②

An Atmospheric Millimeter Wave Propagation Model

AD A139154

(

DTIC
ELECTE
S   MAR 2 0 1984
E   D

NTiA

report series

84 03 19 075

An Atmospheric Millimeter Wave Propagation Model

H. J. Liebe

U.S. DEPARTMENT OF COMMERCE
Malcolm Baldrige, Secretary

David J. Markey, Assistant Secretary
for Communications and Information

December 1983

PREFACE

This report provides a description of the current status of a millimeter wave propagation model based on geophysical input data. The model is being developed by the National Telecommunications and Information Administration, Institute for Tele-communication Sciences, to aid in the development of millimeter wave telecommunication systems.

The laboratory measurements that have been used to verify, and at times, drive the model, have been supported by the Army Research Office, under Contracts ARO 101-83, 6-82, 51-81, and 42-80.

TABLE OF CONTENTS

LIST OF FIGURES

LIST OF TABLES

AN ATMOSPHERIC MILLIMETER WAVE PROPAGATION MODEL
H. J. Liebe*

The neutral atmosphere is characterized for the frequency range from 1 to 300 GHz as a nonturbulent propagation medium. Attenuation and propagation delay effects are predicted from meteorological data sets: pressure, temperature, humidity, suspended particle concentration, and rain rate. The physical data base of the propagation model consists of four terms: (a) resonance information for 30 water vapor and 48 oxygen absorption lines in the form of intensity coefficients and center frequency for each line; (b) a composite (oxygen, water vapor, and nitrogen) continuum spectrum; (c) a hydrosol attenuation term for haze, fog, and cloud conditions; and (d) a rain attenuation model. Oxygen lines extend into the mesosphere, where they behave in a complicated manner due to the Zeeman effect. The geomagnetic field strength H is required as an additional input parameter. Each O_2 line splits proportionally with H into numerous sub-lines, which are juxtaposed to form a Zeeman pattern spread over a megahertz scale. Patterns for three main polarization cases are calculated. Detailed examples for model atmospheres provide basic millimeter wave propagation information over the height range 0 to 100 km of the neutral atmosphere.

Key words: atmospheric attenuation; delay effects; millimeter wave properties of air; propagation model; oxygen Zeeman patterns

1. INTRODUCTION

This report is both an update and a recap of a Millimeter-wave Propagation Model (MPM) based on geophysical input parameters. The atmospheric propagation medium is described by measurable quantities for which spatial and temporal statistics are assumed to be known. Laboratory experiments (Liebe et al., 1977; Liebe, 1984) and analytical efforts (Liebe, 1982; 1983) conducted at the Institute for Telecommunication Sciences (ITS) have played a major role in establishing an MPM which relates easy-to-obtain meteorological data (pressure, temperature, humidity, etc.) to difficult-to-measure propagation factors (attenuation, delay, medium noise, etc.) in a most direct manner. Statistical problems have been treated separately at ITS; for example, those related to specific locations (Allen et al., 1983), to rain climates (Dutton et al., 1983), or to rain clouds (Allen, 1983).

*The author is with the Institute for Telecommunication Sciences, National Telecommunications and Information Administration, U. S. Department of Commerce, 325 Broadway, Boulder, CO 80303.

Atmospheric propagation limitations dominate most consideratons in the advancement of millimeter wave applications (Crane, 1981). Adverse weather causes radio signal degradations due to rain, wet snow, suspended particles, and water vapor. The MPM is structured to solve this complex problem in an efficient manner--complicated microphysical methodology is reduced to simple radio engineering terms. Such propagation modeling provides a cost-effective means of predicting the performance of a system for its intended use. A propagation model can take into account all performance-influencing factors of the atmosphere which in the actual operating environment would be difficult, if not impossible, to identify.

The propagation model is a conglomerate of individual routines. Each routine presents the most practical simulation approach to a particular propagation hindrance and has been validated by calibrated measurements and/or theory. Millimeter wave signal degradations are described by theories of molecular resonances, Rayleigh absorption, Mie scattering loss, and Debye absorption. One role of the MPM is to express these theories or suitable approximations in terms of environmental factors, such as pressure, temperature, humidity, suspended particle concentration, rain rate, and geomagnetic field strength.

The MPM basic to this report was given by Liebe (1981), and a recap of input/output parameters is presented in Section 1.1. The model has found many practical uses, as reflected in Section 1.2 (Allen et al., 1983; Damosso et al., 1982; Pierluissi et al., 1982; and others). The heart of the MPM consists of more than 400 spectroscopic parameters. Some of these have been revised to take into consideration new research findings (Burch, 1982; Davies and Oli, 1973; Endo and Mizushima, 1982; Flaud et al., 1981; Hartmann and Kunzi, 1983; Messer et al., 1983; Pickett et al., 1981; Rosenkranz, 1982; Thomas and Nordstrom, 1982). The updated MPM also contains a rain attenuation term (Olsen et al., 1978; Stutzman and Dishman, 1982). Several physical models of atmospheric millimeter wave properties provided references for the MPM reported here (Waters, 1976; Zrazhevskiy, 1976; Falcone et al., 1979; Mizushima, 1982a, 1982b; Smith, 1981; Smith, 1982).

1.1 The Input/Output Parameters

The Millimeter-wave Propagation Model (MPM) calculates radio path parameters defined in this section based on an earlier paper (Liebe, 1981). For a detailed description of some of the quantities involved and for a discussion of the underlying theory, the reader is referred to that paper. Germane to the propagation model is a macroscopic measure of the interaction between radiation and absorbing species in the form of the complex refractivity N (in parts per million),

2

$$N = N_0 + D(f) + jN''(f) \qquad ppm \qquad (1)$$

The refractivity consists of a frequency-independent refractivity N_0 plus various spectra of refractive dispersion $D(f)$ and absorption $N''(f)$. In radio engineering it is customary to express the imaginary part of (1) as specific power attenuation α and the real part as propagation delay β (with reference to vacuum); that is,

$$\alpha = 0.1820f \; N''(f) \qquad dB/km \quad or$$
$$\alpha^* = \alpha/4.343 \qquad Np/km \quad , \qquad (2)$$

and

$$\beta = 0.02096f[N_0 + D(f)] \qquad radians/km \quad or$$
$$\beta^* = \beta/2\pi f \qquad ns/km \quad , \qquad (3)$$

where the frequency f is in gigahertz (GHz) throughout.

The atmosphere is characterized for the frequency range 1 to 300 (1000) GHz as a nonturbulent propagation medium. The medium is treated as an ensemble of molecules and particles in which spectral features of water vapor, oxygen, suspended water droplets (hydrosols), and precipitation constitute the main absorbers. An adequate permanent spectroscopic data base for the calculation of N consists of seven additive parts:

- the frequency-independent refractivity of moist air given by (Liebe, 1981; Hill et al., 1982)

$$N_0 = (2.589p + 41.6e0 + 2.39e)\vartheta \qquad ppm \quad , \qquad (4)$$

- resonance information for 30 H_2O lines between 22 and 997 GHz $\qquad (N_a)$,
- resonance information for 48 O_2 lines between 49 and 834 GHz $\qquad (N_b)$,
- (·) optional; resonance information for trace gas lines (Section 3.2) $\qquad (N_{e,d,...})$
- continuum absorption due to > 500 H_2O lines above 1000 GHz $\qquad (N_e)$,
- continuum due to nonresonant O_2 and pressure-induced N_2 absorption $\qquad (N_p)$,
- suspended water droplet (haze, fog, cloud) attenuation term $\qquad (N_w)$,
- two-coefficient rain attenuation model (Olsen et al., 1978) $\qquad (N_R)$.

The physical state of the atmosphere, which determines the absorber population in a radio path, is described by the MPM input parameters:

p dry air pressure in kPa (1 kPa = 10 mbar), where the measurable barometric pressure is

$$P = p + e \qquad \text{kPa} ; \tag{5a}$$

T temperature in degrees Kelvin (K), which for the MPM is reduced to a relative inverse temperature parameter

$$\theta = 300/T \qquad ; \tag{5r}$$

e water vapor partial pressure, where vapor concentration is

$$v = 7.219e\theta \quad \text{g/m}^3 \tag{6a}$$

and both e and v are limited by relative humidity

$$RH = (e/e_s)100 = 5.750 \, v\theta^{-6} \times 10^{(9.834\theta - 10)} \leq 100\% \tag{6b}$$

(e_s is the saturation pressure) ;

w suspended water droplet concentration, g/m^3; and

R point rain rate, mm/h

The dispersion and absorption spectra are formulated from

→optional

$$D(f) = \sum_{i=1}^{n_a} (SF')_i + N_p' + \sum_{i}^{n_b} (SF')_i + N_e' + N_w' + N_R' \;\Big|\; + \sum_i^{n_c} (SF')_i + \ldots \quad \text{ppm} \tag{7}$$

and

$$N''(f) = \sum_{i=1}^{n_a} (SF'')_i + N_p'' + \sum_{i}^{n_b} (SF'')_i + N_e'' + N_w'' + N_R'' \;\Big|\; + \sum_i^{n_c} (SF'')_i + \ldots \quad \text{ppm} \tag{8}$$

dry air | humidity | fog,rain | trace gases

where S is a line strength in kHz and F', F'' are real and imaginary parts of a line shape function in GHz^{-1}. Both expressions are discussed in detail in Sections 2 and 3 where the contributing lines are listed in Table 1 (n_a = 48 for O_2), Table 2 (n_b = 30 for H_2O), and Table 6 (n_c = 2 for CO and n_d = 32 for O_3).

For illustrative purposes, it is helpful to introduce Figure 1, which presents an overview of the clear air (w = 0, R = 0) portion of the MPM applied to predict specific attenuation $\alpha(f)$ and refractive dispersion $D(f)$ for sea level conditions at various relative humidities. Significant attenuation extends over several orders

4
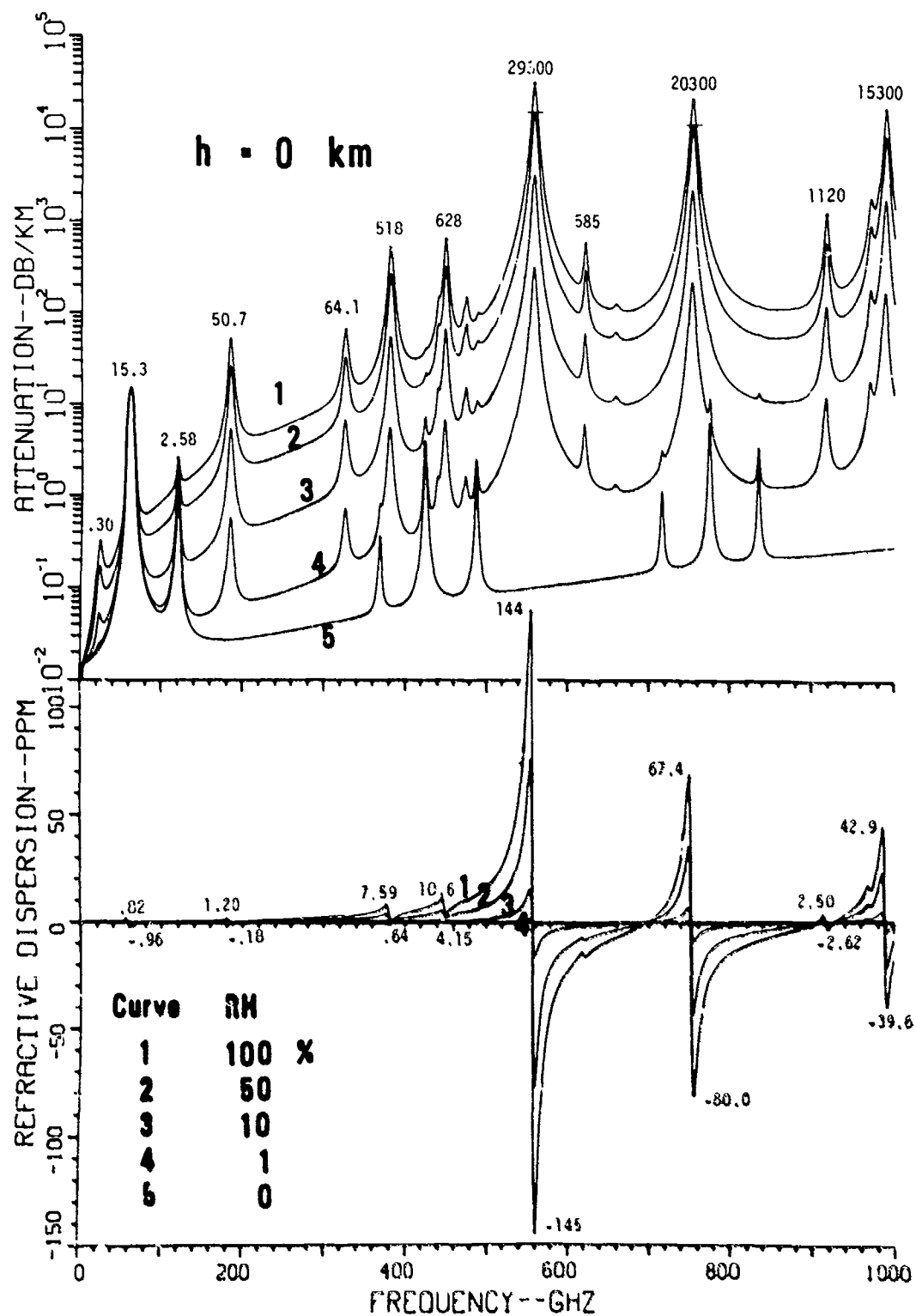
Figure 1. Specific attenuation rate α and refractive dispersion D for moist air (p = 1013 mb, T = 15°C, RH = 0 to 100%) at sea level over a frequency range f = 1 to 1000 GHz.

of magnitude ($<10^{-2}$ to $>10^4$ dB/km). Outside the oxygen resonance regions (see curve 5), the attenuation rate is approximately proportional to absolute humidity v (6a) and is highly frequency-dependent. The low-frequency wing of the dispersion spectrum from the strong 557 GHz H_2O line makes its influence known down to about 100 GHz. The millimeter wave range (30 to 300 GHz) displays four "windows" with relatively low values of α. The frame for these windows is set up by resonance absorption due to oxygen (centered at 60 and 119 GHz) and due to water vapor (centered at 22, 183, and 325 GHz).

Delay (3),(7) and absorption (2),(8) effects of the propagation medium are functions of individual absorber abundances ($\propto$ p/T, v, w, and R) along a radio path, and of frequency f. In addition, emission originates from each absorber volume element in order for the medium to remain in local thermal equilibrium. Radio path measures for these three interrelated effects are:

a) total attenuation in units of decibels (dB) or nepers (Np)

$$A = \int_0^L \alpha(x)dx \qquad dB \qquad or$$

$$A^* = A/4.343 \qquad Np \quad ,$$

(9)

b) total delay in units of radians (rd) or nanoseconds (ns)

$$B = \int_0^L \beta(x)\,dx \qquad rd \qquad or$$

$$B^* = B/2\pi f \qquad ns \quad ,$$

(10)

and

c) sky brightness temperature (Smith, 1982) in units of degrees Kelvin (K)

$$T_B = \int_{h_0}^{\infty} \alpha^*(x)T(x)\ exp[-A^*(x)]dx + 2.9\ exp(-A^*) \qquad K \quad ,$$

(11)

where dx is an increment of the path length L in km, $T(x)$ is the kinetic temperature distribution along the path, and h_0 is the initial (observer) height. Path attenuation A quantifies the amount of energy extracted from a plane wave propagating through the atmosphere, delay B is a measure of the excess traveling time with reference to vacuum, and brightness T_B indicates noise emission (between 2.9 K for $A^* = 0$ and $T_{ambient}$ for $A^* = \infty$) from the medium to the starting level h_0.

6

The cumulative radio path quantities (9) to (11) are the primary output of the MPM. They are evaluated for paths traversing a spherically stratified (concentric layers) atmospheric extending in height between h_o and h_f. The final height is determined by the eventual absence of absorbers. Typically, h_f = 100 km for dry air, 30 km for water vapor, 10 km for water clouds, and 5 to 0 km (height of 0°C isotherm) for rain. The atmosphere is structured in discrete height levels (e.g., 48 layers between h = 0 and 30 km), each identified by a set of p(h), T(h), and RH(h) data that are used to calculate specific values of α, β, and N_o for the layer. Cloud water profiles w(h) can be added to saturated (RH = 100%) air conditions, as well as constant rain rates R. The MPM can draw p-T-RH height profiles from a catalog of ten model atmospheres, and w(h) from several cloud models (Section 4.1).

"Ray tracing" is used to evaluate the path increments dx. A ray is assumed to start from the initial level h_o with an elevation angle ψ (measured from the horizontal) and proceed through the atmosphere, gaining the height interval dh = h - h_o while being subjected to refractive bending. The traveled path differential, including refractive bending, is given by

$$dx = dh / \left\{ 1 - \left[\left(\frac{10^6 + N'(h_o)}{10^6 + N'(h)} \right) \left(\frac{r_E + h_o}{r_E + h} \right) \cos \psi \right]^2 \right\}^{1/2} \quad km , \quad (12)$$

where r_E = 6357 km is a standard (45°N) earth radius. Equation (12) is the spherical form of Snell's law and is strictly valid only when N is purely real, but for the case at hand it is a good approximation, since the values for N" are generally small compared with N' = N_o + D.

The shortest way through the atmosphere is the zenith path ψ = 90°, where dx = dh. A numerical integration through the layered atmosphere implies simply a summation of the specific contributions at each level, applying Simpson's rule. Clear air zenith attenuation A_z is said to be caused by "one air mass." To first order, the air mass for slanted radio paths down to $\psi \geq 10°$ increases according to the secant law, dx = dh/sin ψ, which has been experimentally verified for slant path attenuation A_s (Altshuler et al., 1978). The behavior of slanted ($\psi > 10°$) radio paths can be predicted from

$$A_s = A_z / \sin \psi \qquad \text{and} \qquad B_s = B_z / \sin \psi \qquad (13)$$

Only low elevation angles ($\psi < 10°$) require a detailed evaluation of (12). Refraction is most pronounced in the lowest layers of the atmosphere, which have to be divided into many sublayers for an accurate tracing of the ray path (Gallery et al., 1983). For $\psi < 1°$ and values of h close to h_0, Equation (12) becomes numerically unstable and approximations of the two bracketed terms have to be made by series expansions. At this point, path increments dx become very sensitive to a particular height distribution of absorbers. For example, the tangential ($\psi = 0°$) air mass through the U. S. Standard Atmosphere (NOAA, 1976) for dry air is 38 times the zenith value (Gallery et al., 1983), while for water vapor the tangential mass is about 70 to 180 times the zenith value.

Three useful cumulative measures describing the propagation medium are:

a) the refractive path delay

$$B_0 \cdot \int_0^L N_0(x)dx \quad mm \qquad or \qquad B_0^\star = 3\ 336\ B_0 \quad ps \quad , \qquad (14)$$

b) the total, path-integrated water vapor

$$V = \int_0^L v(x)dx \quad mm \qquad and \qquad (15)$$

c) the total suspended droplet water

$$W = \int_0^L w(x)dx \quad mn \quad . \qquad (16)$$

The MPM operates as follows:

<u>INPUT</u>   frequency range $f_1 (\geq 1\ GHz)$ to $f_2(\ 300\ GHz)$,   (Fig. 1)
            which may be extended to 1000 GHz, although
            purely on theoretical grounds   ,

            horizontal path of length L or slant path with
            elevation angle ψ at h_0 (12),(13)   ,

            pressure and temperature p,θ (5a,5b)   ,

            water vapor concentration v(RH)   (6a,6b)   ,

            hydrosol concentration w   ,

            rainfall rate R   .

8

OUTPUT	specific rates $\alpha(f), \beta(f)$	(2),(3)	,
	cumulative measures $A(f), B(f)$	(9),(10)	,
	medium noise $T_B(f)$	(11)	,
	medium descriptors B_o, V, W	(14)-(16)	.

The heart of the model is a complex refractivity N (7),(8) expressed in measurable quantities. The body of this report consists (a) of improvements and additions to the formulations for N over two separate height ranges, h = 0 to 30 km (Section 2) and 30 to 100 km (Section 3); (b) of a discussion of the MPM computer routine (Section 4); and (c) of samples of representative results in numerical and graphical form (Section 5 and Appendix A).

1.2 Model Applications

Since the introduction of the first MPM version (Liebe, 1981), the model has proven useful for a variety of applications in millimeter wave communications, remote sensing, and radio astronomy. Tape copies of the model together with program listings for P1 and P2 (see Section 4) have been requested by 51 users from industry (23), Government (13), universities (7), and foreign countries (8). The Institute (ITS) has worked with the MPM to lend support to the following applications, to name but a few:

- to develop simple models for predicting transparency in the four atmospheric millimeter wave ranges (Liebe, 1983);
- to present selected examples of the unique transfer characteristics of dry air in the 50 to 70 GHz frequency range (Liebe, 1982);
- to estimate location-dependent attenuation between 10 and 100 GHz for major U. S. population centers (Allen et al., 1983);
- to plan the development of a system performance model for terrestrial millimeter wave communications (Liebe et al., NTIA Technical Memorandum 83-93, August 1983, limited distribution);
- to provide numerical data on the effective height concept $h_s = A/\alpha$ (Section 5.2) over the range 5 to 400 GHz using three model atmospheres (U. S. Standard, Arctic Winter, and Tropical Summer) for CCIR Study Group 5, International Working Party 3, July 1983 (F. Fedi, Chairman);
- to evaluate water-vapor-dependent attenuation data from laboratory and field experiments conducted at 20.6, 31.6, 96.1, 110, and 337 GHz as summarized in Appendix C;

9

- to compare the propagation characteristics over the range 30 to 150 GHz for two sites selected at h = 1 km in Japan and at h = 3 km in Spain for millimeter wave radio astronomy (M. Lebenbaum, private communication, 1983);
- to interpret data from a radiometric observation of the 25⁻ O_2 line (see Section 3.1 and Figure A2) performed over Europe from an aircraft flying at a height of 10 km (Hartmann and Kunzi, 1983).

2. ABSORPTION IN THE LOWER ATMOSPHERE (0 to 30 km)

Strong interactions do occur between millimeter waves and moist air as evident from Figure 1. Other phase states of H_2O also act as strong absorbers in a radio path, each with a behavior that is distinctly different across the millimeter wave spectrum. Specific attenuation for five H_2O states is illustrated in Figure 2, assuming approximately 1 mm absorber thickness ($\approx 3.4 \times 10^{22}$ H_2O molecules). Parameterization of the theories that need to be applied to express the individual spectra of (8) in terms describing atmospheric conditions is outlined in this section including some revisions with regard to the initial model.

2.1 Molecular Effects

Gaseous O_2 and H_2O are considered to be the principal absorbers in moist air. Pressure broadening of spectral lines leads to two different types of frequency responses; namely, sharp resonance lines and continuum spectra, which are treated separately in the following for atmospheric conditions up to heights, h = 30 km. Self- and foreign-gas-broadening influences have to be taken into account.

2.1.1 Local Line Absorption and Dispersion

For the shape of an absorption line, the Van Vleck-Weisskopf function (Kemp, 1979) as modified by Rosenkranz (1975) was chosen in the form

$$F'' = \frac{f}{\nu_0} \left(\frac{\gamma - (\nu_0 - f)\delta}{(\nu_0 - f)^2 + \gamma^2} + \frac{\gamma - (\nu_0 + f)\delta}{(\nu_0 + f)^2 - \gamma^2} \right) \qquad GHz^{-1} . \qquad (17)$$

A Hilbert transform of (17) yields the corresponding dispersion profile (D. Brown, private communication, 1982; R. Hill, private communication, 1982)

10
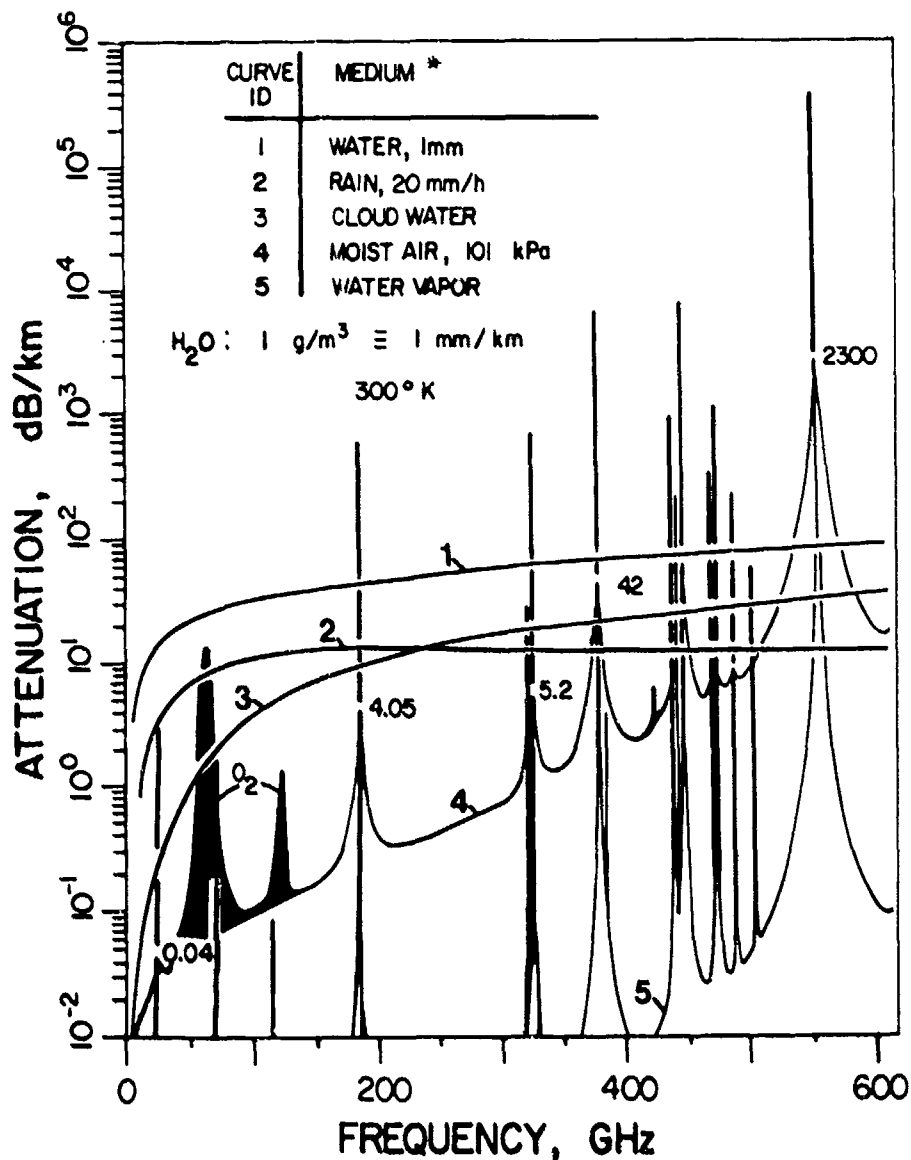
*) Note: The phase states (absorption theories) are: 1) water (Debye relaxation), 2) rain (Mie scattering), 3) hydrosol (Rayleigh absorption, 4) moist air (pressure-broadened spectral line, numbers shown indicate selected peak attenuations), and 5) pure water vapor (self-broadered lines).

Figure 2. Specific H_2O attenuation over a frequency range from 5 to 600 GHz for five phase states normalized to equal absorber amount (1 mm).

$$F' = \left(\frac{(\nu_0 - f) + \gamma(\gamma + f\delta)/\nu_0}{(\nu_0 - f)^2 + \gamma^2} + \frac{(\nu_0 + f) + \gamma(\gamma - f\delta)/\nu_0}{(\nu_0 + f)^2 + \gamma^2} - \frac{2}{\nu_0} \right) \text{GHz}^{-1}, \quad (18)$$

which is slightly different from F' as given by Liebe (1981).

The line parameters are calculated according to the scheme below:

ID	O_2 lines in air a	H_2O lines in air b	Equation (7),(8)
ν_0 , GHz	Table 1	Table 2	
S , kHz	$a_1 p\theta^3 \exp[a_2(1 - \theta)]10^{-6*}$	$b_1 e\theta^{3.5} \exp[b_2(1 - \theta)]$	(19)
γ , GHz	$a_3(p\theta^{(0.8-a_6)} + 1.1e\theta)10^{-3}$	$b_3(p\theta^{0.8} + 4.80e\theta)10^{-3}$	(20)
δ , 1	$a_4 p\theta^{a_5}$	0	(21)

* See Appendix B

Line center frequencies ν_0 and the spectroscopic coefficients a_1 to a_6, b_1 to b_3 for strength S and width γ are listed in Tables 1 and 2. Revisions have been made to:

$\nu_0(O_2)$ (Endo and Mizushima, 1982) ,

a_1 (Appendix B) ,

$a_3(e)$ (Setzer and Pickett, 1977) ,

a_6 (Pickett et al., 1981) ,

$\nu_0(H_2O)$ (Messer et al., 1983) ,

b_1 (Flaud et al., 1981; Mizushima, 1982a) ,

b_3 (Davies and Oli, 1978) ,

$b_3(\theta)$ (Thomas and Nordstrom, 1982) .

The oxygen coefficients a_1 to a_4 are based largely on solid experimental evidence (Liebe et al., 1977). The spectroscopic fundamentals for the molecular calculation procedure of a_1 and a_2 are outlined briefly in Appendix B. Even after drastic simplifications, there remain 336 spectroscopic coefficients (Table 1) to describe for an MPM the detailed line spectrum of dry air. The temperature dependence of the overlap coefficients a_4 evolves from a complicated iterative procedure (Rosenkranz, 1975) that was evaluated over the temperature range T = 200 to 300 K. The results were approximated by a_5 (21). The even simpler approximation $a_5 = 2$ was attempted, and a comparison of both with rigorous calculations, as shown for an example in Table 3, resulted in opting for a_5 as listed in Table 1. A more rigorous theory for a_4, a_5 has been developed by Smith (1981) based on our data.

The spectroscopic water vapor coefficients b_1 also have a molecular base in Equation (B2). The asymmetric H_2O rotor molecule possesses a strong electric dipole moment (μ) and requires different assumptions about selection rules (ν_o), matrix elements ($|\phi|$), energy levels (E_ℓ), partition function (Q), and nuclear spin (g_ℓ). The line strength coefficients b_1 were compared with several reported H_2O line data bases (Rothman et al., 1983a; Poynter and Pickett, 1981; Mizushima, 1982a). These data bases differ slightly from one another and the b_1 values given in Table 2 are derived from Flaud et al. (1981). Linewidth data b_3 for the 22 GHz and 183 GHz lines are based on controlled laboratory experiments; the remaining ones were approximated following the theoretical work by Davies and Oli (1978). The MPM version of the atmospheric water vapor line spectrum requires 120 spectroscopic coefficients (Table 2) since overlap corrections need not be made. Water vapor lines are reported to display small, vapor-pressure-induced shifts of the center frequencies ν_o, which are neglected.

2.1.2 Continuum Absorption

The continuum spectrum in (7) and (8) consists of dry air and water vapor absorption terms,

$$N_c'' = N_p'' + N_e'' \quad , \tag{22}$$

while the respective refractive dispersions are neglected; i.e., $N_p' = 0$ and $N_e' = 0$. The continuum varies monotonically with frequency and needs to be added to the selected group of local O_2 and H_2O resonance lines (Tables 1 and 2) in order to correctly predict atmospheric millimeter wave attenuation in the window ranges in between lines.

Table 1. Revised Oxygen Line Parameters
(compare with Liebe, 1981: Table 4a)

ν_0	a_1	a_2	a_3	a_4	a_5	a_6	$K^\pm$
GHz	$(kHz/kPa)10^{-6}$		MHz/kPa	1/kPa			D=doublet
49.452379	0.12	11.830	8.40	5.60	1.7	0	41−
49.962257	0.34	10.720	8.50	5.60	1.7	0	39−
50.474238	0.94	9.690	8.60	5.60	1.7	0	37−
50.987748	2.46	8.690	8.70	5.50	1.7	0	35−
51.503350	6.08	7.740	8.90	5.60	1.8	0	33−
52.021409	14.14	6.840	9.20	5.50	1.8	0	31−
52.542393	31.02	6.000	9.40	5.70	1.8	0	29−
53.066906	64.10	5.220	9.70	5.30	1.9	0	27−
53.595748	124.70	4.480	10.00	5.40	1.8	0	25−
54.129999	228.00	3.810	10.20	4.80	2.0	0	23−
54.671157	391.80	3.190	10.50	4.80	1.9	0	21−
55.221365	631.60	2.620	10.79	4.17	2.1	0	19−
55.783800	953.50	2.115	11.10	3.75	2.1	0	17−
56.264777	548.90	0.010	16.46	7.74	0.9	0	D1 | 1+
56.363387	1344.00	1.655	11.44	2.97	2.3	0	15−
56.968180	1763.00	1.255	11.81	2.12	2.5	0	13−
57.612481	2141.00	0.910	12.21	0.94	3.7	0	11−
58.323874	2386.00	0.621	12.66	−0.55	−3.1	0	D2 | 9−
58.446589	1457.00	0.079	14.49	5.97	0.8	0	3+
59.164204	2404.00	0.386	13.19	−2.44	0.1	0	7−
59.590982	2112.00	0.207	13.60	3.44	0.5	0	5+
60.306057	2124.00	0.207	13.82	−4.13*	0.7	0	D3 | 5−
60.434775	2461.00	0.386	12.97	1.32	−1.0	0	7+
61.150558	2504.00	0.621	12.48	−0.36	5.8	0	9+
61.800152	2298.00	0.910	12.07	−1.59	2.9	0	11+
62.411212	1933.00	1.255	11.71	−2.66	2.3	0	D4 | 13+
62.486253	1517.00	0.078	14.68	−4.77*	0.9	0	3−
62.997974	1503.00	1.660	11.39	−3.34	2.2	0	15+
63.568515	1087.00	2.110	11.08	−4.17	2.0	0	17+
64.127764	733.50	2.620	10.78	−4.48	2.0	0	19+
64.678900	463.50	3.190	10.50	−5.10	1.8	0	21+
65.224067	274.80	3.810	10.20	−5.10	1.9	0	23+
65.764769	153.00	4.480	10.00	−5.70	1.8	0	25+
66.302088	80.09	5.220	9.70	−5.50	1.8	0	27+
66.836827	39.46	6.000	9.40	−5.90	1.7	0	29+
67.369595	18.32	6.840	9.20	−5.60	1.8	0	31+
67.900862	8.01	7.740	8.90	−5.80	1.7	0	33+
68.431001	3.30	8.690	8.70	−5.70	1.7	0	35+
68.960306	1.28	9.690	8.60	−5.60	1.7	0	37+
69.489021	0.47	10.720	8.50	−5.60	1.7	0	39+
70.017342	0.16	11.830	8.40	−5.60	1.7	0	41+
118.750341	945.00	0.000	15.92	−0.44	0.9	0	1−
368.498350	67.90	0.020	15.60	0	1	0.6	11,23
424.763120	638.00	0.011	14.70	0	1	0.6	21,23
487.249370	235.00	0.011	14.70	0	1	0.6	21,33
715.393150	99.60	0.089	14.40	0	1	0.6	33,45
773.838730	671.00	0.079	14.00	0	1	0.6	43,45
834.145330	180.00	0.079	14.00	0	1	0.6	43,55

* Reduced value (i.e., theory minus 5 percent)

Table 2. Revised Water Vapor Line Parameters
(compare with Liebe, 1981: Table 4b)

ν_0	b_1	b_2	b_3
GHz	kHz/kPa		MHz/kPa
22.235080	0.1120	2.143	28.10
67.813000 *	0.0011	8.730	25.00
120.127000 *	0.0007	8.350	27.00
183.310117	2.4070	0.653	28.20
321.225644	0.0450	6.160	25.50
325.152919	1.5910	1.520	29.00
336.187000 *	0.0009	9.800	24.00
380.197372	12.6400	1.020	28.50
390.134508	0.0041	7.330	25.00
437.346667	0.0625	5.020	25.50
439.150812	0.9250	3.560	25.80
443.018295	0.1900	5.020	25.50
448.001075	10.9900	1.370	27.60
470.888947	0.3310	3.570	26.80
474.689127	1.3100	2.340	26.50
488.491133	0.2550	2.810	26.00
503.568532	0.0354	6.690	24.40
504.482692	0.0118	6.690	24.40
556.936002	538.8000	0.114	31.70
620.700807	5.3960	2.340	27.00
658.015000 *	0.4600	7.760	32.80
752.033227	264.3000	0.336	30.20
841.073593	0.0123	8.110	25.40
859.865000 *	0.0150	7.990	29.00
899.407000 *	0.0910	7.840	30.00
902.555000 *	0.0640	8.350	27.80
906.205524	0.1820	5.040	25.40
916.171582	8.9180	1.370	27.90
970.315022	9.6880	1.840	26.60
987.926764	145.6000	0.180	29.90

* First vibrationally excited line (Flaud et al., 1981)

15

Table 3. Two approximations for the temperature dependence of Rosenkranz's (1975) overlap coefficients for the O_2 microwave spectrum.

1) The "$a_5 = 2$" Approximation:

DRY AIR AT 250 K, P=101 KPA

FREQUENCY (GHZ)	ATTENUATION (DB/KM)	PERCENT ERROR OF APPROX.	PHASE DISPERSION (RAD/KM)	PERCENT ERROR OF APPROX.
40.0	.081	-.04	.113	.02
42.5	.105	-.09	.152	.03
45.0	.166	-.14	.207	.04
47.5	.242	-.18	.291	.05
50.0	.451	-.16	.427	.05
52.5	1.074	.10	.651	.15
55.0	4.974	.57	1.166	.17
57.5	14.649	.04	1.011	
60.0	20.674	-.48	-.175	-1.07
62.5	15.765	.68	-1.605	-4.66
65.0	4.465	.06	-1.653	-.01
67.5	1.129	.90	-1.177	.25
70.0	.511	-1.28	-.916	.11
72.5	.310	-1.39	-.754	.05
75.0	.214	-1.44	-.713	.01
77.5	.159	-1.45	-.649	.01
80.0	.125	-1.41	-.620	.01
82.5	.102	-1.33	-.595	.01
85.0	.086	-1.20	-.572	.00
87.5	.075	-1.01	-.556	.00
90.0	.057	-.75	-.544	.00
92.5	.061	-.42	-.535	.00
95.0	.054	-.01	-.527	.00
97.5	.056	.48	-.521	.00
100.0	.057	1.02	-.516	.00
102.5	.046	1.59	-.513	.00
105.0	.058	2.11	-.505	.00
107.5	.063	2.51	-.504	.01
110.0	.115	2.46	-.498	.01
112.5	.119	2.44	-.484	.04
115.0	.413	1.78	-.460	.10
117.5	1.350	.67	-.454	.17
120.0	1.244	-.82	-.454	.17
122.5	.379	-2.56	-.644	.68
125.0	.161	-4.40	-.621	.04
127.5	.050	-6.23	-.410	.03
130.0	.045	-7.96	-.466	.01
132.5	.043	-9.56	-.665	.01
135.0	.042	-11.01	-.658	.01
137.5	.027	-15.32	-.615	.01
140.0	.013	-13.50	-.612	.00

2) The "a_5" Approximation (Table 1, Eq. 21):

FREQUENCY (GHZ)	ATTENUATION (DB/KM)	PERCENT ERROR OF APPROX.	PHASE DISPERSION (RAD/KM)	PERCENT ERROR OF APPROX.
40.0	.081	.00	.113	.00
42.5	.105	.01	.152	.00
45.0	.166	.02	.207	.00
47.5	.242	.04	.291	.00
50.0	.451	.05	.427	.00
52.5	1.058	.06	.651	.01
55.0	4.934	-.01	1.165	.02
57.5	14.649	-.02	1.011	.03
60.0	20.674	-.00	-.175	.03
62.5	15.765	-.04	-1.605	.02
65.0	4.465	-.10	-1.653	.02
67.5	1.129	-.14	-1.177	.01
70.0	.511	-.17	-.916	.00
72.5	.310	-.19	-.754	.00
75.0	.214	-.23	-.713	.00
77.5	.159	-.25	-.649	.00
80.0	.125	-.27	-.620	.00
82.5	.102	-.27	-.595	.00
85.0	.086	-.26	-.536	.00
87.5	.075	-.24	-.525	.00
90.0	.057	-.18	-.513	.00
92.5	.061	-.14	-.505	.00
95.0	.054	.04	-.504	.00
97.5	.056	.05	-.498	.00
100.0	.115	-.01	-.484	.00
102.5	.119	-.01	-.460	.00
105.0	.413	-.03	-.454	.00
107.5	1.350	.08	-.454	.00
110.0	1.244	.16	-.644	.00
112.5	.379	.36	-.621	.00
115.0	.161	.54	-.410	.00
117.5	.044	.44	-.466	.01
120.0	.043	.53	-.665	.00
140.0	.013	.71	-.612	.00

16

The dry air continuum,

$$N_p'' = [a_o p \theta^2 \gamma_o / (f^2 + \gamma_o^2) + a_n p^2 \theta^{2.5}] f \quad \text{ppm} \quad , \qquad (23)$$

makes a small contribution at ground level pressures due to the nonresonant O_2 spectrum below 10 GHz (Rosenkranz, 1975) and the pressure-induced N_2 spectrum effective above 100 GHz (Dagg et al., 1982). The scale factors in (23) are

$$a_o = 6.14 \times 10^{-4} \quad \text{ppm(kPa GHz)}^{-1} ,$$
$$\qquad (23a)$$
$$a_n = 1.5 \times 10^{-10} \quad \text{ppm(kPa)}^{-2} \text{(GHz)}^{-1} ;$$

and the width parameter (see Eq. 20),

$$\gamma_o = 5.6 \times 10^{-3} \ (p + 1.1e) \theta^{0.8} \quad \text{GHz/kPa} \quad , \qquad (23b)$$

for the Debye spectrum of O_2, is chosen to agree with overlap measurements (Liebe et al., 1977) following a suggestion by Rosenkranz (1982).

The water vapor continuum,

$$N_e'' = [b_f e p \theta^{2.5} + b_s e^2 \theta^{3.5}] f \quad \text{ppm} \qquad (24)$$

has been a major source of uncertainty in predicting millimeter wave attenuation rates, especially in the four window ranges (Waters, 1976; Rice and Ade, 1979; Emery et al., 1980; Crane, 1981; Zammit and Ade, 1981; Burch, 1982; Zammit et al., 1982; Liebe, 1983). Recent laboratory experiments, employing a special high-humidity spectrometer at $f = 138$ GHz, RH = 80 to 100%, and $p = 0$ to 150 kPa (nitrogen), produced the following results (Liebe, 1984), which are reflected in the formulation of (24):

• the scale factors in (24) for moist air are

$$b_f = 1.40 \times 10^{-6} \quad \text{ppm(kPa)}^{-2} \text{GHz}^{-1} . \qquad (24a)$$

and

$$b_s = 5.41 \times 10^{-5} \quad \text{ppm(kPa)}^{-2} \text{GHz}^{-1} ; \qquad (24b)$$

17

- up to saturation (RH = 100%), there was no evidence of anomalous absorption at the two test temperatures, 282 and 300K;

- a strong self-broadening component $b_s e^2$ was measured and tentatively identified to be related to monomer H_2O line absorption, since its temperature dependence is $\theta^{3.5 \pm 1}$, which is a little higher than expected from H_2O line broadening theory.

Predictions with the MPM including (24) show good agreement with absolute laboratory and field results for specific attenuation caused by water vapor (see Appendix C).

2.2 Suspended Particle Effects

Hydrosols in haze, fog, or clouds are the dominant suspended particle absorbers in the lower atmosphere. Their refractivity contribution is labeled $N_W = (N_W' + jN_W'')$. Below 300 GHz, there is relatively little effect on path delay since

$$N_W' \approx 1.4 \, w \quad \text{ppm} \tag{25}$$

It is the Rayleigh absorption approximation

$$N_W'' = \alpha_W / 0.182f = 4.50 \, w \, \varepsilon'' / [(\varepsilon' + 2)^2 + (\varepsilon'')^2] \quad \text{ppm} \tag{26}$$

of Mie scattering losses (appropriate for size ranges of radii $\leq 50 \, \mu m$), which makes a frequency dependent contribution (Falcone et al., 1979). The dielectric data ε', ε'' of bulk water are calculated with the Debye model reported by Chang and Wilheit (1979), which is valid for $f \leq 300$ GHz:

$$\varepsilon' = 4.9 + (185 - 113/\theta)/[1 + (f\tau)^2]$$

and
$$\tag{27}$$

$$\varepsilon'' = (185 - 113/\theta)f\tau/[1 + (f\tau)^2] \quad ,$$

where

$$\tau = 4.17 \times 10^{-5} \, \theta \, \exp(7.13\theta) \quad \text{ns} \quad .$$

Equations (2), (26), and (27) are applied to model specific attenuation by hydrosols (haze, fog, clouds) if their average mass concentration $w(g/m^3)$ and relative temperature θ within a radio path are known. Cloud and fog conditions ($w < 0.01 \, g/m^3$) exist only in nearly saturated air (RH $\approx$ 100%); for haze conditions ($w < 0.01 \, g/m^3$), the relative humidity may be in the 90 to 99 percent range. Table 4 lists

numerical examples of α_w (dB/km) for two temperatures (0° C and 25° C) at selected frequencies.

Table 4. Hydrosol (haze, fog, cloud) attenuation α_w
for a mass concentration $w = 1$ g/m^3

TEMPERATURE		FREQUENCY f , GHz					
T	θ	1	10	30	100	200	300
°C				dB/km			
0	1.0983	.001	.097	.82	5.4	9.3	10.7
25	1.0062	.001	.051	.45	4.2	10.8	15.3

Models for clouds, fog, and haze are available that describe spatial distributions of w(h) (e.g., Chang and Wilheit, 1979; Falcone et al., 1979). Nonprecipitating clouds and clouds producing stratiform rain have limited vertical but, on the average, large horizontal extents. Cloud top/bottom heights typically are in ranges from (2 to 8)/(1 to 6) km, and the liquid water concentration w may vary between 0.01 and 1 g/m^3. Chemical depositions in clouds (e.g., acid content) may alter the dielectric properties (27) of pure water. Also, temperature (roughly between -20 and +5° C) has some influence upon the attenuation (26). Integrated zenith column densities W (16) amount to values between 0.05 and 2 mm, distributed in air masses with water vapor column densities V (15) between 5 and 60 mm. For slant path calculations, both columns are expected to display a secant dependence (13) with elevation angles $\psi > 10°$.

The structure of cumulus-type (convective) clouds, such as occur in thunderstorms, is much more complicated. Here, distinct regions for updrafts (large W) and downdrafts (large R), as well as an irregular horizontal structure, have to be distinguished. An attempt to model their influence upon millimeter wave propagation was reported by Allen (1983). He suggests for both types of rain-producing clouds simple correlations between hydrosol concentration w and rain rate R in the mean (stratus: $w \approx 0.7R^{0.9}$, cumulus-type: $w \approx 3 R^{0.5}$) and proceeds to derive rain cloud properties from readily available rain rate statistics.

2.3 Precipitation Effects

Precipitation originates as a hig ly statistical event within clouds suspended in saturated air. Its vertical distribution is separated into two regions by the height h_f of the $0°$ C isotherm, which can vary between 6 km and ground level depending on season and latitude. The lower part is mostly liquid drops, and the upper region consists of frozen particles with occasional supercooled droplet-loadings by strong updrafts. Widespread steady rain occurs more uniformly and favors small drop sizes ($\leq$ 1 mm diameter) which stay in the air longer. Heavy showers are more localized, favor larger drops, and occur less frequently.

The refractivity spectrum of rain is identified in (7) and (8) by $N_R = N_R' + jN_R''$. Drop diameters (0.1 - 6 mm) and millimeter wavelengths are comparable, thus causing appreciable interactions due to Mie absorption and scattering. A very crude approximation for delay effects yields

$$N_R' \approx 0.06 \ R \quad ppm \quad for \ f \leq 10 \ GHz \ and$$

$$N_R' \approx 0.6R/f \quad ppm \quad for \ f > 10 \ GHz \ . \tag{28}$$

The absorption spectrum is formally expressed by

$$N_R'' = \alpha_R/0.182 \ f \quad ppm \ .$$

Bypassing elaborate, lengthy Mie calculations (e.g., Falcone et al., 1979), which require drop shape and size distributions, as well as the complex dielectric constant of water (27), Olsen et al. (1978) approximated the specific rain attenuation by the power law model

$$\alpha_r = u(f)R^{v(f)} \quad dB/km \ . \tag{29}$$

The frequency-dependent coefficient u and exponent v were calculated using dropsize spectra of Laws and Parsons and a temperature of $T = 0°$ C. A regression fit to individual (u,v)-pairs over the frequency range from 1 to 1000 GHz resulted in the following calculation scheme (Olsen et al., 1978):

20

$$u = x_1 f^{x_2} \qquad\qquad v = x_3 f^{x_4} \qquad (29a)$$

f	x_1	x_2	f	x_3	x_4
GHz			GHz		
1 to 2.9	6.39×10^{-5}	2.03	1 to 8.5	0.851	0.158
2.9 to 54	4.21×10^{-5}	2.42	8.5 to 25	1.41	−0.0779
54 to 180	4.09×10^{-2}	0.699	25 to 164	2.63	−0.272
180 to 1000	3.38	−0.151	164 to 1000	0.616	0.0126

An evaluation of (29) for point rainfall rates R between 0.25 (light drizzle) and 150 (severe thundershower) mm/h is shown in Figure 3. The validity of this approach, which reduces theoretical complexity to empirical simplicity, is fairly well established (Stutzman and Dishman, 1982).

Rain can be a serious attenuator at frequencies above 20 GHz; however, experience is: "it rains only occasionally." Actually, events of serious consequences $(\alpha_R > 1 \text{ dB/km})$ occur typically less than one percent over the period of a year. Long-term statistics of rain attenuation, however, are beyond the scope intended for the MPM. Statistical estimation methods and models for the occurrences of rain attenuation are discussed in detail, for example, by Crane (1980,1981) and by Dutton et al. (1983). Rain cell extent L_R and path-averaged rain rate $\bar{R}$ are obtained from cumulative distributions of path attenuation A or point rate R at many locations over long time periods, preferably several years.

The MPM is capable of treating rain identified by a point rate R (mm/h) measured somewhere along the path extending over a horizontal length L (km). Then an average rate $\bar{R}$, which is calculated with an empirical model proposed by Stutzman and Dishman (1982), can be assumed to fill the entire path homogeneously. According to that model, the path-averaged rain rate is

$$\bar{R} = R \qquad\qquad \text{when } R \leq 10, \text{ and is for } R > 10 \text{ given by}$$

$$\bar{R} = R \ \frac{1 - \exp[-(L/22) \ \ln(R/10)]}{(L/22) \ \ln(R/10)} \quad \text{mm/h} \quad . \qquad (30)$$

For slant path calculations, the rain cell extent is limited to height level h_f (0° C) and the secant law (13) is applied for predicting elevation angle (ψ) dependences.
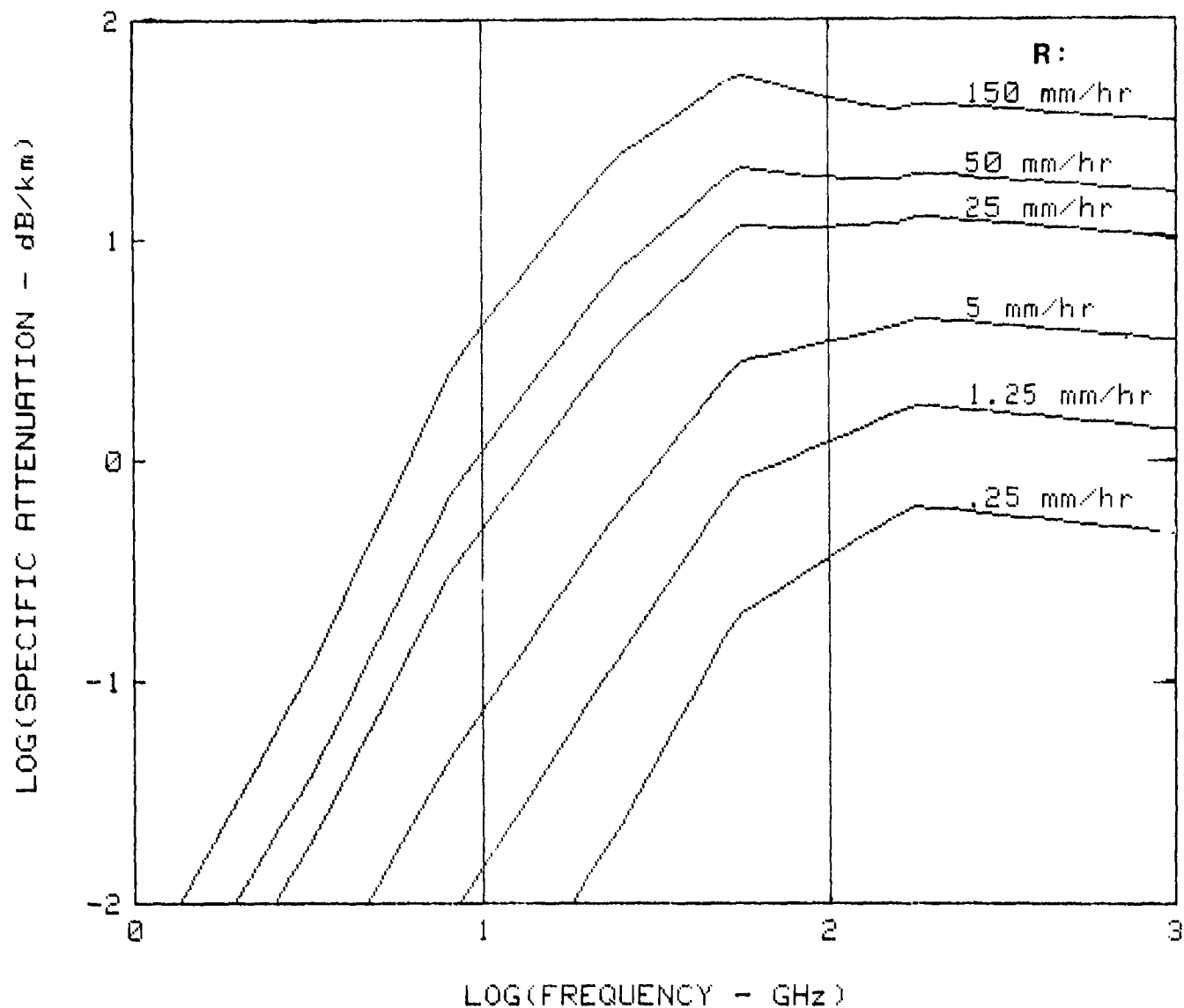
21

Figure 3. Specific rain attenuation α_R over a frequency range from 1 to 1000 GHz for various rainfall rates, R = 0.25 to 150 mm/h using a four-segment approximation for equation (29).

22

The MPM is restricted to approximate only the most fundamental effects by rain, formulated by (28) to (30). Considerable refinements need to be added if other precipitation-induced signal degradations (e.g., depolarization, scatter interference between links sharing the same frequency, etc.) are to be predicted (Oguchi, 1983).

3. ABSORPTION IN THE UPPER ATMOSPHERE (30 TO 100 km)

An auxiliary model to the MPM calculates specific attenuation due to isolated lines above h = 30 km. All line overlap has disappeared and even closely-spaced doublets in the O_2 spectrum (Table 1) can be treated as isolated lines. Increasing height implies exponentially decreasing pressure p, which causes a single line to narrow. The attenuation peak at line center begins to diminish when the absorber abundance disappears or when Equation (20) approaches the finite Doppler width

$$\gamma_D = 6.20\nu_0/\sqrt{m\theta} \qquad kHz \qquad (31)$$

where m is the molecular weight (e.g., O_2, m = 32, θ = 1, ν_0 = 60 GHz, then γ_D = 65.8 kHz). An adequate approximation can be made by replacing γ with

$$\gamma_h = \sqrt{\gamma^2 + \gamma_D^2} \quad , \qquad (32)$$

while retaining the first term (Lorentzian) of the line profiles F" (17) and F' (18). Actually, during this process, the line profile also changes from a Lorentzian to a Gaussian. This transition is described by a Voigt profile (Liebe, 1981) that, for the purpose of the MPM, can be passed over. Water vapor height profiles indicate that e(h > 20 km) $\simeq$ 0, except for a very small residual,which can exist up to about 70 km. Mesospheric water vapor lines can be neglected for the MPM. The oxygen mixing ratio, however, remains constant up to about 80 km where dissociation to atomic oxygen begins. At 120 km, the ratio O_2/O has dropped off to 0.25. Oxygen lines have to be traced above 30 km and the situation grows complicated due to Zeeman splitting caused by the geomagnetic field.

3.1 Oxygen Zeeman Patterns

Zeeman splitting of isolated oxygen lines due to the influence of the earth's magnetic field strength H (in Gauss) introduces considerable complications. Each line is identified by a quantum number K. The presence of the steady field H splits $K^{\pm}$ lines into three groups of $(2K^{\pm} \pm 1)$ sublines, thereby redistributing line atten-

uation over a fixed frequency range. In principle, three different Zeeman patterns, $\alpha_{1,2,3}$, are possible for any $K^{\pm}$ line. These patterns are obtained by evaluating η and ξ coefficients in π and $\sigma^{\pm}$ groups. Each sum of sublines determines a Zeeman pattern according to

$$\alpha_{1,2,3} = \alpha_0 \sum_{\eta} \xi/\{1 + [(f - \nu_0^z)/\gamma_h]^2\} \tag{33}$$

where the scale factor $\alpha_0 = \alpha(\nu_0)$ follows with (2), (8), (19), (17), (20), (32) to be

$$\alpha_0 = 0.182 \ \nu_0(a_1 p/\gamma_h)\theta^3 \exp[a_2(1 - \theta)] \qquad dB/km \quad . \tag{34}$$

The line center frequency ν_0^z of each Zeeman component is given by

$$\nu_0^z = \nu_0 + \eta \ 2.803 \ H \times 10^{-3} \qquad GHz \quad . \tag{35}$$

A scheme to calculate number, position (η), and intensity (ξ) of individual Zeeman components was derived from the work of Lenoir (1968) by Liebe (1981; Table 6). The component number increases with quantum number $K^{\pm}$ (line ID, Table 1). Numerical and graphical results for the first eight lines $K^{\pm} = 1$ to 7 illustrate in Table 5 and Figure 4 the organization of Zeeman components into three groups labeled π, σ^+, and σ^-. Each component is treated as a separate independent line having identical shape and width. The intensity sum, both for the π components and for the $\sigma^+ + \sigma^-$ components, is equal to the integrated intensity of the unsplit line repreresented by the scale factor α_0 (34).

The three main patterns $\alpha_1(\pi), \alpha_2(\sigma^+)$ and $\alpha_3(\sigma^-)$ for lines $K^{\pm} = 1$ to 29 (Table 1) have been calculated at local $p - \theta - H$ conditions of the U. S. Standard Atmosphere (NOAA, 1976) over the height range 30 to 100 km at two magnetic field strengths, $H = 0.3$ and 0.6 G. A catalog of the complete set is presented in graphical form in Appendix A. Above $h = 70$ km, individual, now mostly Doppler-broadened components become discernible. The results, in combination with beginning dissociation to atomic oxygen, establish $h = 100$ km as the boundary to outer space for radio path modeling. Over the height range 30 to 100 km and a narrow frequency band around ν_0 one is confronted with direction-dependent (unisotropic) attenuation rates. The first step towards tying the three main Zeeman patterns to a global coordinate system for H and antenna position and expressing them for two principal directions and various wave polarizations is discussed in Section 4.2.

24

Table 5. The Frequency Shifts $\eta(K,M)$ and Relative Intensity Factors $\zeta(K,M)$ for the ZEEMAN Components of the $K=1^{\pm}$ to $7^{\pm}$ Oxygen Lines (Table 1).
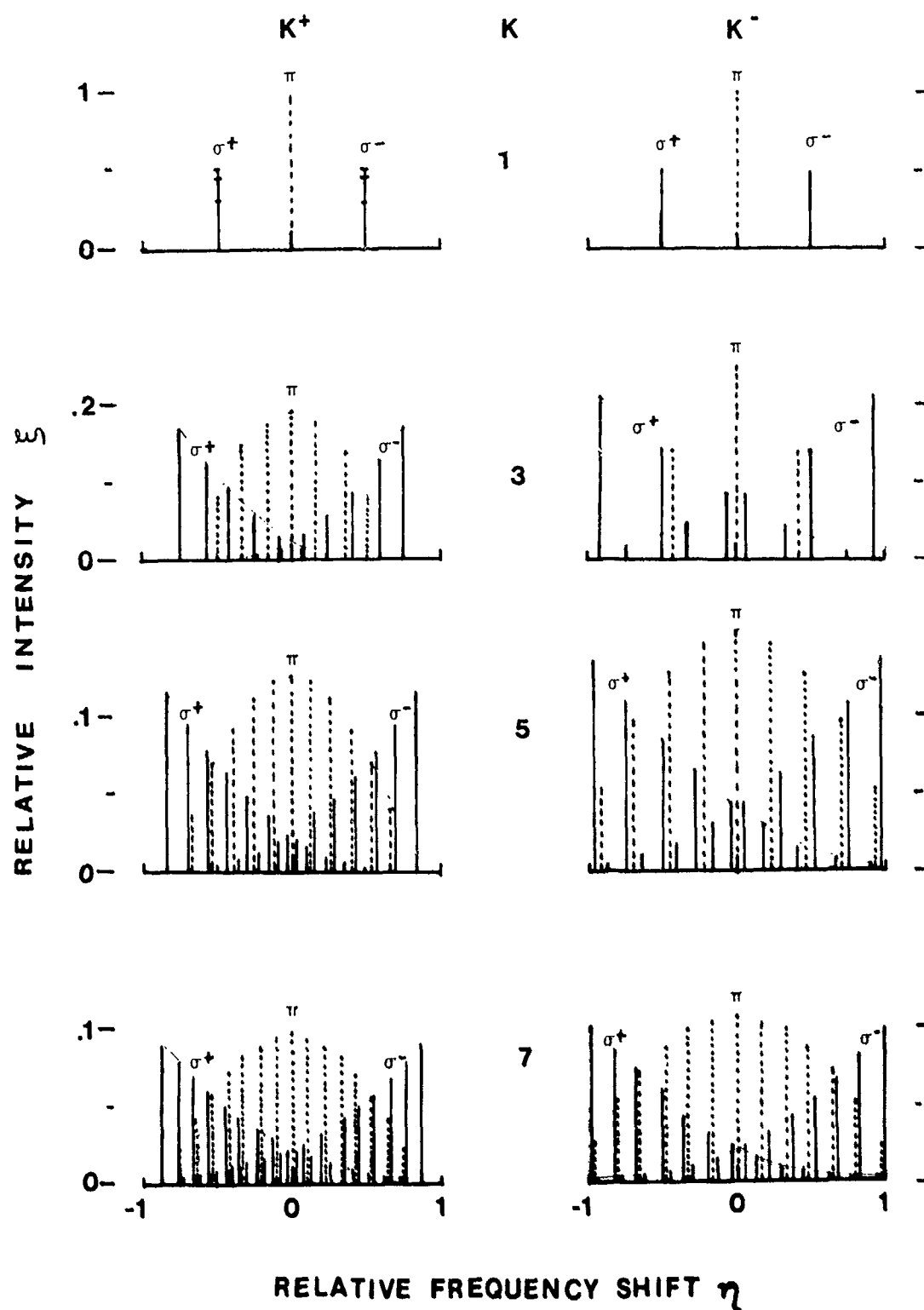
Figure 4. Relative shift η and relative intensity ξ of the Zeeman components for O_2 microwave lines $K^{\pm} = 1$ to 7.

3.2 Trace Gas Spectra

Atmospheric trace gases such as carbon monoxide (CO), ozone (O_3), nitrous oxide (N_2O), nitric oxide (NO), and sulfur dioxide (SO_2) are potential millimeter wave absorbers. In particular, the asymmetric rotor molecules O_3 and SO_2 exhibit a rich millimeter wave line spectrum (Rothman et al., 1983b; Park et al., 1981). Scanty abundances (< 2 ppm/vol.) of trace gas absorbers and dominant pressure-broadening by the major constituents ($\propto p$) make none of these lines detectable in the troposphere. When linewidths (2θ) have narrowed to a few megahertz ($h \geq 20$ km), stronger lines may affect the millimeter wave behavior of radio paths to outer space, especially if abundances have increased with height, as is the case for ozone. Tiny absorption spikes may be observed on an earth-space path operating at low elevation angles in transparent portions of the spectrum.

Spectra are modeled with the formulations described in Section 2.1.1. Tables of the spectroscopic coefficients have to be prepared before line spectra of trace gas molecules can be added to (8). Several millimeter wave lines of the species CO and O_3 have been observed in the atmosphere. Their calculation scheme is detailed below:

	CO lines in air	O_3 lines in air	Equation
ID	c	d	(7),(8)
ν_0,GHz	Table 6	Table 6	
S,kHz	$c_1 M_c 10^{-18}\theta^2 \exp[c_2(1-\theta)]$	$d_1 M_d 10^{-18}\theta^{2.5}\exp[d_2(1-\theta)]$	(36)
γ,GHz	$c_3 p\theta^{0.8}$	$d_3 p\theta^{0.5}$	(37)
δ	0	0	

Line strengths S are defined to be proportional to the number density M in molecules/cm^3. The spectroscopic coefficients c_1 to c_3, d_1 to d_3 are given in Table 6. Models exist for the height profiles $M_{c,d}(h)$ (NOAA, 1976). For example, ozone displays a maximum $M_d = 5 \times 10^{12} cm^{-3}$ in the profile $M_d(h)$ at a height of $h = 22$ km ($p = 4$ kPa, $\theta = 1.37$) where the air density is $M_a = 1.3 \times 10^{18} cm^{-3}$. Under these conditions, the peak attenuation is $\alpha(\nu_0) = 7.6 \times 10^{-3}$ dB/km for the line centered at $\nu_0 = 101.7$ GHz (Table 6).

Table 6. Carbon monoxide (CO) and selected Ozone (O_3)
line parameters (Waters, 1976; Rothman et al., 1981)

Carbon monoxide (CO):

ν_0	c_1	c_2	c_3
GHz	$(\frac{kHz \ cm^3}{molec.})10^{-18}$		$\frac{GHz}{kPa}$
115.27120	2.09	0	0.023
230.53797	7.92	0.018	0.023

Ozone ($^{16}O_3$):

ν_0	d_1	d_2	d_3
67.35624	2.36	0.074	0.032
96.22834	3.19	0.012	0.032
101.73687	5.74	0.040	0.032
103.87839	1.93	0.542	0.032
109.55933	2.28	0.902	0.032
110.83604	8.22	0.084	0.032
124.08746	10.6	0.144	0.032
125.38958	6.16	0.124	0.032
142.17512	12.7	0.124	0.032
164.95182	4.41	0.012	0.032
165.78445	14.4	0.311	0.032
184.37831	11.5	0.191	0.032
195.43051	15.6	0.418	0.032
208.64244	8.26	0.040	0.032
231.28125	16.2	0.540	0.032
235.70964	22.9	0.578	0.032
237.14600	21.9	0.449	0.032
239.43195	23.0	0.720	0.032
242.31860	20.2	0.338	0.032
243.45370	18.2	0.272	0.032
248.18332	22.5	0.880	0.032
249.78846	13.0	0.084	0.032
249.96190	17.8	0.243	0.032
258.71610	14.7	0.164	0.032
263.69236	21.3	1.055	0.032
267.26694	11.3	0.102	0.032
273.05063	16.2	0.677	0.032
286.08720	11.1	0.675	0.032
286.15650	19.8	1.246	0.032
288.95895	18.5	0.144	0.032
293.17125	9.09	0.074	0.032
301.801	25.5	0.370	0.032

In principle, line tables for trace gases could be included in the MPM; in practice, it turns out that these lines are relatively weak, that their main importance lies more in remote sensing applications of abundances and, most important, that their assessment requires considerable computing time. For these reasons, so far, we have omitted trace gas spectra from the MPM.

4. MODELING STRATEGY

The MPM systematizes radio path parameter calculations (see Section 1.1) in two computer routines P1 and P2. Routine P1 constitutes the main model, while the auxiliary routine P2 is activated only if line details over the height range h = 30 to 100 km are required. This simplifies the handling of the large number of spectroscopic quantities and computational steps involved. The computations are performed in a user-friendly, interactive mode designed to minimize possibilities for error. An operator needs to specify a frequency range $f_1 (\geq 1$ GHz) to $f_2 (\leq 1000$ GHz) and the following.

> <u>Horizontal</u> path: height level h, model atmosphere or set of appropriate
> p,T-values, relative humidity RH, hydrosol concentration w,
> rainfall rate R, and path length L.
>
> <u>Slant</u> path: initial height level h_o, elevation angle ψ, relative
> humidity RH at h_o, final height h_f, and model atmosphere.
> For an earth-space path h_f = 30 km, unless routine P2 is
> called to include oxygen line details ($\nu_o \pm$ 50 MHz) up to
> h_f = 100 km.

Routine P1 generates a frequency grid with a resolution tied to the line center frequencies that fall within the desired range. Two consecutive values, ν_o and ν_o', are taken and the number of points between them is specified (usually 2 to 5). Also automatically added to the grid are the half-power points at $\nu_o \pm \gamma$. Thus, it is assured that attenuation maxima and dispersion peaks will be plotted. The program feeds one frequency at a time into the subroutine and receives values of α and β, which are stored temporarily in two files. When all numbers of the grid have been handled, a numerical integration is performed layer-by-layer over the height range of the desired radio path and the output is presented in a numerical printout and processed by a graphics routine. In the troposphere (h < 10 km), only absorption by H_2O (vapor and liquid) and O_2 is important. Above h = 5 km, spectral lines of

29

weak trace gas abundances (O_3, CO, N_2O, etc.) become detectable over narrow ($\nu_0 \pm 0.2$ GHz) frequency ranges (Waters, 1976; Poynter and Pickett, 1981), but they are not included in the MPM, in keeping with the goal of modeling simplicity. Also, computational economy cannot be overlooked, since each specific value of α and β requires the summation of up to 82 contributions (8) at one frequency and the height integration typically is carried out over as many as 56 layers.

4.1 Spectroscopic Data File and Synthetic Atmospheres

The system of attenuation/dispersion routines consists of four FORTRAN 4 programs and 11 permanent data files. Of these data files, No. 1 is the permanent spectroscopic line data file LNDAT which contains line center frequencies and other spectroscopic parameters (strength, width, interference) for each of 48 O_2 lines and 30 H_2O lines in air (Tables 1 and 2). Files No. 2 to 11 are synthetic atmosphere data bases that list height, pressure, temperature, and maximum relative humidity data for 45 discrete height levels (Valley, 1965); they are called by the following names:

> STDATM 1 - U. S. Standard Atmosphere 1976,
> STDATM 2 - Tropical 15 degrees north,
> STDATM 3 - Subtropical 30 degrees north, July,
> STDATM 4 - Subtropical 30 degrees north, January,
> STDATM 5 - Midlatitude 45 degrees north, July,
> STDATM 6 - Midlatitude 45 degrees north, January,
> STDATM 7 - Subarctic 60 degrees north, July,
> STDATM 8 - Subarctic 60 degrees north, January,
> STDATM 9 - Arctic 75 degrees north, July,
> STDATM 0 - Arctic 75 degrees north, January.

The permanent line data file and a model atmosphere are assigned to each job as two local file tapes (TAPE6,7).

4.2 P1: Lower Atmosphere Program (0 to 30 km)

There are three FORTRAN 4 programs that make up the attenuation/delay system for this height range. The file names are as follows:

SETPLT - interactive run set-up program;
ATNPLT - computation program according to the physical model
for N, including the revisions discussed in Section 2;
ATNOUT - output routine producing listings, plots, and
numerical integration for cumulative calculations
through the array of discrete height levels.

A control language procedure file DERP is used to properly set up a job.

The three programs communicate with each other through several local files. Local files TAPE1 to TAPE10 are reserved for these programs. The first program is interactive and requests from the user the frequency range, climatological data, plot sizes, and several output options. It then writes the input information to local file TAPE1, the line data base used for calculations is assigned to TAPE2, and if a plot is requested, the plot parameters are stored in TAPE5.

The second program, in generating the attenuation/delay data, performs the majority of all calculations. This program sets up a grid of frequency (x-axis) values consisting of any combination of line center frequencies, half-power points, and even increment values. Then, if a plot is desired, the program automatically adds additional resolution points to the frequency grid so that a smooth curve is obtained. On cumulative path calculations, no half-power and additional resolution points are added because this mode requires considerably more computational effort. In this case, the grid increment has to be chosen for the desired frequency range as a compromise between cost and needed resolution. The elements of the frequency grid are then passed step-by-step through the propagation model, and two arrays with attenuation-vs.-frequency and delay-vs.-frequency data for each set of climatological data are completed, each constituting a "curve." The points are written to binary local files TAPE3 and TAPE4, curve by curve.

The third program handles output. Based on user specifications, a listing and a plot (if desired) are produced. The listing is sent to local file TAPE10, and the plots are made using the DISSPLA plotting routine in conjunction with the FR-80 microfilm plotter. If a horizontal path mode was specified, the output program prints a heading that consists of climatological data and N_0. Multiple curves are combined in the same plot frame. If a cumulative (zenith) path was specified, the output prints a table of climatological data used at each height level. Attenuation and delay data for these levels are summed to approximate integration over height.

31

For each frequency, attenuation and delay values on two consecutive height levels are averaged, then multiplied by the height difference (layer thickness within model atmosphere). Zenith attenuation (dB) and delay (s) are accumulated at each frequency as the program moves from the specified initial to the final height level. Large frequency ranges and small frequency grid elements should be avoided to keep expenses under control.

Details for user-specified parameters are discussed below.

1. RUN TYPE -- a code number 1 to 6 specifies the following outputs:

CODE	PLOT	EVEN GRID	LINE CENTERS
1	no	no	yes
2	no	yes	no
3	no	yes	yes
4	yes	no	yes
5	yes	yes	no
6	yes	yes	yes

A repeat run may be done by specifying a negative run type code. For example, run code 3 is specified, then the user decides he would like a plot of the same data. By rerunning the system and specifying a code (-4), a plot is produced using identical climatological data but without even grid frequencies. This is cheaper and produces a neater output than specifying code 6, since the listing does not contain the resolution points used in plotting.

2. FREQUENCY RANGE -- beginning and ending frequency are specified. For calculations from 30 to 300 GHz, the proper response is "30., 300.".

3. EVEN GRID -- this number is the increment for an even frequency grid. For 2 GHz steps, the response is: "2."

4. WATER VAPOR CONTINUUM ABSORPTION -- is modeled by the expression

$$N''_e = (b_f e p f^x \theta^y + b_s e^2 f^{x'} \theta^{y'}) 10^{-6} \quad ppm$$

Coefficients $b_{f,s}$ and exponents x,y can be specified, or the default values (new continuum model, Eq. 24)

32

$$b_f = 1.40 \quad , \quad x = 1 \quad , \quad y = 2.5 \quad ,$$
$$b_s = 54.1 \quad , \quad x' = 1 \quad , \quad y' = 3.5$$

are used automatically.

5. LINE STRENGTH CUT-OFF -- in order to reduce computer run time, a cut-off value can be applied to the resonance line strength factors. All lines in the permanent file are checked, and those falling below the specified cut-off are disregarded in attenuation/delay calculations.

6. PATH MODE -- horizontal or zenith paths may be selected. In the horizontal path mode, discrete height h, pressure p, temperature T, relative humidity RH, and droplet concentration w or rain rate R for each curve are entered. Combinations of $h(p,T)$ can be also drawn from the 10 atmospheric local files.

In the slant path mode, a model atmosphere and elevation angle ψ are specified, together with a height range between 0 and 30 km and a relative humidity at h_0. A cloud height range may be defined when 100 percent relative humidity conditions exist, where the mean droplet concentration w is entered. For example, "2., 4., .1" establishes a cloud between 2 and 4 km with a droplet concentration of $w = 0.1$ g/m^3. Zenith path behavior is calculated when $\psi = 90°$.

7. PLOT PARAMETERS -- if a plot has been requested, the program asks for plot axis length and labeling inputs.

8. ERROR CORRECTION -- at this point, if any errors in entry have been made, or if the user changes his mind, any input parameter may be changed. A final reply "NO" to the option of initiating changes executes the program and produces the requested output in microfilm plots and/or printed listings on local file TAPE10.

4.3 P2: Isolated Lines in the Upper Atmosphere (30 to 100 km)

The routine P2 calculates the response of isolated lines over the height range h = 30 to 100 km as formulated in Section 3.1. The routine takes into account the complicated Zeeman effect of the O_2 microwave lines. Formally, each oxygen splits proportionally with the geomagnetic field strength H into numerous sub-lines, which superimpose to three main Zeeman patterns $\alpha_{1,2,3}$ spread over a megahertz frequency

33

scale (see Appendix A). Routine P2 stops at this point and additional information has to be provided before a mesospheric O_2 line pattern α_z can be calculated.

The propagation medium is anisotropic in close vicinity of O_2 spectral lines. Transformation formulae which reduce the three Zeeman components $\alpha_{1,2,3}$ into an observable attenuation rate α_z with respect to given coordinates for the geomagnetic field vector and the propagating radio wave (or receiving antenna) have been given by Hartmann and Künzi (1983). Here, only the simpler case of angle dependence between wave plane and geomagnetic field direction is discussed. For linearly polarized radiation, an angle of orientation ϕ is defined between the wave's magnetic field component in a plane of constant phase (i.e., perpendicular to the direction of propagation) and the geomagnetic field direction H. For circularly polarized radiation, the angle ϕ is defined between the plane of constant phase and H. A mesospheric O_2 line α_z then generally consists of a mixture of the three Zeeman patterns:

Wave polarization	Zeeman line α_z =
linear	$\alpha_1 \cos^2\phi + (\alpha_2 + \alpha_3) \sin^2\phi$
circular, right-handed	$2\alpha_2 \sin^2\phi + 0.5(\alpha_1 + \alpha_2 + \alpha_3)\cos^2\phi$ $\quad$ (38)
circular, left-handed	$2\alpha_3 \sin^2\phi + 0.5(\alpha_1 + \alpha_2 + \alpha_3)\cos^2\phi$.

These equations assure that in all cases the sum of the Zeeman components equals the integrated absorption strength of the unsplit (H = 0) line.

5. RESULTS

The quest for a model that accurately describes the mean of millimeter wave properties of the atmosphere in terms of measurable primary parameters has been a goal of the ITS millimeter wave program. The current status of an MPM (ITS version) has been described in the preceding sections. The model provides a capability to forecast atmospheric transmission effects on communications and sensor systems. The influence of the atmosphere was structured in four categories; namely, dry air (p,v), humidity (v,RH), hydrosol (w), and rain (R) for the lower part, h = 0 to 30 km, and dry air (p,θ) and magnetic field strength (H) for the upper part, h = 30 to 100 km. In this section, graphical and numerical results are presented in the form of predictions over a frequency range from 10 to 300 GHz by assuming typical

34

climatic conditions. Part of the results can be validated by comparison with data from field and laboratory measurements, of which there are presently but a few above 100 GHz; another part (i.e., the opaque medium, A > 40 dB), will always rest on the underlying theory. As more data become available, further revisions and extensions of the MPM's data base will have to be considered.

5.1 Horizontal Radio Paths

A homogeneous absorber population characterizes a horizontal radio path. One set of p-θ-v + w + R combinations is used to predict the specific rates of α and β. The dispersive delay $\beta(f)$ is presented in three units of measure (see Equation 3): $\beta(f)$ in radians/km, $\beta^*(f)$ in ns/km, or $D(f)$ in ppm. A typical output is illustrated in Figure 5. Dry and moderately humid air (curves 1,2) under sea level conditions allow four millimeter wave window ranges W1 to W4. Transmission through these windows is reduced by high humidity, fog, and light rain (curves 3 to 5), and is seriously impeded by steady rain and thundershowers (curves 6,7). The delay spectrum β^* from gaseous resonance contributions displays frequency gradients around the line centers v_0 that can distort broadband signal transmission (e.g., ns-pulses). Details around the 22 GHz water vapor line are enhanced in Figure 6. This relatively weak line imposes no serious effects upon signal transmissions. As demonstrated in Figure 7, the influence of water vapor becomes important above 70 GHz and, with increasing frequency, actually dominates more and more the milli- meter wave properties of clear air.

The frequency range 45 to 75 GHz is dominated by oxygen absorption, as evident from Figure 8. The change in attenuation from h = 0 to 6 km is small. The lines are merged into a more or less unstructured band with a pressure-proportional atten- uation maximum. Above h = 10 km, however, one can see a significant difference--the unstructured 60 GHz band shape transforms into a highly-structured isolated line response with distinct peaks and valleys. The lines narrow with increasing altitude, deepening the valleys while the line peaks stay approximately constant. This behavior is detailed in Appendix A.

Tracing the line peaks to zero intensity over the range h = 30 to 100 km intro- duces complications of Zeeman splitting by the geomagnetic field H, which has been treated with program P2. Model calculations for O_2 lines labeled $K^\pm$ = 1 to 29 (see Table 1) are displayed in Appendix A assuming two geomagnetic field strengths, H = 0.3 and 0.6 Gauss. Numerical values for peak attenuations of the $\alpha_1(\pi)$-patterns are listed in Table 7. A comparison between programs P1 and P2 at h = 30 km for the unsplit line (H = 0) peak reveals the validity of switching at that point to a
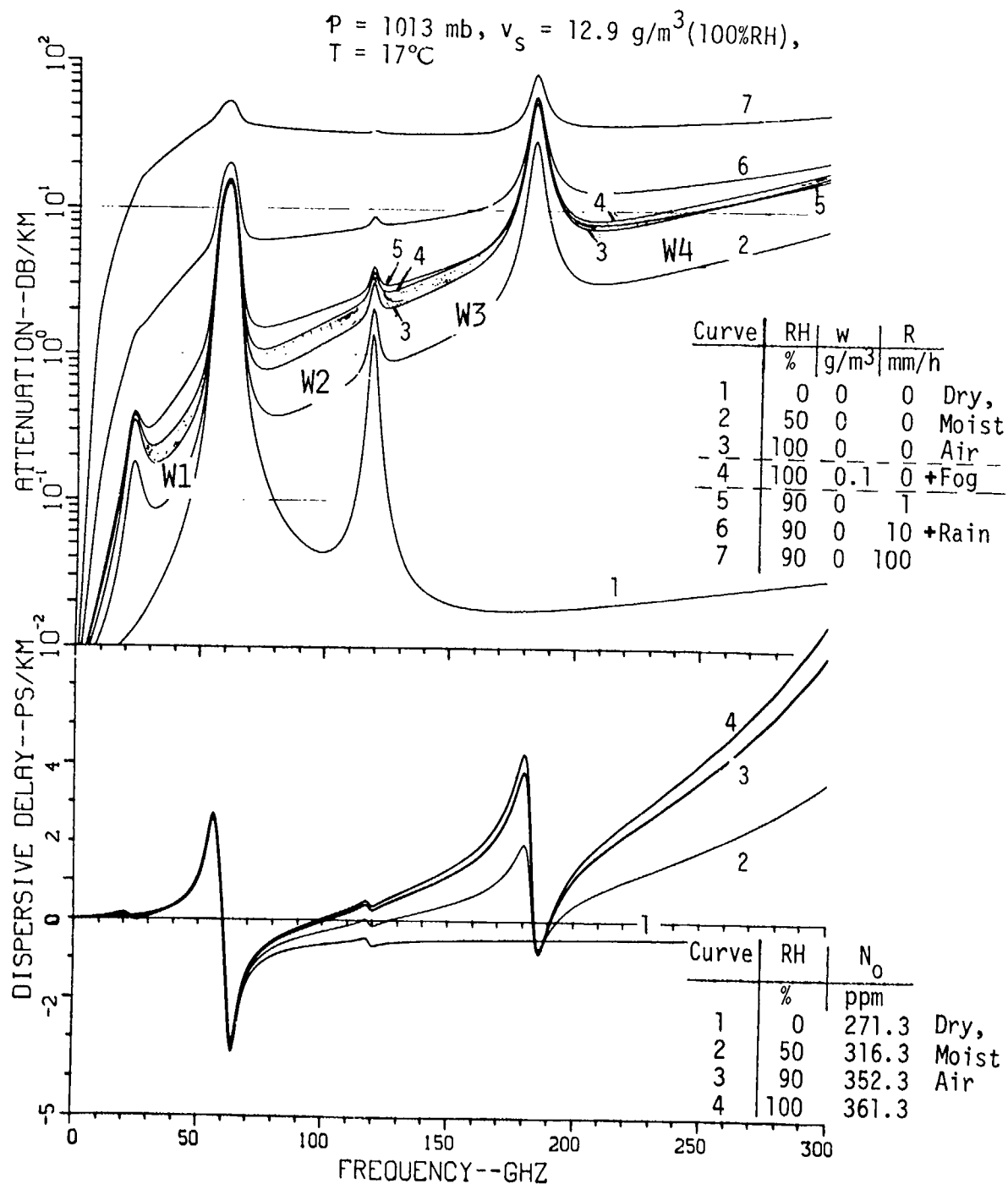
35

Figure 5. Specific attenuation α (dB/km) and dispersive delay β^*(ps/km) for humid air at sea level (RH = 0 to 100%). Also shown is fog attenuation for a liquid water concentration w = 0.1 g/m^3 (about 300 m visibility) and rain attenuation for the rates R = 1, 10, and 100 mm/h.
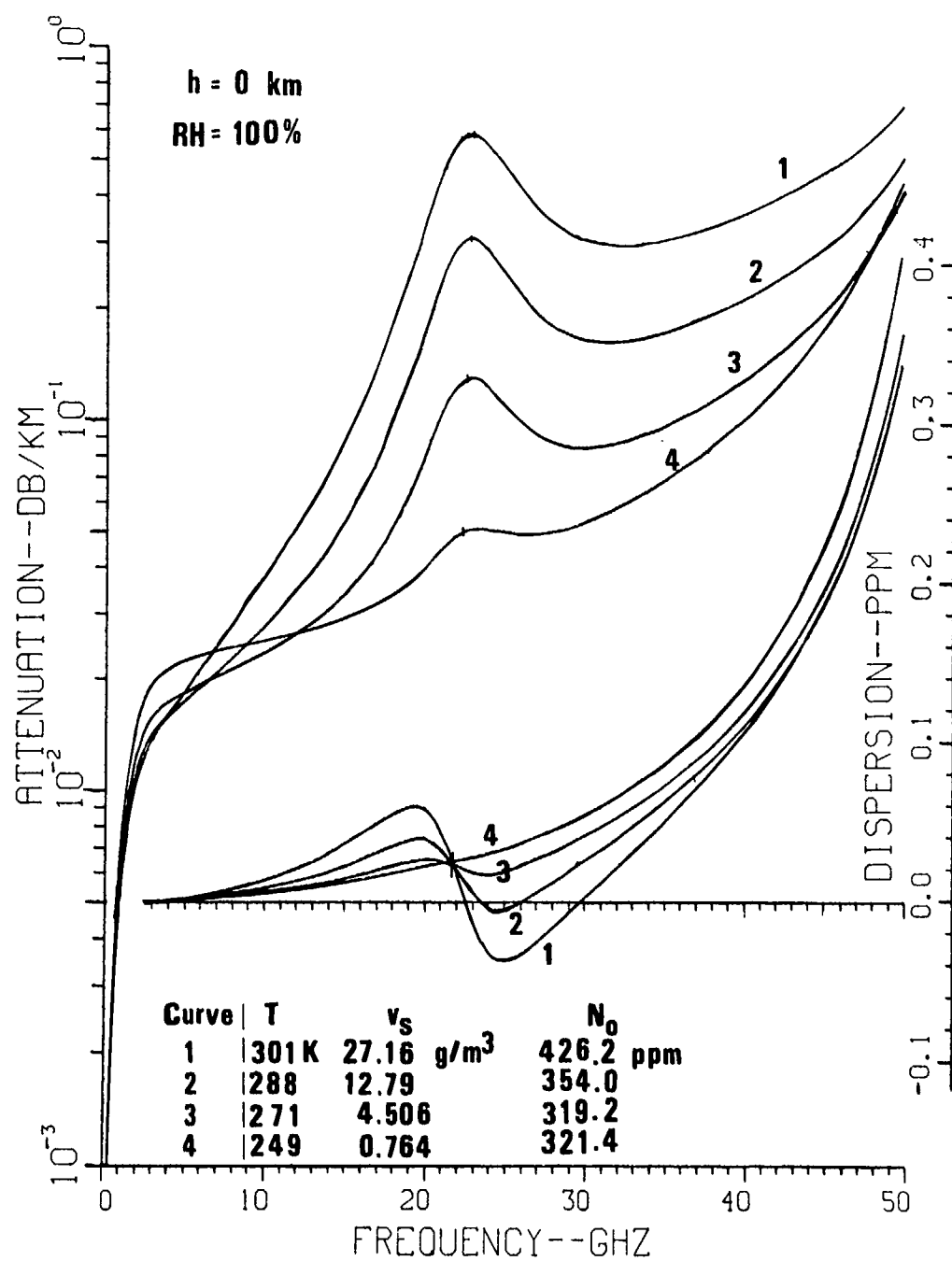
36

Figure 6. Specific attenuation α and refractive dispersion D over a frequency range from 0.5 to 50 GHz for saturated (RH = 100%) sea level air (p = 101.3 kPa) at four temperatures.
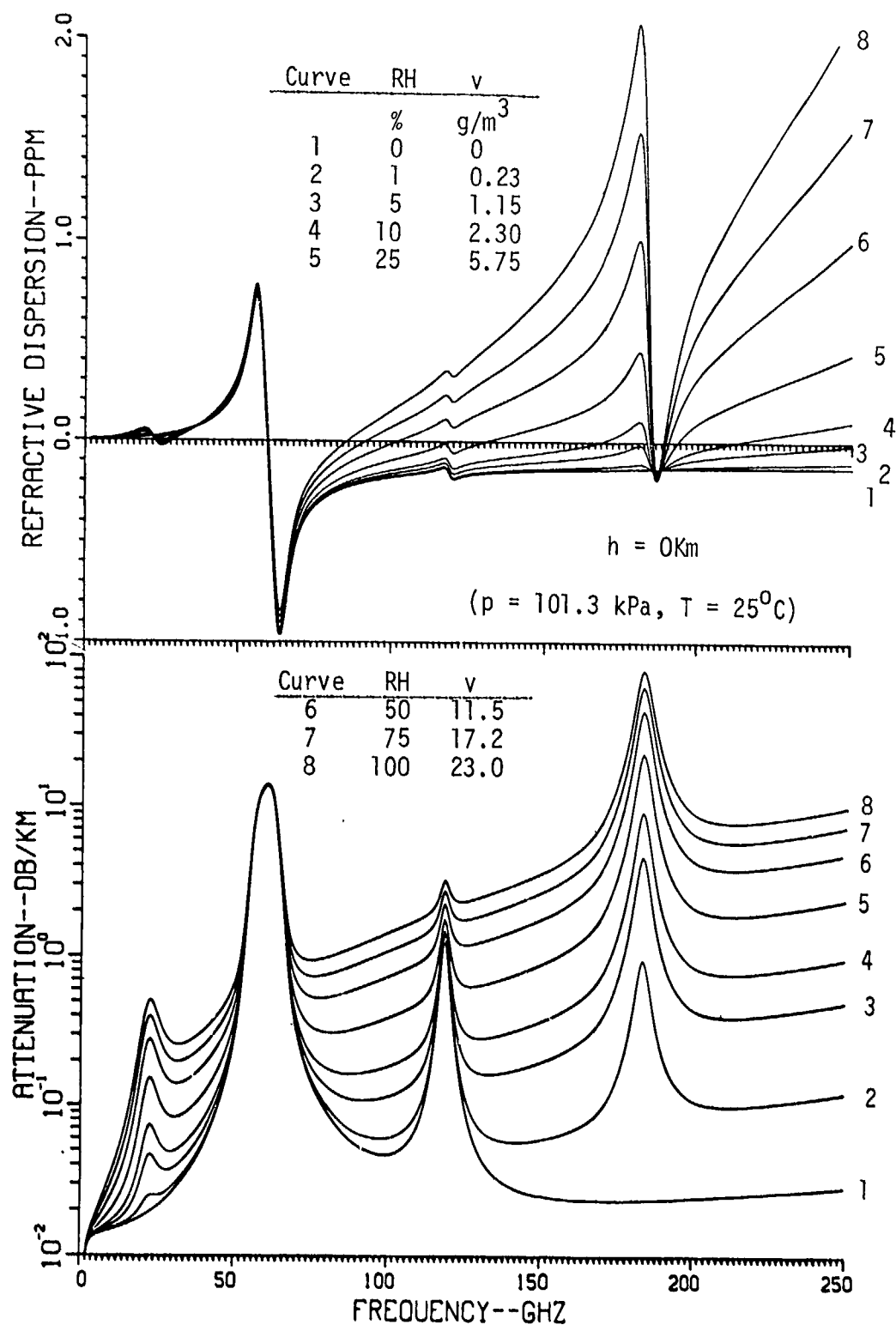
37

Figure 7. Refractive dispersion D and specific attenuation α over a frequency range from 1 to 250 GHz for sea level air at various relative humidities (RH = 0 to 100%).
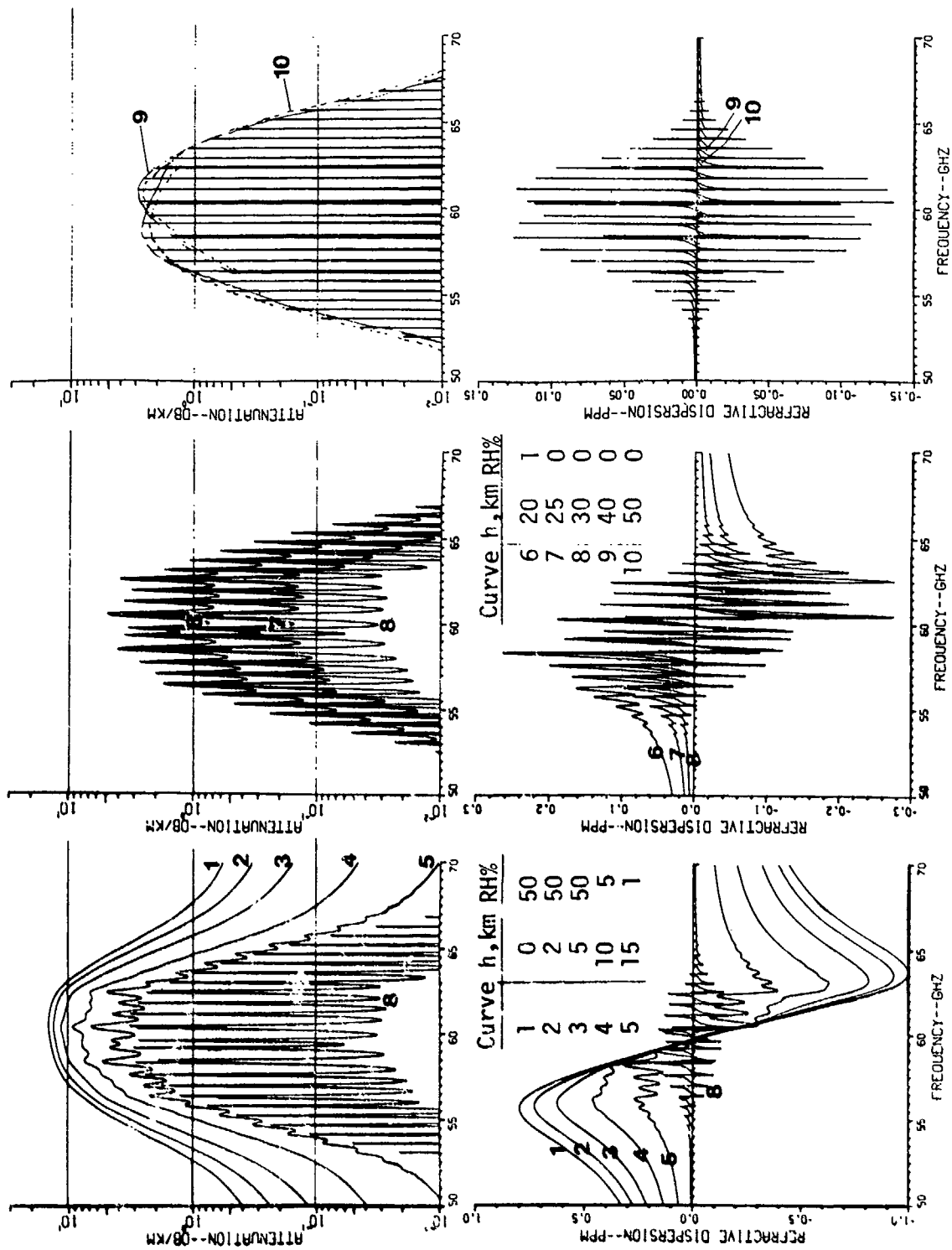
Figure 8. Specific attenuation α and refractive dispersion D of moist air (U.S. Std. Atm. 76) over a frequency range from 50 to 70 GHz (dominated by oxygen line absorption) at various heights between h = 0 and 50 km calculated with Program P1 (for details see Appendix A).

39

Table 7. Peak attenuation calculated for the Zeeman π patterns of $K^{\pm} = 1$ to 29 with Program P2 for magnetic field strengths $H = 0$, 0.3, and 0.6 G assuming a U.S. Standard Atmosphere (NOAA, 1976).

a) Specific attenuation $\alpha_1(\nu_o)$ for h = 30 (see also P1 for comparison), 40, 50, ... 100 km (see Appendix A).

b) Zenith attenuation $A_z^1(\nu_o)$ for h = 30 to 100 km.

a)

U.S. Std. Atm. 76	h p T	km Pa K	30 1197.0 226.5			40 287.1 250.4			50 79.78 270.7		
	H	Gauss	0	0.3	0.6	0	0.3	0.6	0	0.3	0.6
Line K±						$\alpha_1(\nu_o)$, dB/km					
29-			.008	.008	.008	.008	.014	.014	.013	.020	.017	.013
27-			.021	.021	.021	.021	.033	.033	.031	.045	.038	.029
25-			.051	.051	.051	.051	.073	.072	.069	.092	.079	.061
23-			.115	.115	.115	.114	.150	.148	.143	.179	.154	.120
21-			.238	.236	.236	.236	.287	.283	.274	.323	.280	.219
19-			.453	.451	.450	.450	.508	.502	.487	.545	.475	.374
17-			.791	.787	.786	.785	.833	.824	.799	.853	.747	.592
15-			1.306	1.262	1.262	1.260	1.261	1.247	1.211	1.240	1.091	.869
13-			1.853	1.847	1.846	1.843	1.753	1.736	1.688	1.664	1.471	1.179
11-			2.459	2.451	2.450	2.446	2.228	2.206	2.148	2.049	1.820	1.466
9-			2.994	2.930	2.928	2.925	2.568	2.544	2.480	2.302	2.054	1.663
7-			3.116	3.112	3.111	3.107	2.644	2.621	2.557	2.319	2.072	1.691
5-			2.911	2.826	2.824	2.821	2.350	2.331	2.276	2.030	1.825	1.491
3-			2.177	2.051	2.050	2.047	1.679	1.666	1.629	1.435	1.295	1.062
1-			2.288	2.287	2.287	2.287	1.854	1.854	1.854	1.568	1.568	1.568
1+			.652	.610	.610	.610	.495	.495	.495	.420	.420	.420
3+			1.946	1.866	1.866	1.865	1.528	1.522	1.513	1.305	1.261	1.157
5+			2.837	2.821	2.821	2.819	2.347	2.337	2.309	2.027	1.916	1.686
7+			3.381	3.299	3.298	3.295	2.807	2.792	2.750	2.464	2.296	1.974
9+			3.281	3.270	3.269	3.266	2.866	2.848	2.798	2.568	2.369	2.005
11+			2.865	2.855	2.854	2.851	2.595	2.577	2.526	2.386	2.182	1.825
13+			2.417	2.235	2.234	2.232	2.122	2.106	2.061	2.013	1.827	1.509
15+			1.590	1.584	1.583	1.581	1.581	1.568	1.532	1.555	1.402	1.150
17+			1.029	1.023	1.023	1.022	1.083	1.073	1.047	1.109	.993	.803
19+			.610	.608	.608	.607	.685	.679	.661	.735	.654	.528
21+			.332	.331	.330	.330	.401	.397	.386	.452	.399	.320
23+			.167	.166	.166	.166	.218	.214	.209	.258	.228	.181
25+			.077	.077	.077	.077	.109	.108	.105	.139	.121	.096
27+			.033	.033	.033	.033	.051	.051	.049	.069	.060	.047
29+			.013	.013	.013	.013	.023	.022	.021	.033	.028	.022

Full Line Spectrum ——— Single Line Treatment ——————➤

P1   **P2**

U.S. Std. Atm. 76	h	km	60			70			80		
	p	Pa	21.96			5.221			1.052		
	T	K	247.0			219.6			198.6		
	H	Gauss	0.3	0.6	0	0.3	0.6	0	0.3	0.6	
Line K:						$\alpha_1(\nu_0)$, dB/km					
29-			.013	.006	.004	.005	.001	.001	.001	.000	.000
27-			.031	.015	.009	.015	.003	.002	.004	.000	.000
25-			.068	.034	.020	.037	.008	.004	.009	.001	.001
23-			.142	.072	.043	.085	.018	.009	.023	.003	.002
21-			.275	.141	.085	.180	.039	.020	.054	.007	.004
19-			.492	.256	.154	.354	.076	.040	.116	.015	.008
17-			.813	.429	.260	.635	.138	.074	.225	.029	.017
15-			1.241	.663	.404	1.046	.230	.125	.401	.053	.031
13-			1.738	.994	.576	1.565	.349	.192	.644	.086	.052
11-			2.222	1.223	.750	2.121	.481	.270	.929	.126	.082
9-			2.576	1.436	.884	2.584	.595	.348	1.197	.169	.120
7-			2.665	1.504	.930	2.794	.659	.416	1.362	.203	.164
5-			2.377	1.355	.845	2.573	.643	.464	1.307	.239	.209
3-			1.703	.982	.656	1.889	.587	.513	.992	.270	.259
1-			1.835	1.835	1.835	1.717	1.717	1.717	.674	.674	.674
1+			.505	.505	.505	.591	.591	.591	.359	.359	.359
3+			1.551	1.190	.872	1.741	.671	.445	.945	.241	.197
5+			2.373	1.635	1.089	2.566	.813	.496	1.300	.258	.190
7+			2.825	1.836	1.193	2.929	.850	.491	1.394	.247	.166
9+			2.869	1.793	1.146	2.832	.781	.437	1.265	.213	.132
11+			2.581	1.565	.990	2.409	.641	.353	1.006	.165	.097
13+			2.096	1.239	.777	1.385	.475	.259	.713	.116	.065
15+			1.550	.897	.558	1.262	.318	.173	.453	.073	.040
17+			1.052	.596	.369	.789	.195	.106	.260	.042	.023
19+			.659	.367	.225	.403	.102	.055	.136	.022	.012
21+			.381	.208	.127	.237	.057	.031	.064	.010	.006
23+			.205	.110	.067	.114	.027	.015	.028	.005	.002
25+			.102	.054	.033	.051	.012	.006	.011	.002	.001
27+			.047	.024	.015	.021	.005	.003	.005	.001	.000
29+			.020	.010	.006	.008	.002	.001	.002	.000	.000

U.S. Std. Atm. 76	h	km	90			100			30 to 100		
	p	Pa	0.184			0.032					
	T	K	187.2			199.0					
	H	Gauss	0.3	0.6	0	0.3	0.6	0	0.3	0.6	
Line K:					$\alpha_1(\nu_0)$,		dB/km			$A_1(\nu_0)$, dB	
29-			.000	.000	.000	.000	.0000	.0000	.61	.46	.38
27-			.001	.000	.000	.000	.0000	.0000	1.50	1.10	.91
25-			.002	.00	.000	.001	.0000	.0000	3.25	2.45	2.06
23-			.005	.001	.000	.001	.0001	.0000	7.10	5.09	4.31
21-			.009	.001	.001	.002	.0002	.0001	13.7	9.85	8.39
19-			.021	.003	.001	.004	.0005	.0003	24.8	17.8	15.1
17-			.042	.005	.003	.007	.0009	.0005	42.0	29.6	25.3
15-			.078	.010	.006	.013	.0016	.0010	65.9	45.6	39.1
13-			.130	.016	.010	.021	.0026	.0016	93.7	64.5	55.4
11-			.195	.025	.017	.030	.0039	.0026	122.3	83.3	71.8
9-			.258	.034	.025	.039	.0052	.0039	145.2	97.7	84.5
7-			.302	.044	.036	.044	.0065	.0052	152.5	102.3	89.1
5-			.295	.052	.047	.043	.0076	.0067	138.9	92.8	81.6
3-			.227	.061	.059	.032	.0087	.0084	101.3	69.2	62.3
1-			.148	.148	.148	.021	.021	.021	101.1	101.1	101.1
1+			.086	.036	.036	.012	.012	.012	31.2	31.2	31.2
3+			.218	.053	.045	.031	.0076	.0064	92.6	68.1	61.0
5+			.293	.055	.042	.042	.0080	.0061	137.8	98.4	86.4
7+			.307	.051	.035	.045	.0076	.0052	161.5	113.8	99.1
9+			.271	.043	.027	.041	.0065	.0041	159.9	113.2	98.3
11+			.209	.032	.019	.032	.0051	.0030	140.8	100.2	86.9
13+			.143	.022	.012	.023	.0035	.0020	109.1	80.2	69.2
15+			.087	.013	.007	.014	.0022	.0012	80.9	59.1	50.4
17+			.048	.007	.004	.008	.0013	.0007	53.8	39.3	33.7
19+			.024	.004	.002	.004	.0007	.0004	32.6	23.3	20.9
21+			.011	.002	.001	.002	.0003	.0002	18.8	14.0	12.0
23+			.005	.001	.000	.001	.0001	.0001	9.90	7.50	6.4
25+			.002	.000	.000	.001	.0001	.0000	4.89	3.73	3.18
27+			.001	.000	.000	.000	.0000	.0000	2.21	1.73	1.47
29+			.000	.000	.000	.000	.0000	.0000	.97	.74	.63

the unsplit line (H = 0) peak reveals the validity of switching at that point to a single-line treatment. The error is less than -6 percent for the four doublets and less than -1 percent for lines.

Line intensities are sensitive to temperature variations at various rates. Useful approximations at a fixed frequency are the power laws

$$\alpha(T) = \alpha(300K)\theta^y \qquad \text{and} \qquad \beta(T) = \beta(300K)\theta^{y'} \quad . \tag{39}$$

For sea level air, we obtain

f,GHz	50	55	60	65	70	119	120
y	2.49	1.30	2.35	1.20	2.72	2.13	2.70
y'	1.84	1.98	3.30	1.87	1.88	1.96	1.98

5.2 Zenith Path Behavior

Cumulative transfer characteristics of the neutral atmosphere are evaluated by a numerical integration of (9) and (10). For a zenith path, the increments dx are equal to dh, and dh is chosen so that each slab is quasi-homogeneous (p,T,v,w and R are constant). The formalism developed in Sections 2 to 4 is applied to calculate $\alpha(dh)$ and $\beta(dh)$. Height profiles of the meteorological quantities are obtained from model atmospheres. A standard example is the one-way zenith response through the U. S. Standard Atmosphere (NOAA, 1976). The calculation is performed with P1 "layer-by-layer," encompassing 48 slabs between h = 0 and 30 km. Examples for zenith attenuation and delay are presented in Figures 9 to 11. One notices that outside the O_2 absorption frequency ranges (50 to 70 GHz and 115 to 123 GHz), water vapor content V (15) and cloud water content W (16) play a dominant role. The refractive delay of the air mass (14) is $\beta_0^* = 7.62 + 0.09 + 0.21$ V ns, where the 0.09 ns term is the contribution from the height range 30 to 100 km. Selected attenuation values A_z are collected in Table 8.

One can attempt to predict zenith path attenuation A_z from the specific attenuation rate $\alpha_0(h_0)$ by reducing the inhomogeneous atmosphere to an equivalent homogeneous "thickness"

$$h_s = A_z/\alpha_0 \quad \text{km} \quad . \tag{40}$$
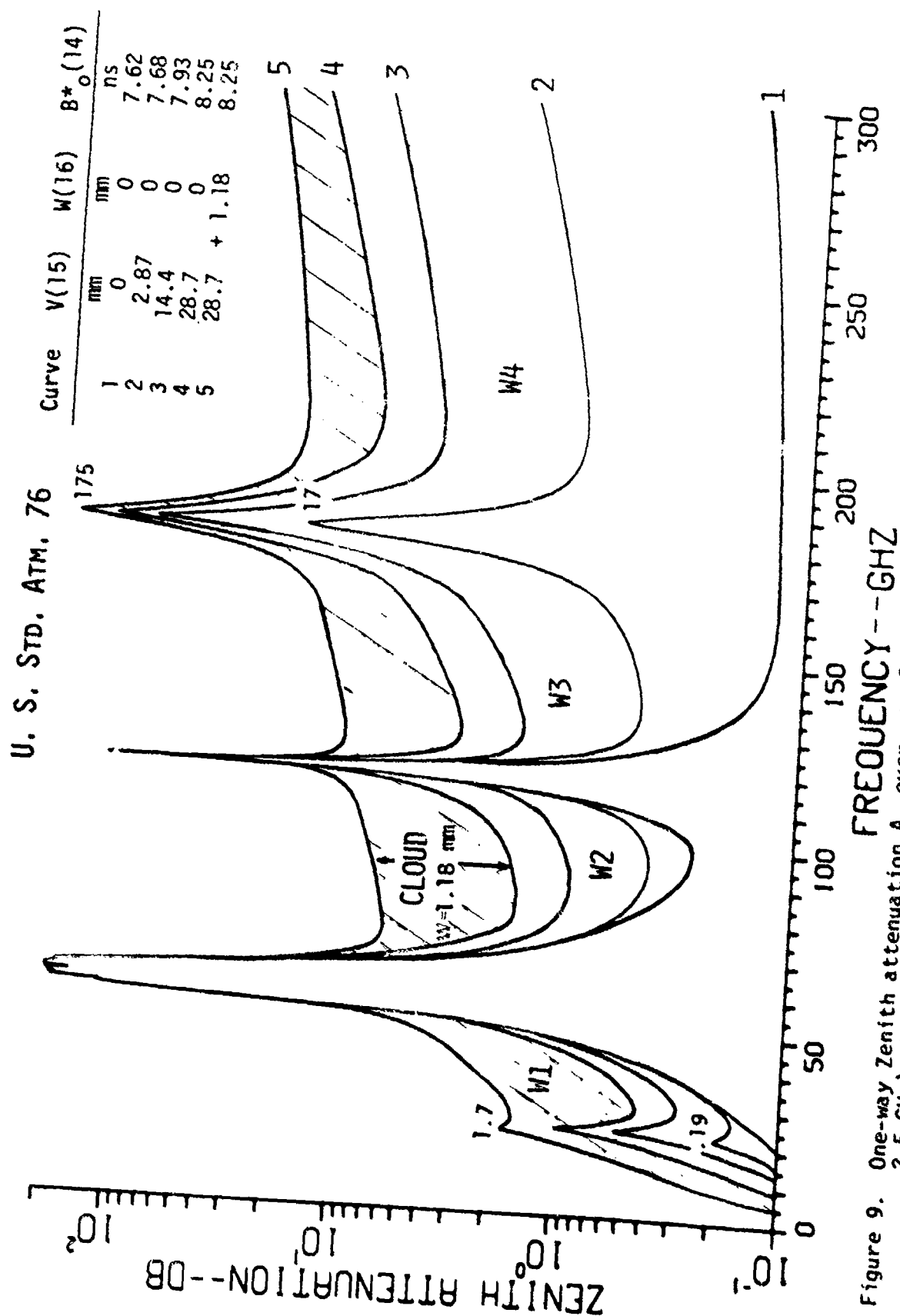
Figure 9. One-way Zenith attenuation A over a frequency range from 5 to 300 GHz (resolution 2.5 GHz) through the U.S. Standard Atmosphere (NOAA, 1976) assuming dry and moist air masses including a rain-bearing cloud calculated with Program Pl. The symbols W1 to W4 indicate the millimeter wave window ranges.
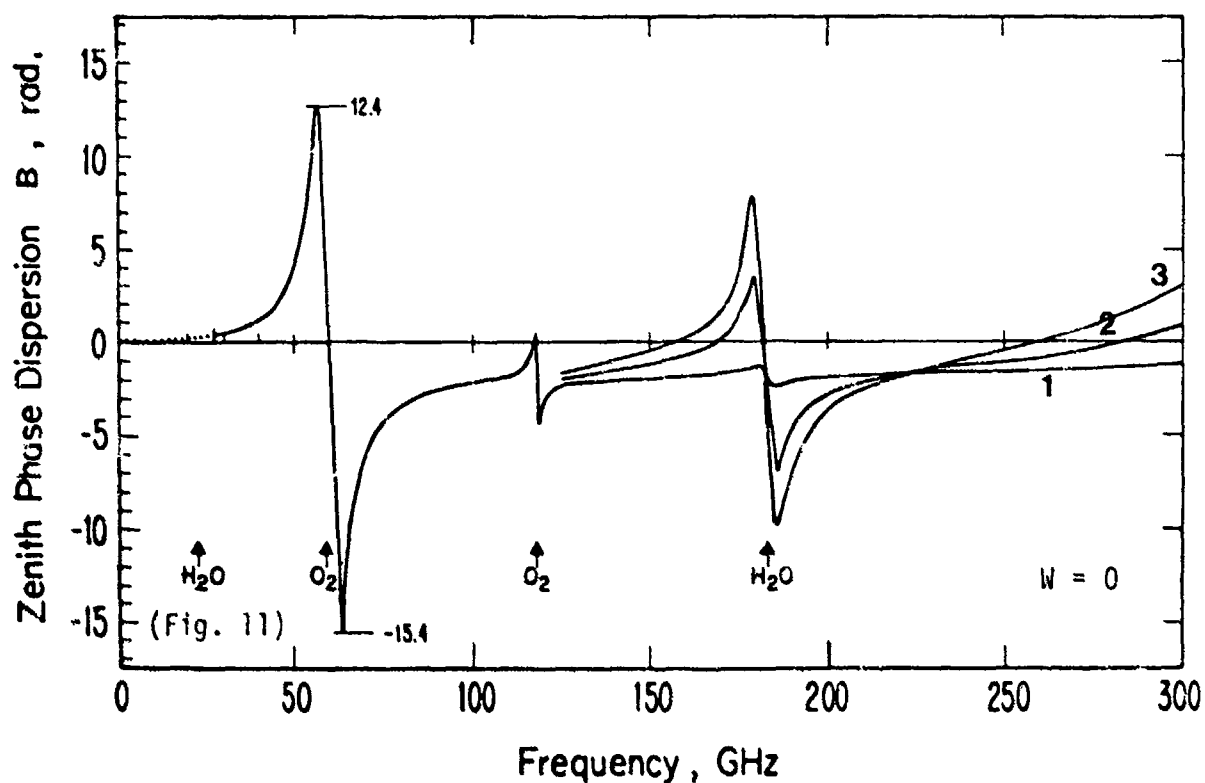
Curve	V	B_0^*
	mm	ns
1	1.53	7.67
2	15.3	7.98
3	30.5	8.27

$\left.\begin{array}{c}\end{array}\right\}$ + 0.09 ns for h = 30 to 100(∞) km

Figure 10. One-way zenith phase dispersion B_z over a frequency range from 1 to 300 GHz for three values of water vapor content V (15) over the height range h = 0 to 30 km (P1) assuming a cloud-free U. S. Standard Atmosphere.

44
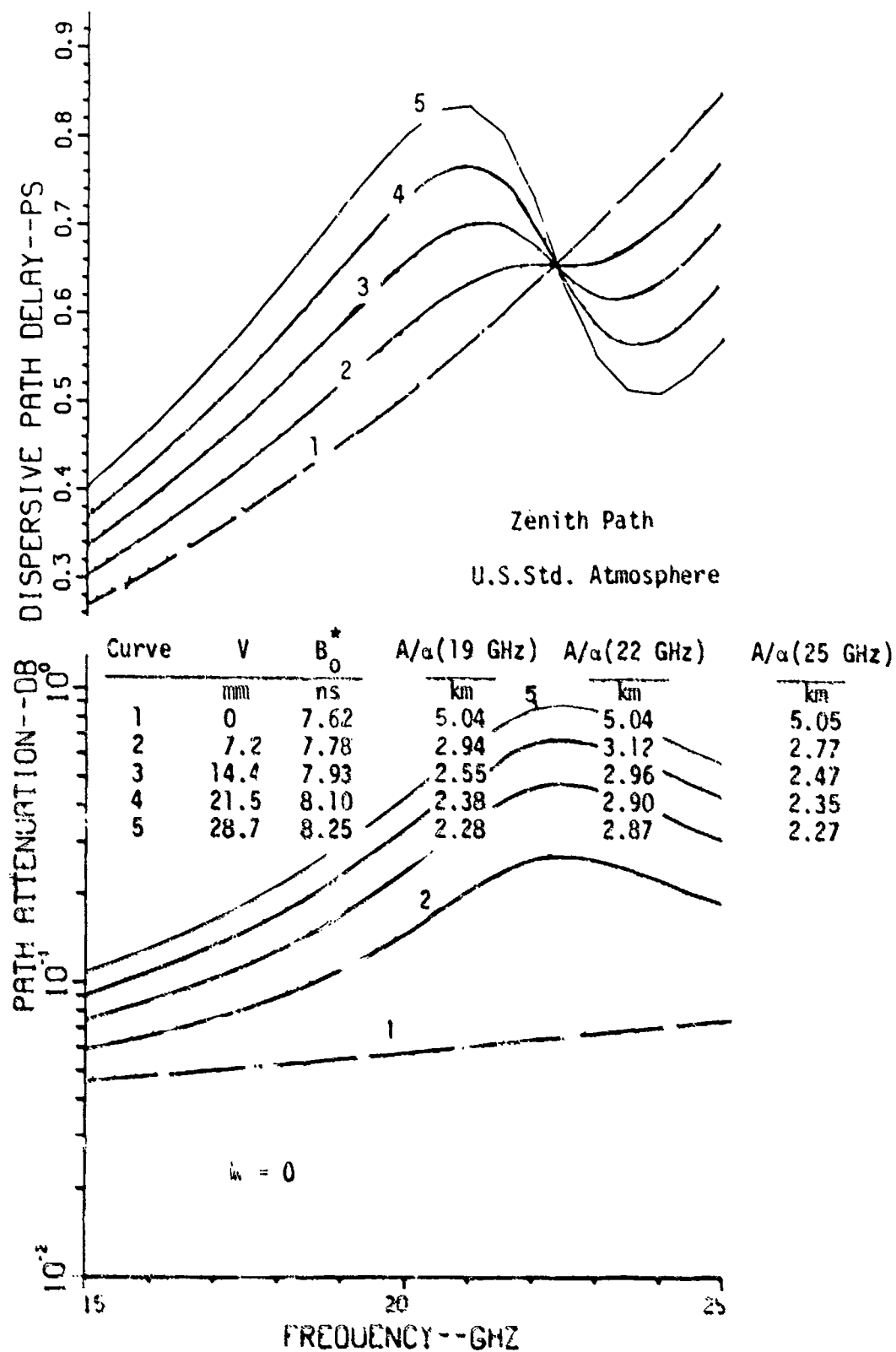
Figure 11. One-way zenith path delay B_z^* and attenuation A_z over a frequency range from 15 to 25 GHz through the cloud-free U. S. Std. Atm. 76 for five values of water vapor content V over the height range h = 0 to 30 km (P1).

Table 8. One-way zenith attenuation A_z through the U. S. Standard Atmosphere at frequencies dominated by water vapor absorption, covering the range 20 to 300 GHz.

	MODEL P1		
Frequency	$A_z(50\%)^*$	$A_z(100\%)^*$	$\alpha(30)$
f	(h = 0-30 km)		(h = 30)
GHz	dB		dB/km
20	.27	.44	.00
22.235(H_2O)	.54	.91	.00
25	.34	.57	.00
30	.24	.35	.00
32	.25	.25	.00
35	.28	.39	.00
40	.40	.52	.00
45	.68	.82	.00
50	1.64	1.81	.00
60	Oxygen Line Absorption		
70	2.27	2.66	.00
80	.96	1.37	.00
90	.87	1.38	.00
100	.97	1.60	.00
105	1.08	1.78	.00
110	1.33	2.10	.00
115	2.57	3.42	.00
120	9.22	10.1	.00
125	1.78	2.79	.00
130	1.53	2.64	.00
140	2.45	2.99	.00
150	1.99	3.62	.00
160	2.59	4.75	.00
170	4.46	8.25	.00
180	30.2	55.6	.00
183.31(H_2O)	93.3	168	.19
185	60.7	109	.00
190	13.1	24.3	.00
200	5.00	9.26	.00
210	4.14	7.63	.00
220	4.08	7.52	.00
230	4.25	7.82	.00
240	4.52	8.32	.00
250	4.85	8.93	.00
260	5.23	9.64	.00
270	5.67	10.4	.00
280	6.18	11.4	.00
290	6.82	12.6	.00
300	7.74	14.3	.00

*The cumulative values $A_z(50\%)$, $A_z(100\%)$ are for water vapor contents V = 14.4 and 28.7 mm, respectively; $\alpha(30)$ is the specific attenuation at the level h = 30 km.

The relations between A_z and α_0 have been calculated with P1 and examples for $h_0 = 0$ km and the U. S. Standard Atmosphere are listed below (see also Figure 11):

f, GHz	15	22	35	60*	90	119*	140	183	220
V, mm				h_s, km					
0	5.0	5.0	5.0	15.4	4.8	50	4.8	4.5	4.6
15	3.1	3.0	2.9	15.3	2.2	35	1.9	3.2	1.8
30	2.4	2.9	2.3	15.2	1.9	25	1.7	3.2	1.7
60	2.2	2.6	2.1	15.1	1.8	20	1.7	3.2	1.7

*Valid for h = 0 to 30 km; see Table 9 for contributions over the range h = 30 to 100 km.

Scale heights h_s assume different values depending on frequency f and water vapor content V, which makes the effective height concept not very universal.

Phase-coherent satellite beacon signals at frequencies around the 22 GHz line experience, in principle, different delays B_z due to a line component which depends linearly upon water vapor content V. This is demonstrated in Figure 11. Analysis reveals that the water vapor group delay between two signals placed symmetrically about ν_0 is extremely small; for example, when

a) $f_1, f_2 = \nu_0 \pm 0.5$ GHz: $B_1^* - B_2^* = (0.0087 \, V - 0.07) \, ps$ and

$$A_z = (0.07 + C \, 028 \, V) \quad dB; \quad or$$

b) $f_1, f_2 = \nu_0 \pm 2.0$ GHz: $B_1^* - B_2^* = (0.020 \, V - 0.27)(\text{max.}) \quad ps$ and

$$A_z = (0.07 + 0.017 \, V) \quad dB.$$

The frequency-dependent delay (14) of each signal traversing the moist air mass is $B_0^* = (7747 + 22.1 \, V)$ ps. The 22 GHz water vapor line is not a good water vapor detector. Sensitivity can be increased by a factor of 3 by looking at the signals under an elevation angle ψ 20°, or by a factor of about 180 by shifting to the 183 GHz line.

Examples of zenith attenuation through a cloudless atmosphere are shown for the frequency range 10 to 350 GHz in Figure 12. The atmosphere is opaque for any system attempting to operate from the ground to outer space when $A_z > 30$ dB. The 55 to 65 GHz band has especially stable shielding qualities. The shielding factor of the air mass has to be evaluated by analytical means; the correct attenuation at the

47
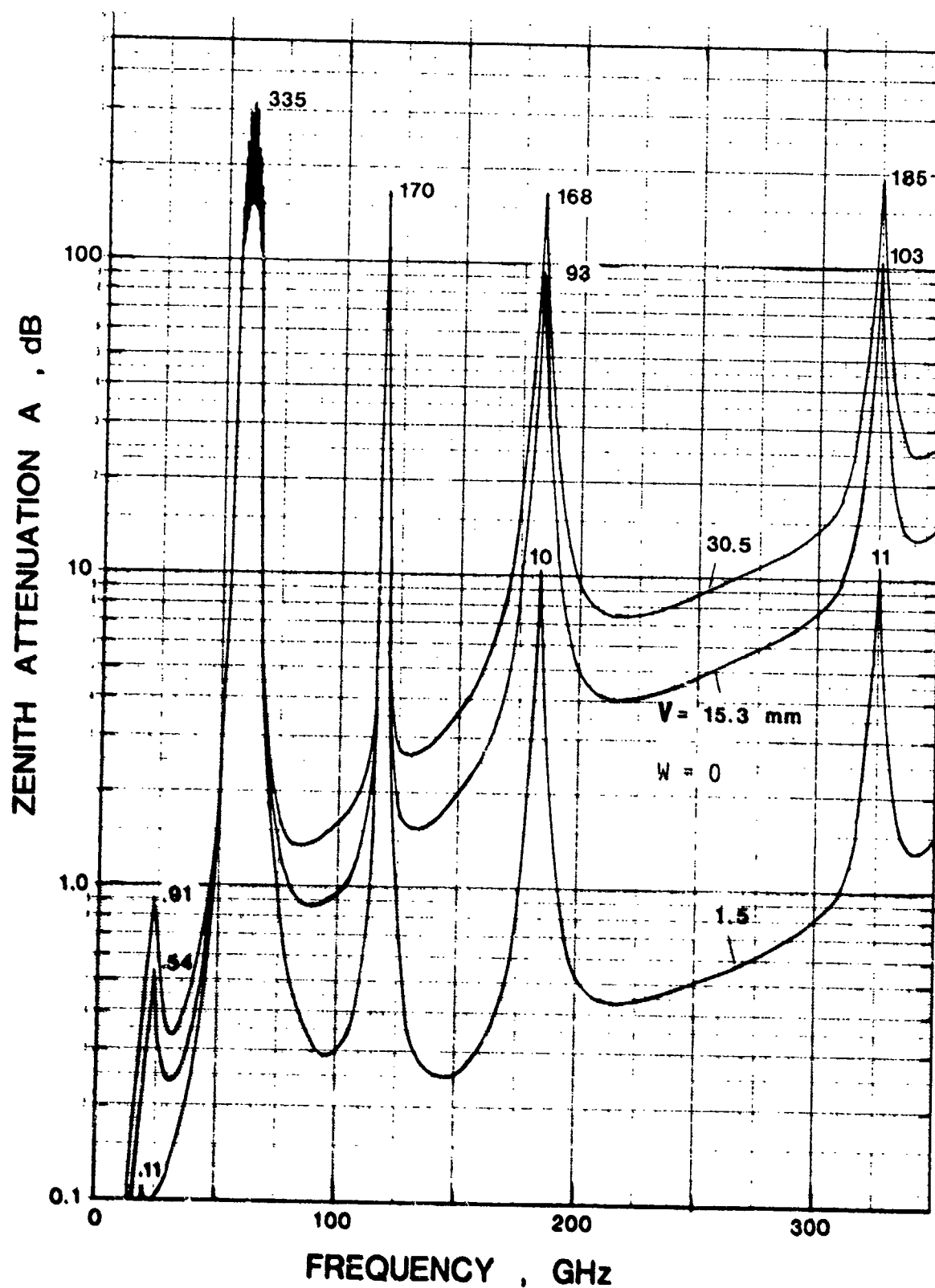
Figure 12. One-way zenith attenuation A_z over a frequency range from 10 to 350 GHz through the cloud-free U. S. Standard Atmosphere 76 for three values of water vapor content V over the height range h = 0 to 100 km (P1 + P2).

oxygen line centers calls for a detailed analysis with P2. An example of such an exercise is exhibited in Figure 13. The numerical account of the integration over h = 30 to 100 km at selected frequencies can be found in Table 9 for the opaque region (a) and for semi-transparent regions (b) to either side of the 60 GHz band. Maximum shielding ($A_z \geq 150$ dB) of satellite-based systems against interference from ground levels can be achieved between 58.9 and 61.2 GHz.

For earth-to-space radio paths, both climatic variations in the state of the atmosphere and elevation angle dependence determine communications link performance at a given frequency. Assessing the low elevation behavior of A by evaluating ray curvature with (12) yields the following selected results:

Cumulative Path Attenuation A

f	$\psi = 90°$ (zenith)		$\psi = 10°$ (slanted)		$\psi = 0°$ (tangential)	
	(a)	(b)	(a)	(b)	(a)	(b)
GHz	dB		dB		dB	
30	0.13	0.35	0.75	2.0	7.4	30
70	2.0	2.7	11.5	15.3	115	175
90	0.31	1.4	1.8	8.0	19	126
140	0.26	3.0	1.5	17.2	18	270

(a) V = 1.5 mm   ,   (b) V = 30 mm   (see Figure 12, Table 8)

This section has presented results of calculations with the ITS version of an MPM. Atmospheric transfer properties in the millimeter wave range are different from those in the lower frequency bands--the lower air mass can become opaque depending on frequency, path length, elevation angle, and climatic conditions.

6. SUMMARY AND RECOMMENDATIONS

The neutral atmosphere ($h \leq 100$ km) has been characterized as a propagation medium for millimeter waves. The basic physics of signal degradations by the atmosphere has been cast into a model (MPM) capable of predicting attenuation and delay effects caused by moist air containing suspended and precipitating water drops. The MPM was streamlined for optimum computer run time but without undue approximations for the clear air case. Exact line-by-line calculations are performed below 1000 GHz for 78 resonance features of the gases O_2 and H_2O. Experimentally confirmed dry and wet continuum absorption terms (22)-(24) have been added to account for attenuation in between lines. Nevertheless, more than 300 spectroscopic coefficients are

49
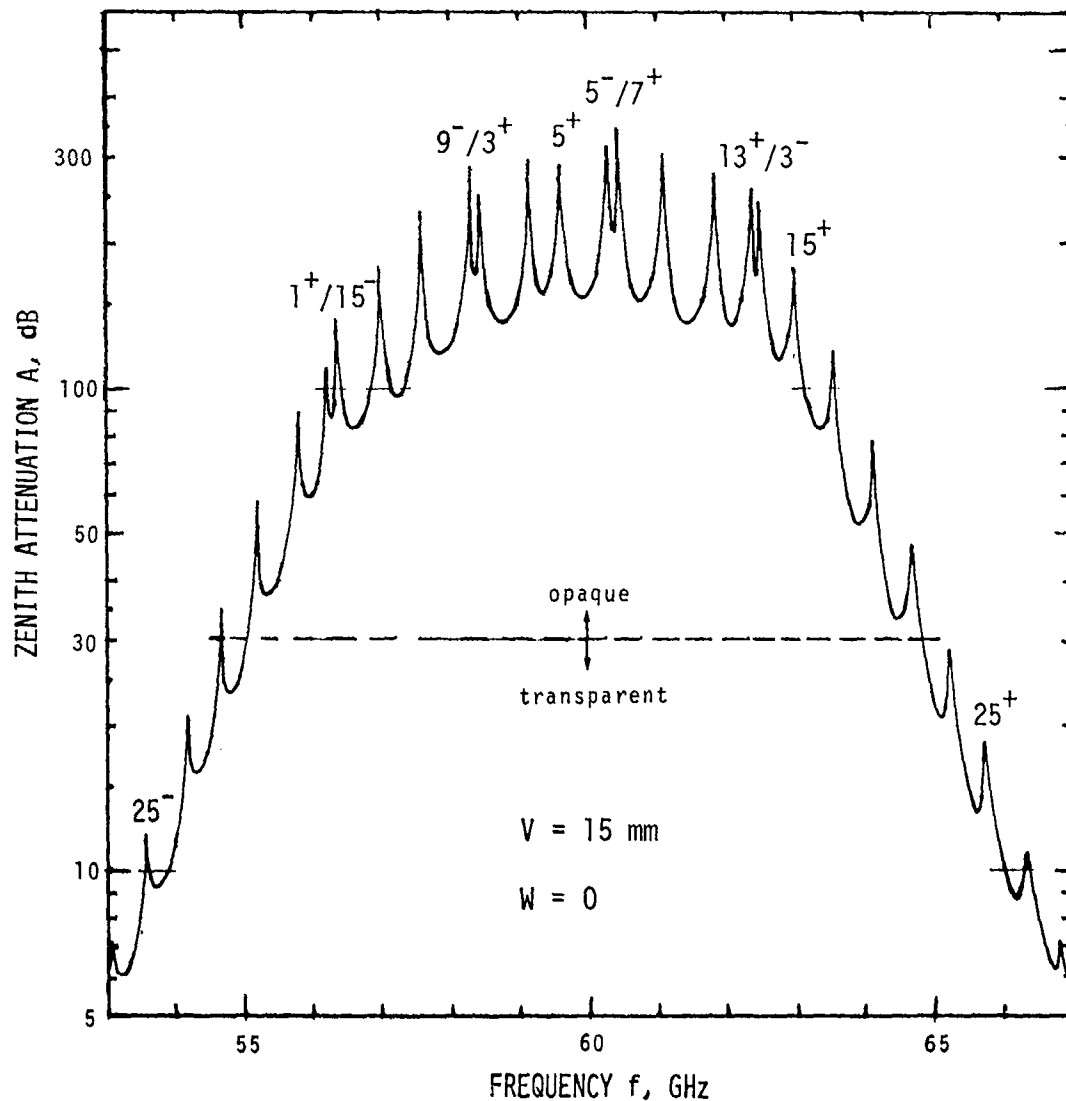
Figure 13. One-way zenith attenuation A_z over a frequency range from 53 to 67 GHz dominated by oxygen line absorption for V = 15 mm over the height range h = 0 to 100 km (P1 + P2). The line peaks are for π patterns and H = 0.3 G (see Table 7).

50

Table 9. One-way zenith attenuation A_z through the U.S. Standard Atmosphere at selected frequencies (max/min values) dominated by oxygen absorption: (a) Opaque Region (> 30 dB) and (b) Semi-Transparent Region (< 30 dB) (see Fig. 13).

The cumulative values A(50%), A(100%) are for V = 14.4 and 28.7 mm, respectively; $\alpha(30)$ is the specific attenuation at h = 30 km; $A_{0.3}$ and $A_{0.6}$ are contributions of mesopheric Zeeman π-patterns assuming a geomagnetic field strength, H = 0.3 or 0.6 Gauss.

(a) Opaque Region (> 30 dB)

Frequency f	Line ID K±	MODEL P1 A(50%) (h = 0 -30 km)	MODEL P1 A(100%) (h = 0 -30 km)	α(30) (h = 30)	MODEL P2 $A_{0.3}$ (π) (h = 30 -100 km)	MODEL P2 $A_{0.6}$ (h = 30 -100 km)	MODEL P1 + P2 A_z (h = 0 -100 km)
GHz		dB		dB/km	dB		dB
55.22	19-	38.9	39.2	.45	17.8	15.1	55 (1)*
55.50		40.0	40.3	.01			41 (1)
55.78	17-	61		.79	29.6	25.3	89 (2)
56.02		60		.02			61 (1)
56.27	1+	83		.65	31.2	31.2	114 (0)
56.36	15-	95		1.30	45.6	39.1	137 (4)
56.67		80		.02			81 (1)
56.97	13-	117		1.85	64.5	55.4	177 (5)
57.29		97		.02			98 (1)
57.61	11-	146		2.46	83.3	71.8	244 (6)
57.97		119		.02			120 (1)
58.32	9-	190		2.99	97.7	84.5	128 (7)
58.45	3+	180		1.94	68.1	61.0	245 (3)
58.81		139		.03			140 (1)
59.16	7-	195		3.11	102	89.1	291 (6)
59.95		159		.03			160 (1)
60.31	5-	223		2.91	92.8	81.6	310 (6)
60.43	7+	228		3.38	114	99.1	335 (7)
60.79		151		.03			151 (1)
61.15	9+	196		3.28	113	98.2	302 (1)
61.48		139		.03			139 (1)
61.80	11+	180		2.86	100	86.9	274 (7)
62.11		134		.03			134 (1)
62.41	13+	179		2.42	80.2	69.2	254 (5)
62.49	3-	171		2.18	69.2	62.3	237 (4)
62.74		113		.03			113 (1)
63.00	15+	117		1.59	59.1	50.4	172 (5)
63.28		98		.02			98 (1)
63.57	17+	79		1.03	39.3	33.7	115 (3)
63.85		53		.01			52.8(2)
64.13	19+	52		.61	23.3	20.9	74 (2)
64.40		35.5	35.8	.01			35.7(2)
64.68	21+	33.7	34.0	.33	14.0	12.0	46.7(1)
118.75	1-	67.9	68.8	2.28	101.1	101.1	170 (1)

* Digit in parenthesis gives the Standard Deviation from the mean (in terms of the final listed digits) due to magnetic field (H = 0.3 to 0.6 G) and humidity (V = 0 to 30 mm) variations.

Frequency f	Line ID K±	MODEL P1			MODEL P2		MODEL P1 + P2
		$A(50\%)$	$A(100\%)$	$\alpha(30)$	$A_{0.3}$ (π)	$A_{0.6}$	A_z
		(h = 0 -30 km)		(h = 30)	(h = 30 -100 km)		(h = 0 -100 km)
GHz		dB		dB/km	dB		dB
50.99	35-	2.19	2.38	.00	.03	.02	2 3(1)*
51.25		2.40	2.59	.00			2.5(1)
51.50	33-	2.66	2.86	.00	.07	.06	2.8(1)
51.76		2.96	3.16	.00			3.1(1)
52.02	31-	3.38	3.58	.00	.18	.15	3.6(2)
52.28		3.82	4.02	.00			3.9(1)
52.54	29-	4.53	4.74	.01	.46	.38	5.1(2)
52.81		5.20	5.41	.00			5.3(1)
53.07	27-	6.46	6.68	.02	1.10	.91	7.6(2)
53.33		7.44	7.66	.00			7.7(1)
53.60	25-	9.75	9.97	.05	2.45	2.06	11.9(3)
53.86		11.1	11.3	.00			11.2(1)
54.13	23-	15.3	15.6	.12	5.09	4.31	20.2(4)
54.40		17.0	17.2	.00			17.1(1)
54.67	21-	24.5	24.7	.24	9.85	8.39	33.7(8)
54.95		26.2	26.4	.00			26.3(1)
		Oxygen Band Center (Table 9a)					
64.95		23.6	24.0	.00			23.8(2)
65.22	23+	21.6	21.9	.17	7.50	6.40	28.8(5)
65.49		15.7	16.1	.00			15.9(2)
65.77	25+	13.9	14.3	.08	3.73	3.18	17.7(4)
66.03		10.7	11.0	.00			10.8(2)
66.30	27+	9.35	9.73	.03	1.73	1.47	11.1(4)
66.57		7.53	7.92	.00			7.7(2)
66.84	29+	6.62	7.02	.01	.74	.63	7.5(3)
67.10		5.60	6.00	.00			5.8(2)
67.37	31+	4.99	5.40	.01	.30	.27	5.5(2)
67.64		4.40	4.81	.00			4.6(2)
67.90	33+	3.99	4.40	.00	.12	.10	4.5(2)
68.17		3.62	4.03	.00			3.8(2)
68.43	35+	3.33	3.74	.00	.04	.03	3.5(2)

* Digit in parenthesis gives the Standard Deviation from the mean (in terms of the final listed digits) due to magnetic field (H = 0.3 to 0.6 G) and humidity (V = 0 to 30 mm) variations.

still involved to various degrees in the calculation of one output value. The presented MPM version is physically sound, has been tested with available data (see Appendix C), and was organized to adapt easily to requirements for communications applications. The MPM, which inputs routinely measured meteorological parameters, can serve as a source for simpler, engineering-type approximations that suffice when applications are limited in frequency or height range (Pierluissi et al., 1982; Liebe, 1983).

The MPM consists of a main program P1 for the lower atmosphere ($\leq$ 30 km) supplemented by a second program P2 for the upper atmosphere ($\leq$ 100 km). Both are written in FORTRAN IV and structured to be operated interactively in a user-friendly mode by nonexperts. Test runs provided a wide selection of numerical and graphical examples, which elucidate unique millimeter wave properties of the atmosphere. However, the model is by no means complete and work should continue to perfect it towards more specific telecommunications requirements. We recognize a need for adding subroutines for the following effects: (a) wet snow attenuation, (b) dust and sandstorm attenuation, (c) dispersive rain delay, (d) spectral line data for trace gases and man-made pollutants, and (e) statistical data on spatial and temporal distributions of the input parameters over scales from centimeters and milliseconds to kilometers and years. Implications and potential of the MPM for performance evaluation and forecasting require more attention, and integration into system models is suggested to allow optimal compromises between environmental and technical constraints. These efforts should proceed hand-in-hand with extensive testing and updating using data from carefully calibrated field tests and well controlled laboratory experiments.

7. REFERENCES

Altshuler, E. E., M. A. Gallop, and L. E. Telford (1978), Atmospheric attenuation statistics at 15 and 35 GHz for very low elevation angles, Radio Sci. 13, No. 5, pp. 839-852.

Allen, K. C. (1983), Attenuation of millimeter waves on earth-space paths by rain clouds, NTIA Report 83-132, September.

Allen, K. C., H. J. Liebe, and C. M. Rush (1983), Estimates of millimeter wave attenuation for 18 United States cities, NTIA Report 83-119, May (NTIS Acces. No. PB83-240630).

Burch, D. E. (1982), Continuum absorption by H_2O, Ford Aerospace and Communications Corp., Aeronutronic Div., Final Report AFGL-TR-81-0300.

Chang, A. T., and T. T. Wilheit (1979), Remote sensing of atmospheric water vapor, liquid water, and wind speed at the ocean surface by passive microwave techniques from the NIMBUS 5 satellite, Radio Sci. 14, No. 5, pp. 793-802.

Crane, R. K. (1980), Prediction of attenuation by rain, IEEE Trans. Comm. COM-28, pp. 1717-1733.

Crane, R. K. (1981), Fundamental limitations caused by RF propagation, Proc. IEEE 69, No. 2, pp. 196-209.

Dagg, I. R., L. A. Read, and J. Vanderkooy (1982), Far infrared laser system for the measurement of collision-induced absorption spectra, Rev. Sci. Instru. 53 No. 2, pp. 187-193.

Damosso, E., P. Porzio-Giusto, L. Stola, and D. Tarducci (1982), Study of propagation properties of the 50- to 70-GHz band and its potential applications for space communication systems, Report by Centro Studi E Laboratori Telecomunicazioni, Torino, Italy (CSELT No. 82.01.043) for European Space Agency (ESA Contr. 4535/80/NL/MS), Parts I and II, January.

Davies, R. W., and B. A. Oli (1978), Theoretical calculations of H_2O linewidths and pressure shifts: Comparison of the Anderson theory with quantüm manybody theory for N_2 and air-broadened lines, J. Quant. Spect. Rad. Transfer 20, pp. 95-120.

Dutton, E. J., C. E. Lewis, and F. K. Steele (1983), Climatological coefficients for rain attenuation at millimeter wavelengths, NTIA Report 83-129, August.

Emery, R. J., A. M. Zavody, and H. A. Gibbie (1980), Measurements of atmospheric absorption in the range 5-17 cm^{-1} and its temperature dependence, J. Atm. Terrestr. Phys. 42, pp. 801-807.

Endo, Y., and M. Mizushima (1982), Microwave resonance lines of $^{16}O_2$ in its electronic ground state, Jap. J. Appl. Phys. 21, No. 6, pp. L379-L380.

Flaud, J.-M., C. Camy-Peyret, and R. A. Toth (1981), Water Vapor Line Parameters from Microwave to Medium Infrared (Pergamon Press, Oxford, England).

Falcone, V. J., Jr., L. W. Abreu, and E. P. Shettle (1979), Atmospheric attenuation of millimeter and submillimeter waves: Models and computer code, Environmental Res. Paper 679, October (available as Rep. AFGL-TR-79-0253, U. S. Air Force Geophysics Lab., Hanscom Air Force Base, MA), also SPIE-259, pp. 5866 (Oct. 1980).

Gallery, W. O., F. X. Kneizys, and S. A. Clough (1983), Air mass computer program for atmospheric transmittance/radiance calculation: FSCATM, Air Force Geophysics Lab., Report No. AFGL-TR-83-0065 (Environm. Res. Papers, No. 828).

Hartmann, G. K., and K. F. Künzi (1983), The Zeeman effect of O_2 and its influence on the brightness temperature of the earth's atmosphere, MPI-Aeronomy Report MPAE-W-66-22, Lindau, W-Germany, May.

Hill, R. J., R. S. Lawrence, and J. T. Priestley (1982), Theoretical and calculational aspects of the radio refractive index of water vapor, Radio Sci. 17, No. 5, pp. 1251-1257.

Kemp, A. J. (1979), Line shape functions for the computation of the absorption coefficient of water vapour at submillimetre wavelengths, Infrared Phys. 19, pp. 595-598.

Lenoir, W. B. (1968), Microwave spectrum of molecular oxygen in the mesosphere, J. Geophys. Res. 73, pp. 361-376.

Liebe, H. J., G. G. Gimmestad, and J. D. Hopponen (1977), Atmospheric oxygen micro-wave spectrum--Experiment versus theory. IEEE Trans. Ant. Prop. AP-25, No. 3, pp. 327-335.

Liebe, H. J. (198`), Modeling attenuation and phase of radio waves in air at fre-quencies below .100 GHz, Radio Sci. 16, No. 6, pp. 1183-1199.

Liebe, H. J. (1982), The atmospheric propagation medium between 45 and 75 GHz, AGARD Conf. Proc., AGARD-CP-331, pp. 4/1 to 12.

Liebe, H. J. (1983), Atmospheric EHF window transparencies near 35, 90, 140, and 220 GHz, IEEE Trans. Ant. Prop. AP-31, No. 1, pp. 127-135.

Liebe, H. J. (1984), The atmospheric water vapor continuum below 300 GHz, Int. J. Infrared Millimeter Waves 5, No. 2.

Messer, J. K., F. C. DeLucia, and P. Helminger (1983), The pure rotational spectrum of water vapor--a millimeter, submillimeter, and far infrared analysis, Int. J. Infrared Millimeter Waves 4, No. 4, pp. 505-539.

Mizushima, M. (1982a), Absorption of millimeter to submillimeter waves by atmospheric water molecules, Int. J. Infrared Millimeter Waves 3, No. 3, pp. 379-384.

Mizushima, M. (1982b), Transparency of earth's atmosphere in the frequency region below 1 THz, Int. J. Infrared Millimeter Waves 3, No. 6, pp. 889-895.

NOAA (1976), U. S. Standard Atmosphere, 1976, NOAA,S/T 76-1562 (U. S. Government Printing Office, Washington, DC).

Oguchi, T. (1983), Electromagnetic wave propagation and scattering in rain and other hydrometeors, Proc. IEEE 71, No. 6, pp. 1029-1078.

Olsen, R. L., D. V. Rogers, and D. B. Hodge (1978), The aR^b relation in the calcula-tion of rain attenuation, IEEE Trans. Ant. Prop. AP-26, No. 2, pp. 318-329.

Park, J. H., L. S. Rothman, C. P. Rinsland, M. A. Smith, D. T. Richardson, and J. C. Larsen (1981), Atlas of absorption lines from 0 to 17900 cm^{-1}, NASA Reference Publication 1084, December.

Pickett, H. M., E. A. Cohen, and D. E. Brinza (1981), Pressure-broadening of oxygen and its implications for cosmic background measurements, Astrophys. J. 258, pp. L49-L51.

Pierluissi, J. H., K. Tomiyama, W. D. Fowler, and R. B. Gomez (1982), Resonant transmittance model for millimeter wave propagation, IEEE Trans. Ant. Prop. AP-30, No. 4, pp. 741-746.

Poynter, R. L., and H. M. Pickett (1981), Submillimeter, millimeter, and microwave spectral line catalogue, JPL Publication 80-23, Rev. 1, Jet Propulsion Lab., NASA, Pasadena, CA.

Rice, D. P., and P. A. Ade (1979), Absolute measurements of the atmospheric trans-parency at short millimetre wavelengths, Infrared Phys. 12, pp. 575-584.

Rosenkranz, P. W. (1975), Shape of the 5 mm oxygen band in the atmosphere, IEEE Trans. Ant. Prop. AP-23, No. 4, pp. 498-506.

Rosenkranz, P. W. (1982), Comment on absorption and dispersion in the O_2 microwave spectrum at atmospheric pressures, J. Chem. Phys. 77, No. 4, pp. 2216-2217.

Rothman, L. S., R. R. Gamache, A. Barbe, A. Goldman, J. R. Gillis, L. R. Brown, R. A. Toth, J.-M. Flaud, and C. Camy-Peyret (1983a), AFGL atmospheric absorption line parameters compilation: 1982 edition, Appl. Opt. 22, No. 12, pp. 2247-2256.

Rothman, L. S., A. Goldman, J. R. Gillis, R. R. Gamache, H. M. Pickett, R. L. Poynter, N. Husson, and A. Chedin (1983b), AFGL trace gas compilation: 1982 version, Appl. Opt. 22, No. 11, pp. 1616-1627.

Setzer, B. J., and H. M. Pickett (1977), Pressure broadening measurements of the 118.750 GHz oxygen transition, J. Chem. Phys. 67, No. 1, pp. 340-343.

Smith, E. K. (1982), Centimeter and millimeter wave attenuation and brightness temperature due to atmospheric oxygen and water vapor, Radio Sci. 17, No. 6, pp. 1455-1464.

Smith, E. W. (1981), Absorption and dispersion in the O_2 microwave spectrum at atmospheric pressures, J. Chem. Phys. 74, No. 12, pp. 6658-6673.

Stutzman, W. L., and W. K. Dishman (1982), A simple model for the estimation of rain-induced attenuation along earth-space paths at millimeter wavelengths, Radio Sci. 17, No. 6, pp. 1465-1476.

Thomas, M. E., and R. J. Nordstrom (1982), The N_2-broadened water vapor absorption line shape and infrared continuum absorption-II. Implementation of the line shape, J. Quant. Spectrosc. Radiat. Transfer 28, No. 2, pp. 103-112.

Valley, S. L. (1965), Handbook of Geophysics and Space Environments, Chapter 2 (McGraw-Hill Book Co., NY).

Waters, J. R. (1976), Absorption and emission by atmospheric gases, Methods of Experimental Physics 12B, edited by M. L. Meeks, Chapter 2.3 (Academic Press, New York).

Zammit, C. C., and P. A. Ade (1981), Zenith atmospheric attenuation measurements at millimetre and sub-millimetre wavelengths, Nature 293, No. 5833, pp. 550-552.

Zammit, C. C., R. E. Hill, and R. W. Baker (1982), Atmospheric emission and attenuation in the range 100 to 600 GHz measured from a mountain site, Int. J. Infrared Millimeter Waves 3, No. 2, pp. 189-203.

Zrazhevskiy, A. Y. (1976), Method of calculating atmospheric water vapor absorption of millimter and submillimeter waves, Radio Engineering and Electronic Phys. 21, No. 5, pp. 31-36.

APPENDIX A.

DETAILED ATMOSPHERIC (0 to 100 km) ATTENUATION AND DISPERSION
IN FREQUENCY RANGES DOMINATED BY OXYGEN LINES
(52 to 67 GHz and 117 to 121 GHz)

The catalog of graphical results, Figures A1 to A15, is valid for the U. S. Standard Atmosphere (1976) assuming a relative humidity of 50 percent between 0 and 8 km height. Shown are responses at height levels h = 0, 5, 10, 15, 20, and 30 km obtained with program P1 over a limited frequency range (typically 400 MHz), followed by Zeeman patterns of O_2 lines which lie within this range. The three principal attenuation patterns $\alpha_1(\pi)$ $\alpha_{2,3}(\sigma^{\pm})$ for lines identified by the quantum $K^{\pm}$ (Table 1) are calculated over the height range h = 30 to 100 km using program P2.

Figure A1 to A15. Attenuation α and dispersion D over 15 frequency ranges between 52 and 67 GHz, and 117 to 121 GHz displaying the O_2 lines $K^{\pm} = 1$ to 29 over the height range h = 0 to 30 km. Also shown are associated Zeeman attenuation patterns for altitudes h = 30 to 100 km.

Note: Each frame displays $\pi(\alpha_1)$, $\sigma^+(\alpha_2)$, and $\sigma^-(\alpha_3)$ patterns for the magnetic field strengths H = 0.3 (left hand) and H = 0.6 G (right hand) which are symmetric with respect to the center axis (interchange σ^+ and σ^-). The frequency deviation $\Delta\nu = (f - \nu_0)$ is between ±40 MHz for H = 30 and ±2 MHz for h = 60 to 100 km. The maximum attenuation rate $\underline{\alpha_0}$ is that of the isolated unsplit line (H = 0); the value in parentheses is calculated with program P1. The values of $\alpha_1(\nu_0)$ in decibels per kilometer are for 0.3 and 0.6 gauss.

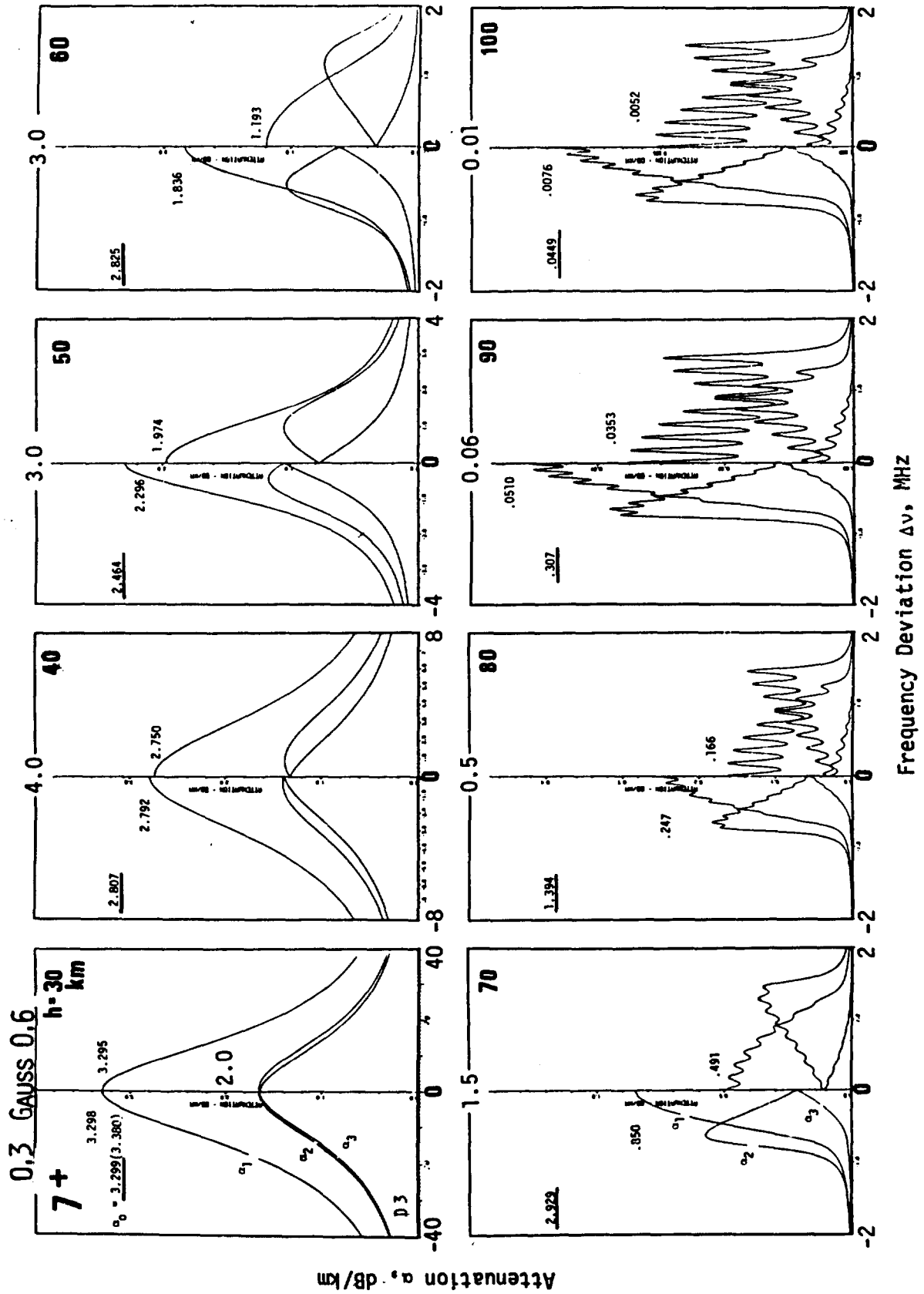|	h = 0 to 30 km			h = 30 to 100 km	
FIGURE	ATTENUATION α AND DISPERSION D			ZEEMAN PATTERNS $\alpha_{1,2,3}$	Page
		f,GHz		$K^{\pm}$	
A1	52.0	to	53.4	29^-, 27^-	59
A2	53.4	to	53.8	25^-	61
A3	53.8	to	56.2	23^- to 17^-	63
A4	56.1	to	56.5	$1^+/15^-$ = D1	67
A5	56.5	to	58.5	13^-, 11^-	70
A6	58.2	to	58.6	$9^-/3^+$ = D2	73
A7	58.6	to	59.4	7^-	76
A8	59.4	to	59.8	5^+	78
A9	59.8	to	60.6	$5^-/7^+$ = D3	80
A10	60.6	to	61.4	9^+	84
A11	61.6	to	62.0	11^+	87
A12	62.2	to	62.6	$13^+/3^-$ = D4	89
A13	62.8	to	63.2	15^+	92
A14	63.0	to	67.0	17^+ to 29^+	94
A15	117.0	to	121.0	1^-	100

Figure A1.

Figure A1. continued

Frequency Deviation Δv, MHz

Attenuation α, dB/km

Figure A2.

$\frac{h}{0 \text{ km}}$

5

10

25°

.051

15

20

30

ATTENUATION--dB/km

53.4   53.5   53.6   53.7   53.8
FREQUENCY--GHZ

REFRACTIVE DISPERSION--ppm

0 km

5

10

15

20

30

53.4   53.5   51.6   53.7   53.8
FREQUENCY--GHZ

61

Figure A2. continued

Frequency Deviation Δν, MHz

Attenuation α, dB/km

Figure A3.

63

Figure A3. continued

Frequency Deviation $\Delta\nu$, MHz

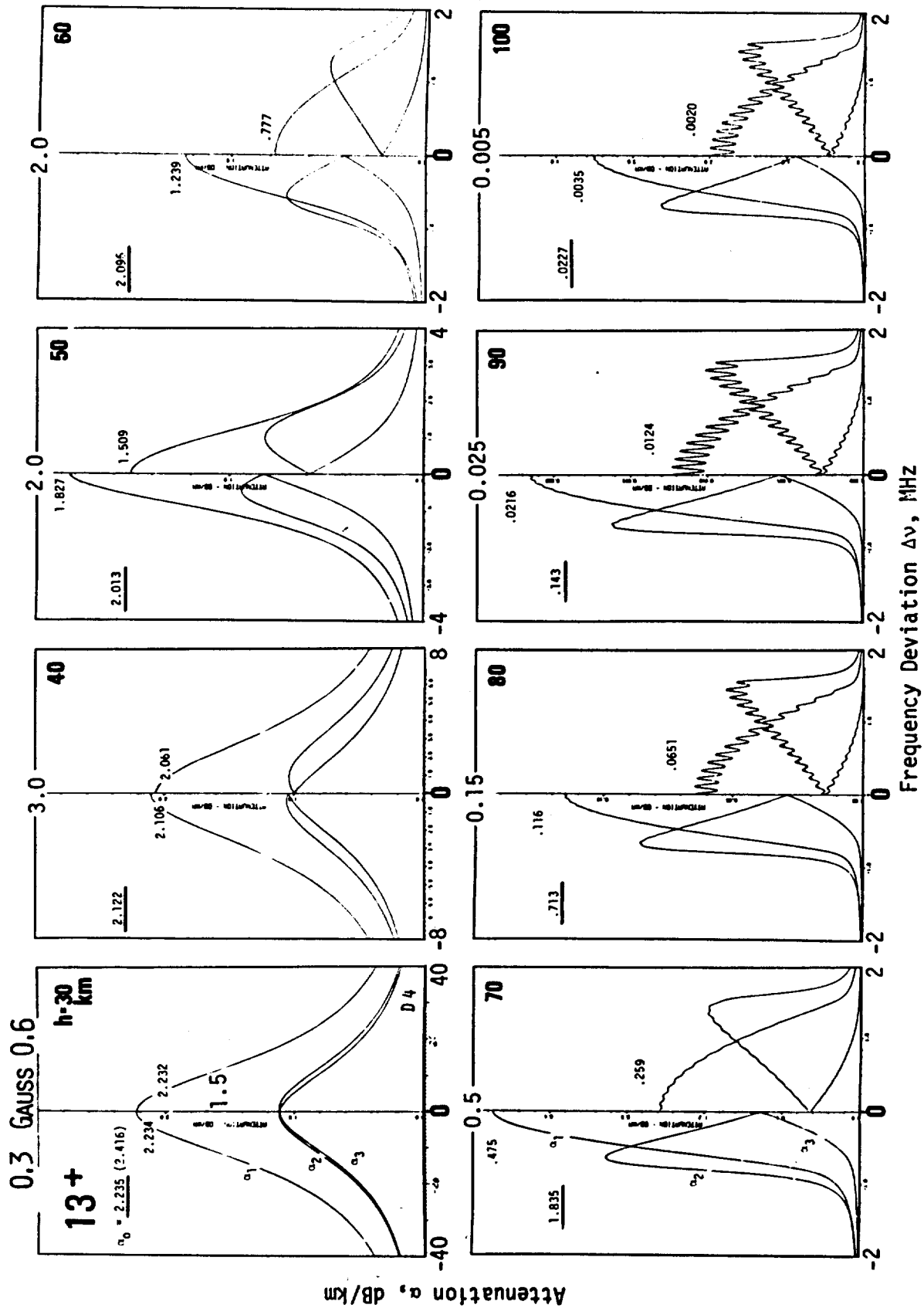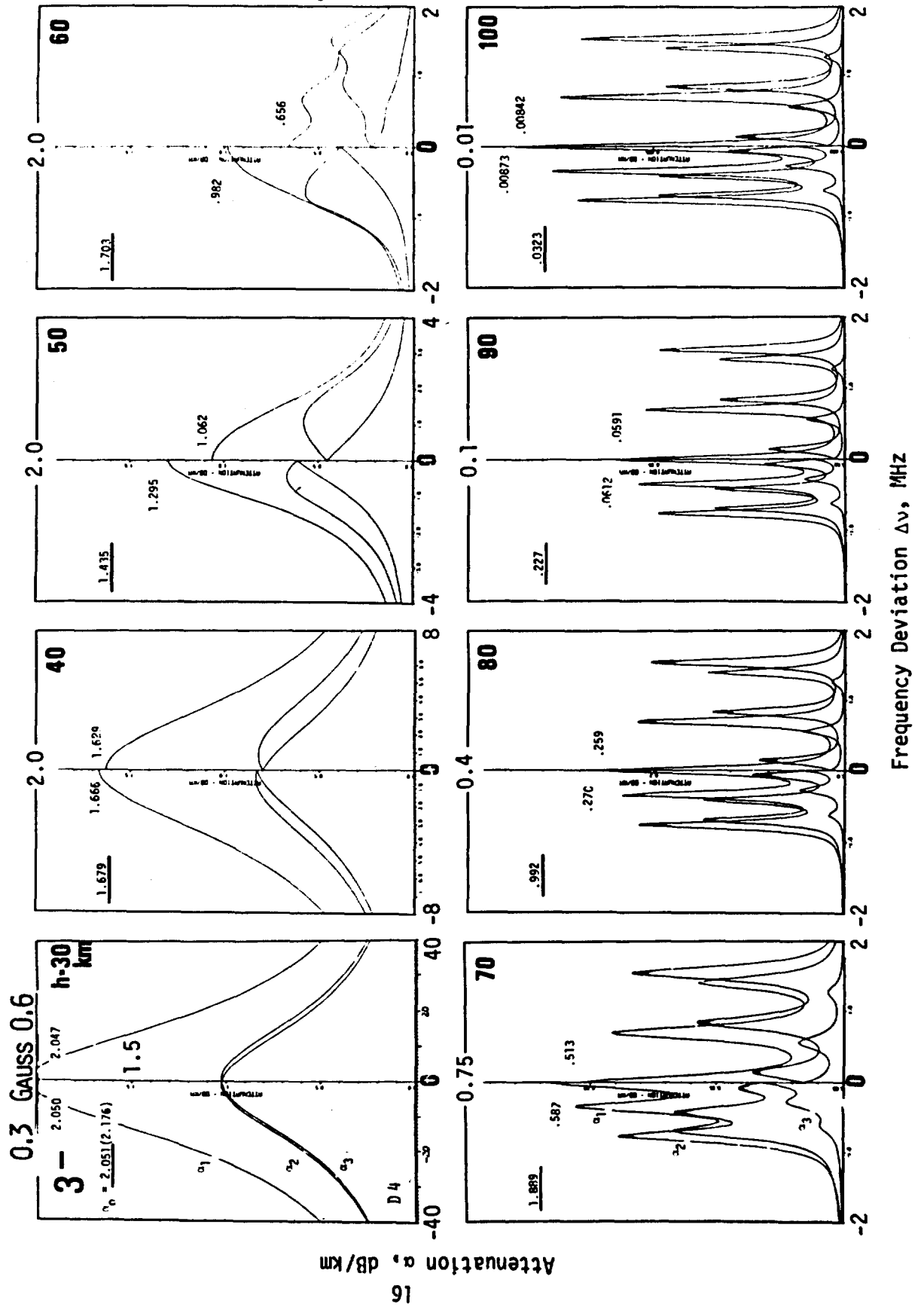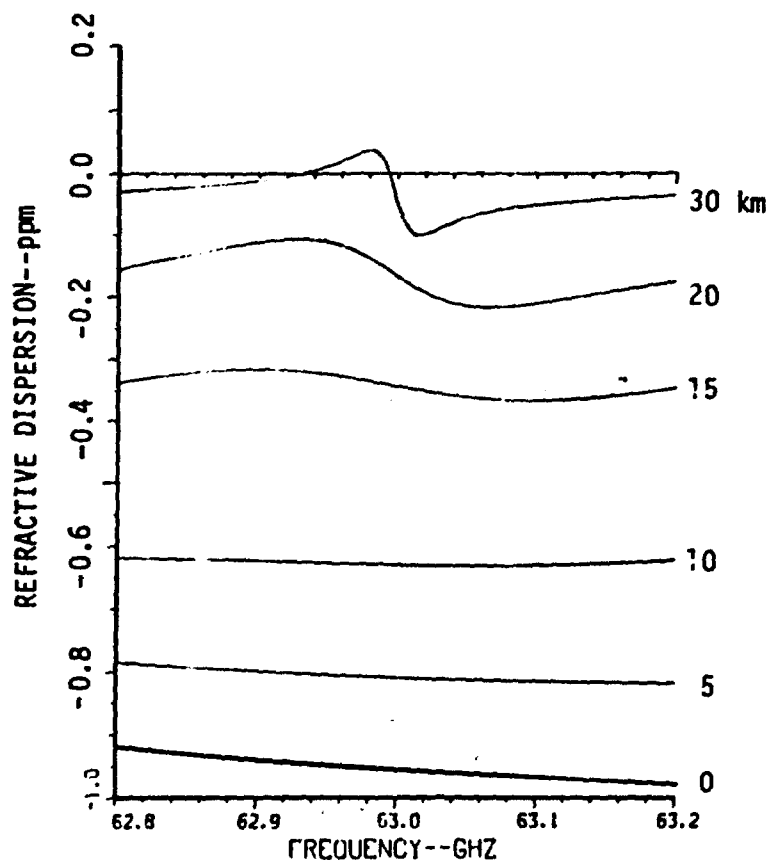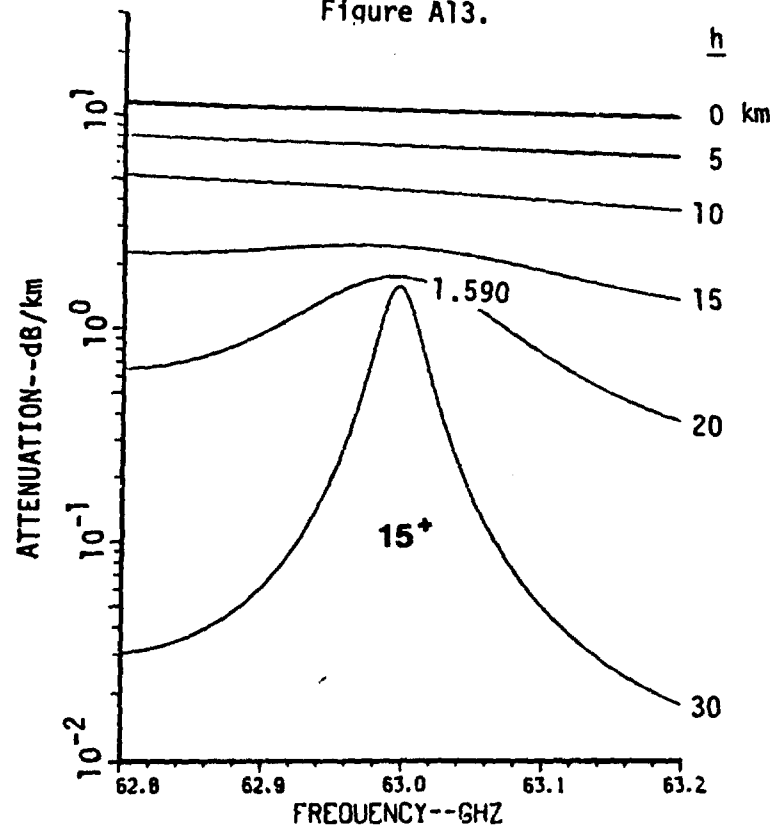Attenuation α, dB/km

64
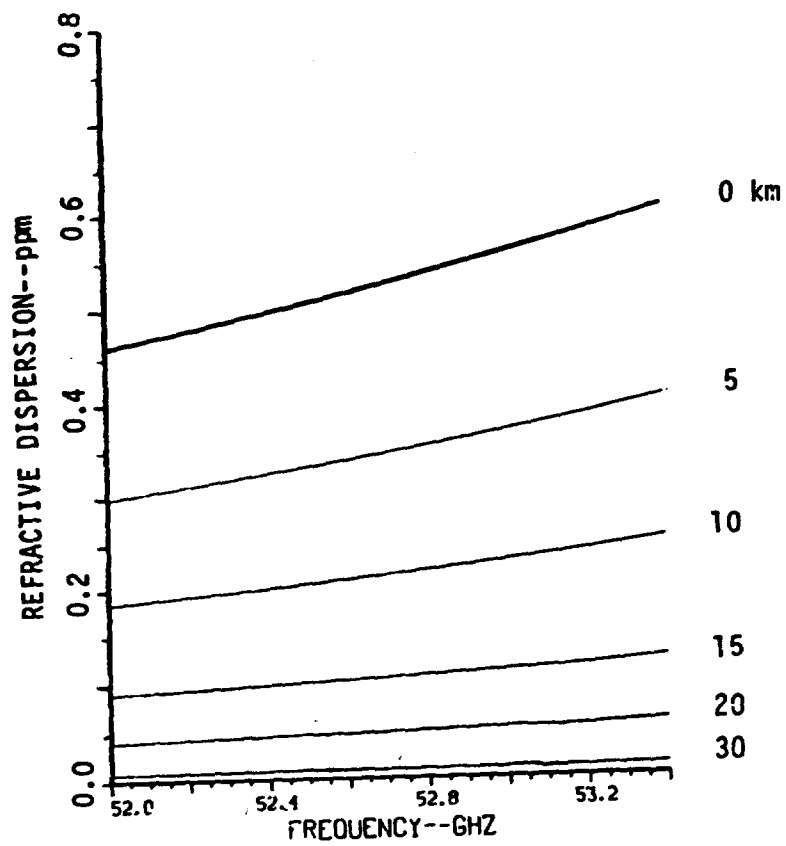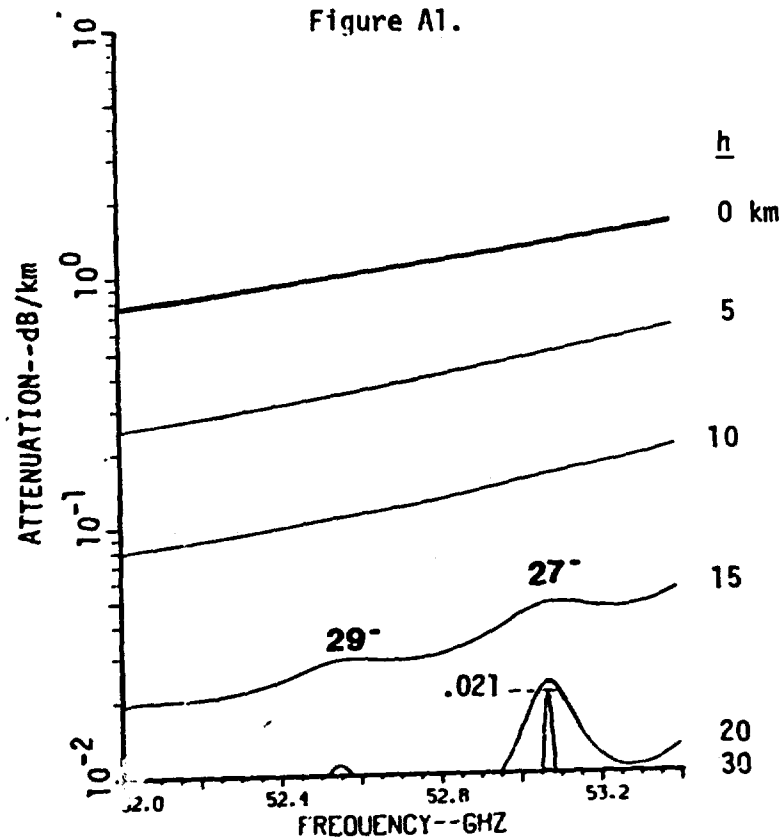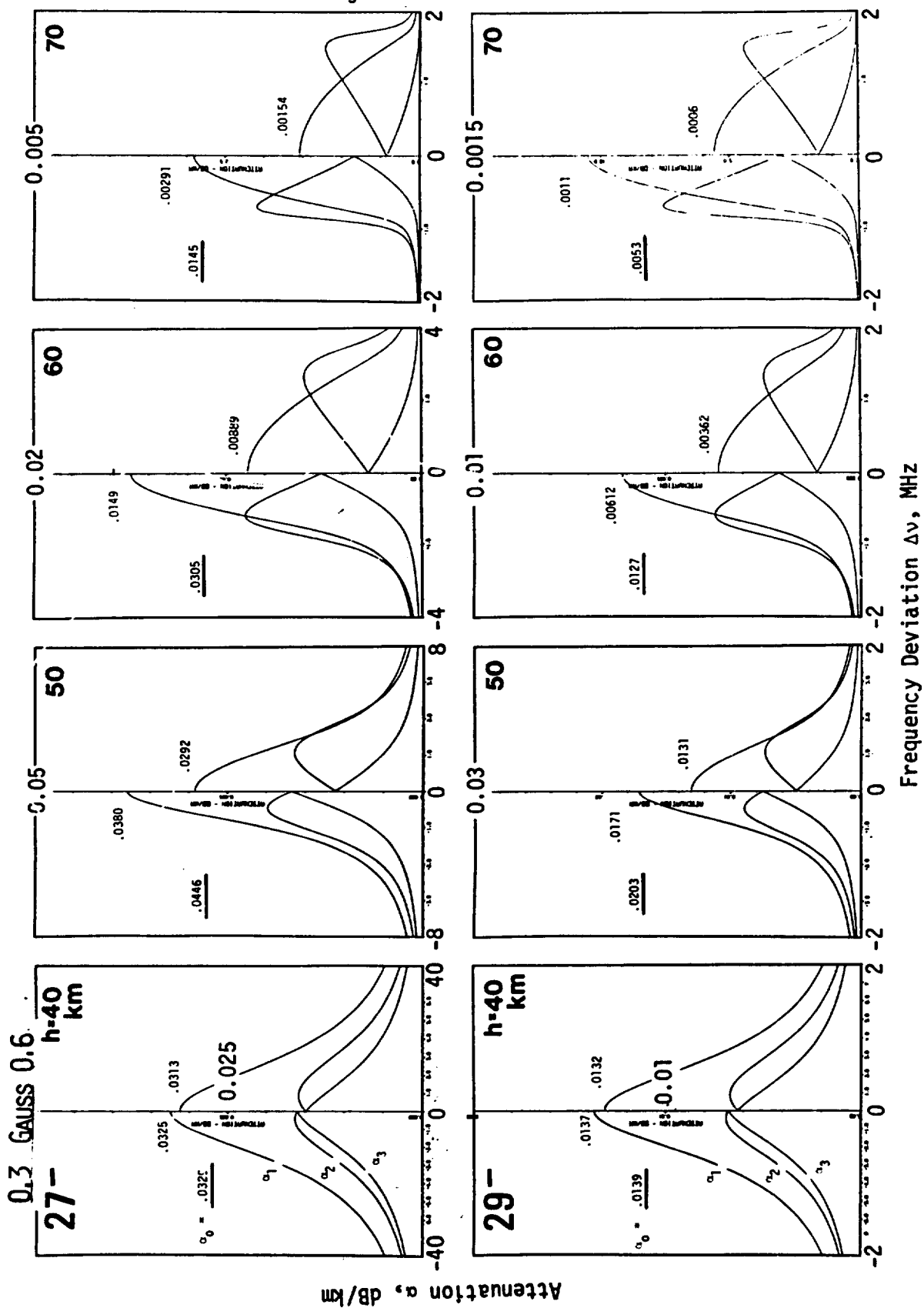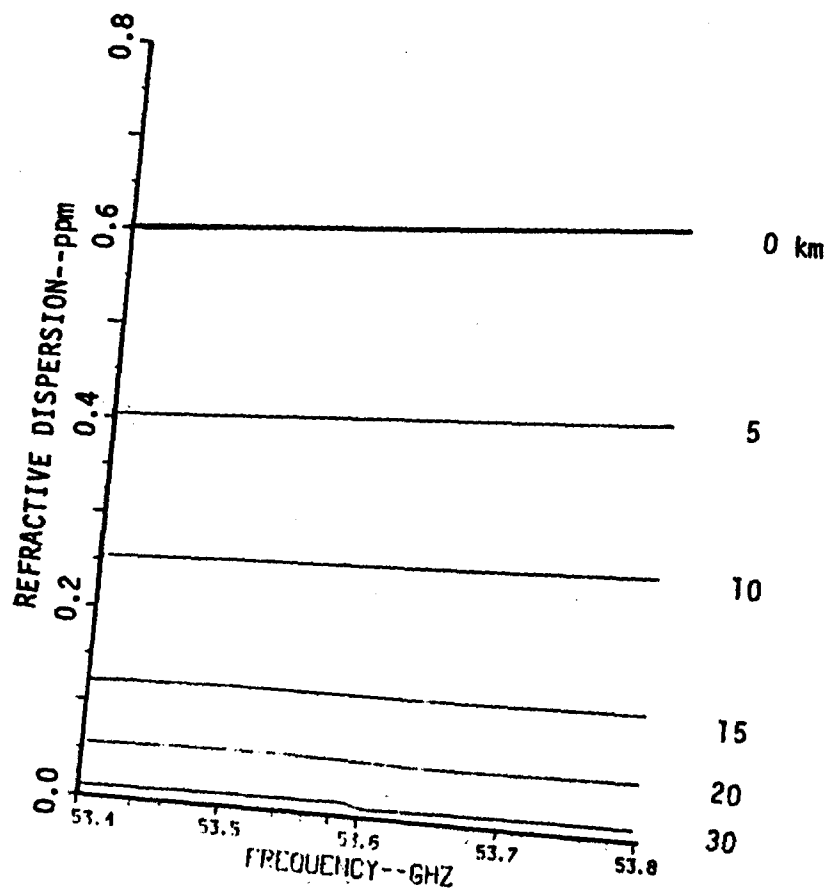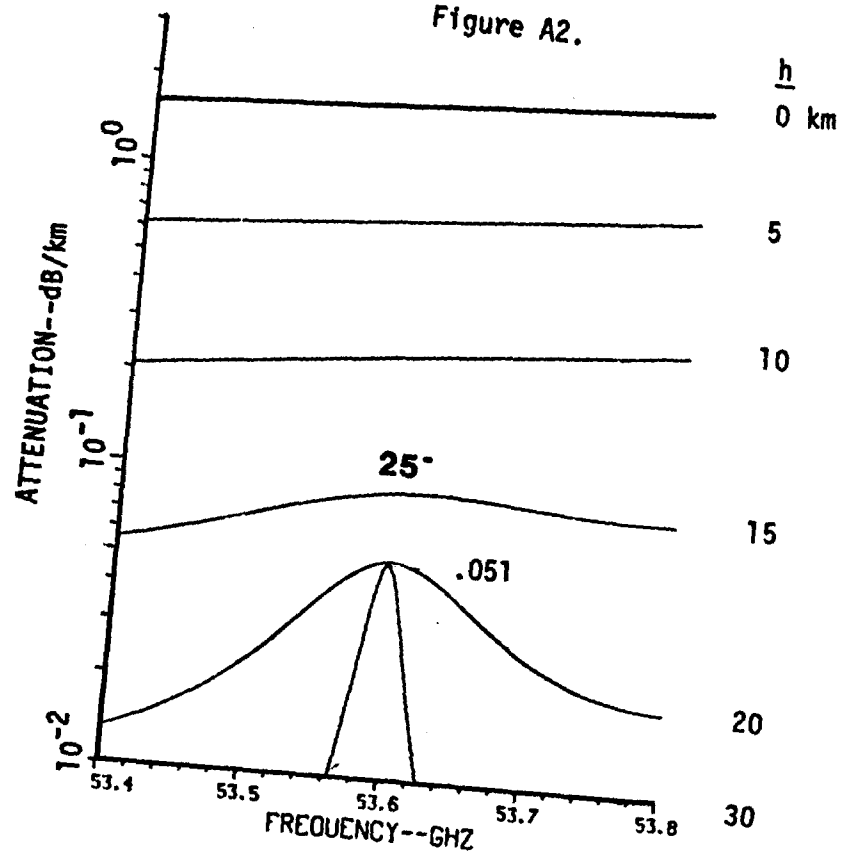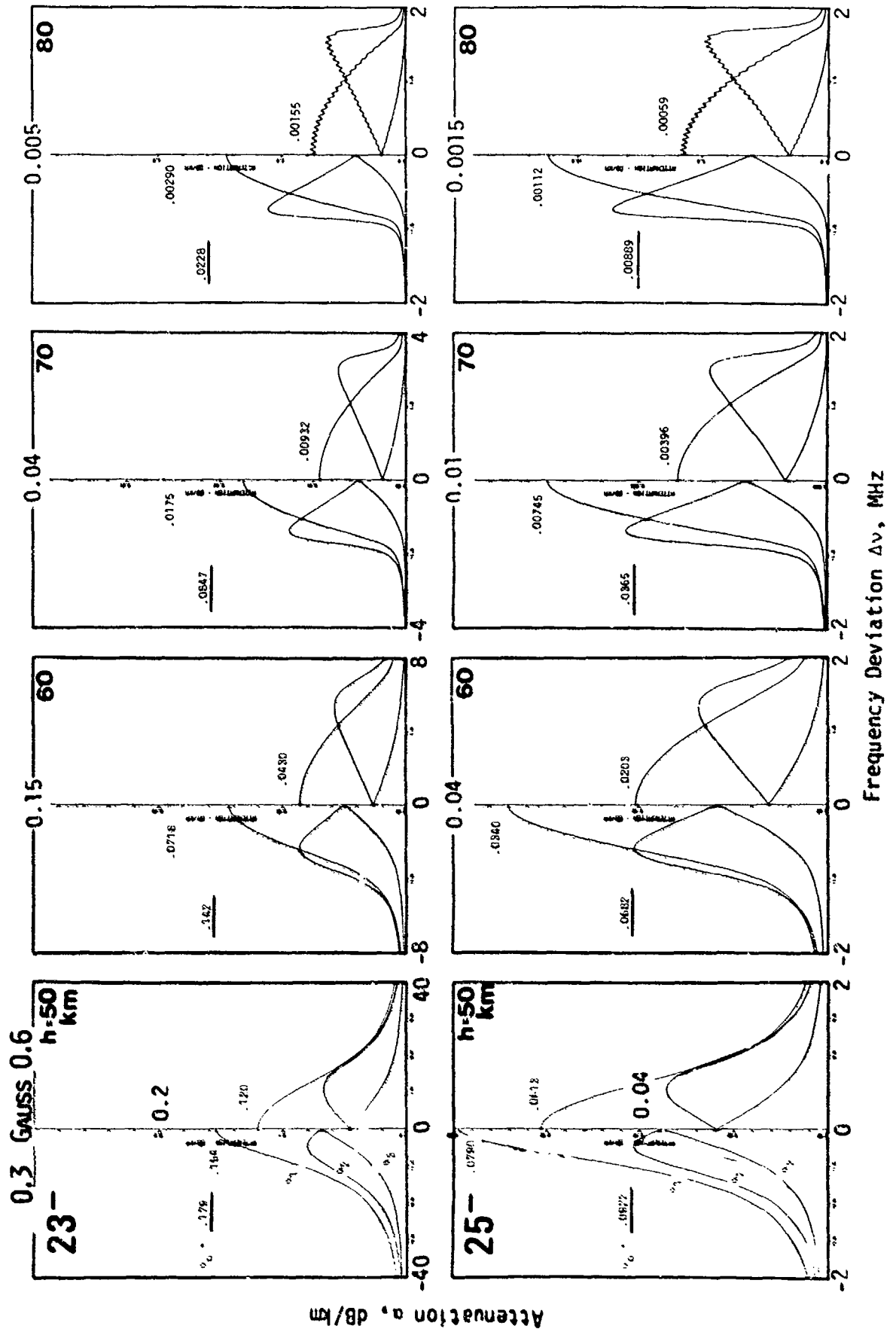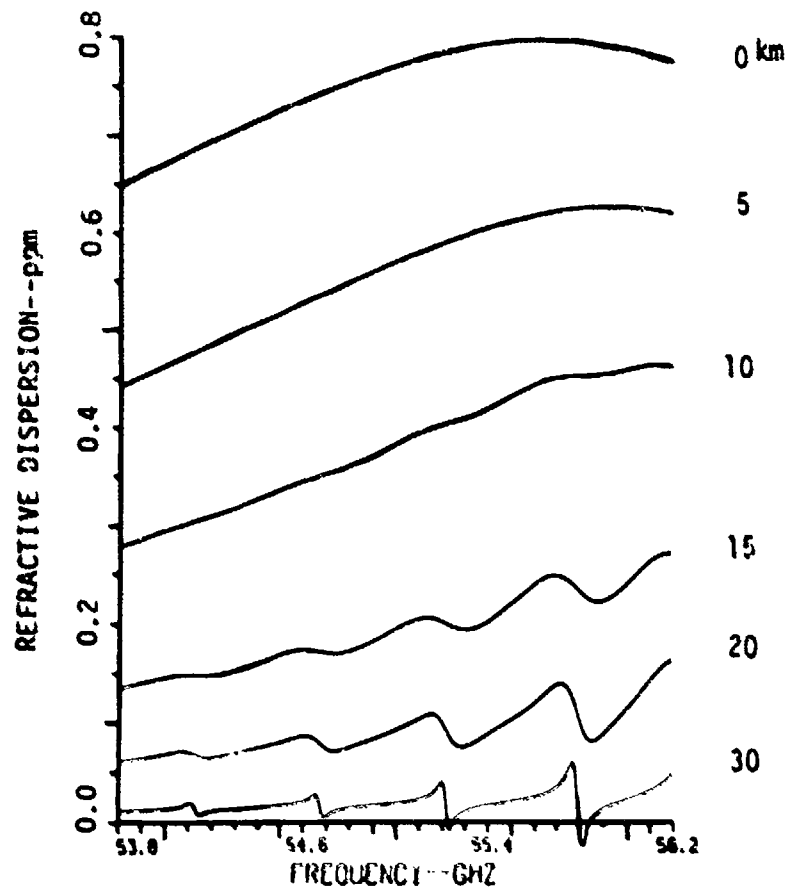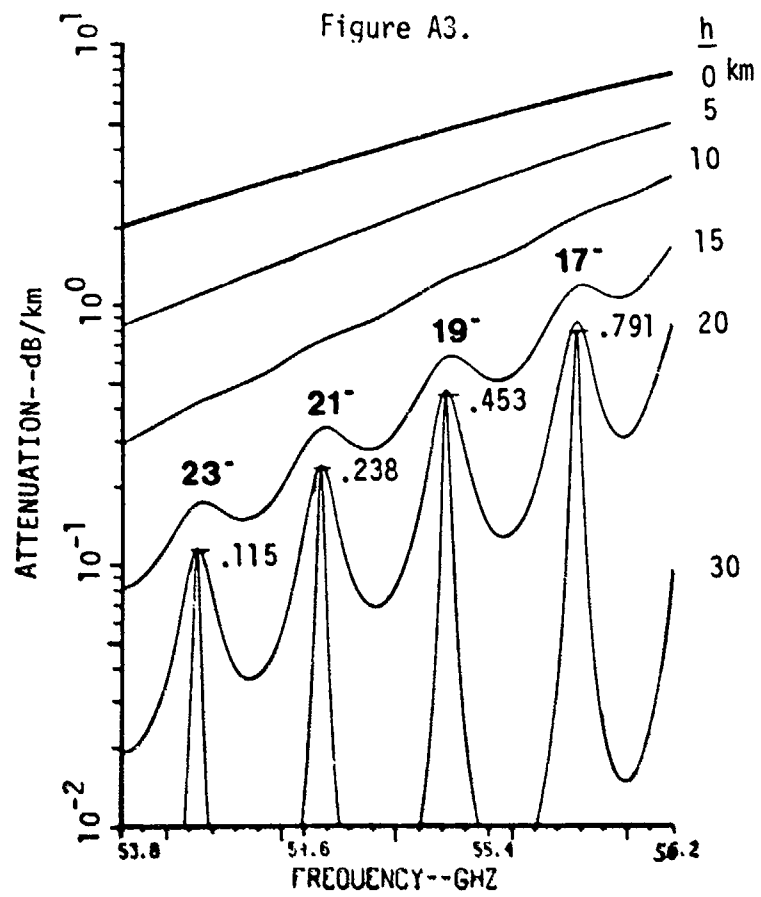
Figure A3. continued
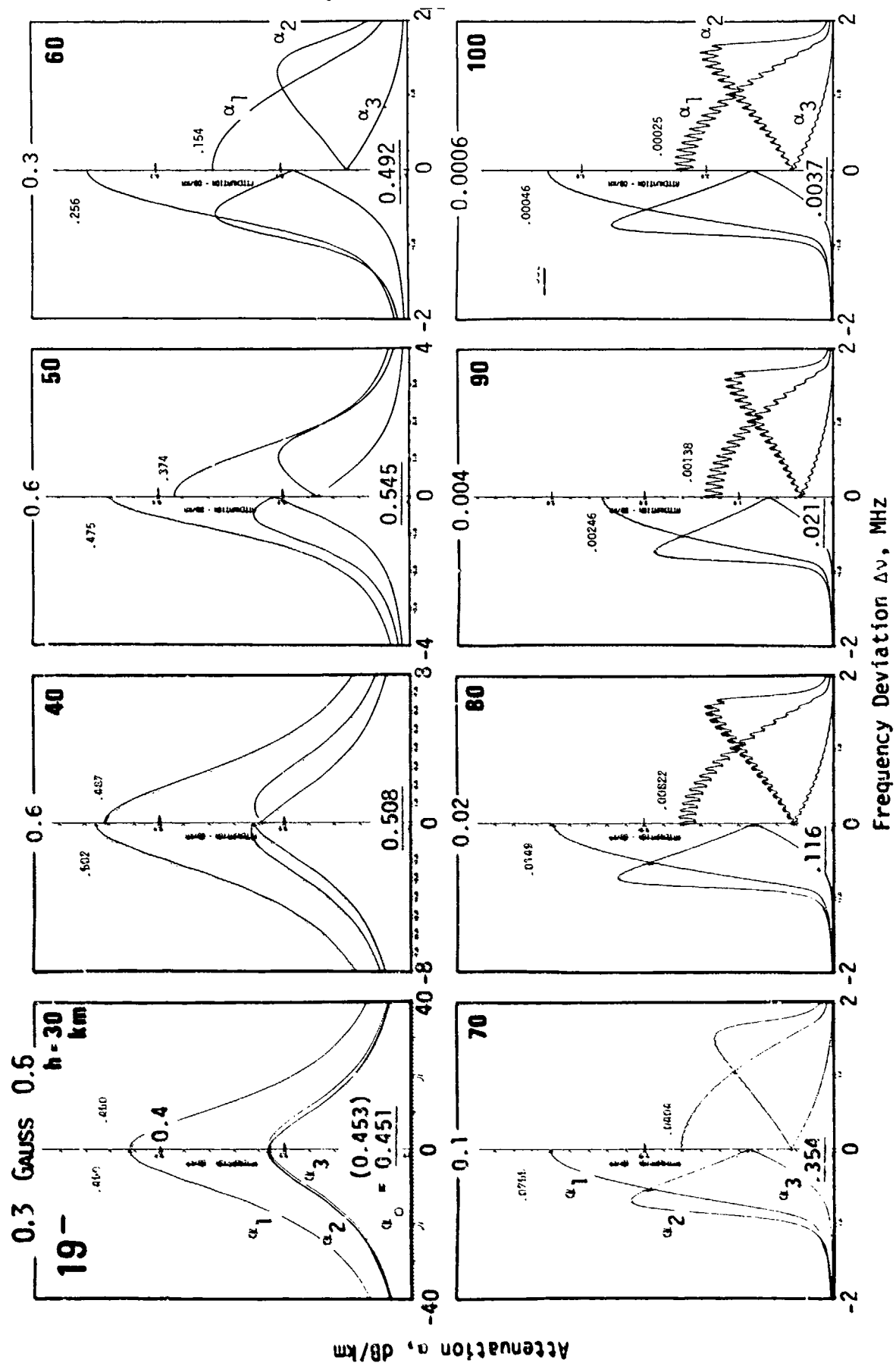
Figure A3. continued

Figure A4.

67
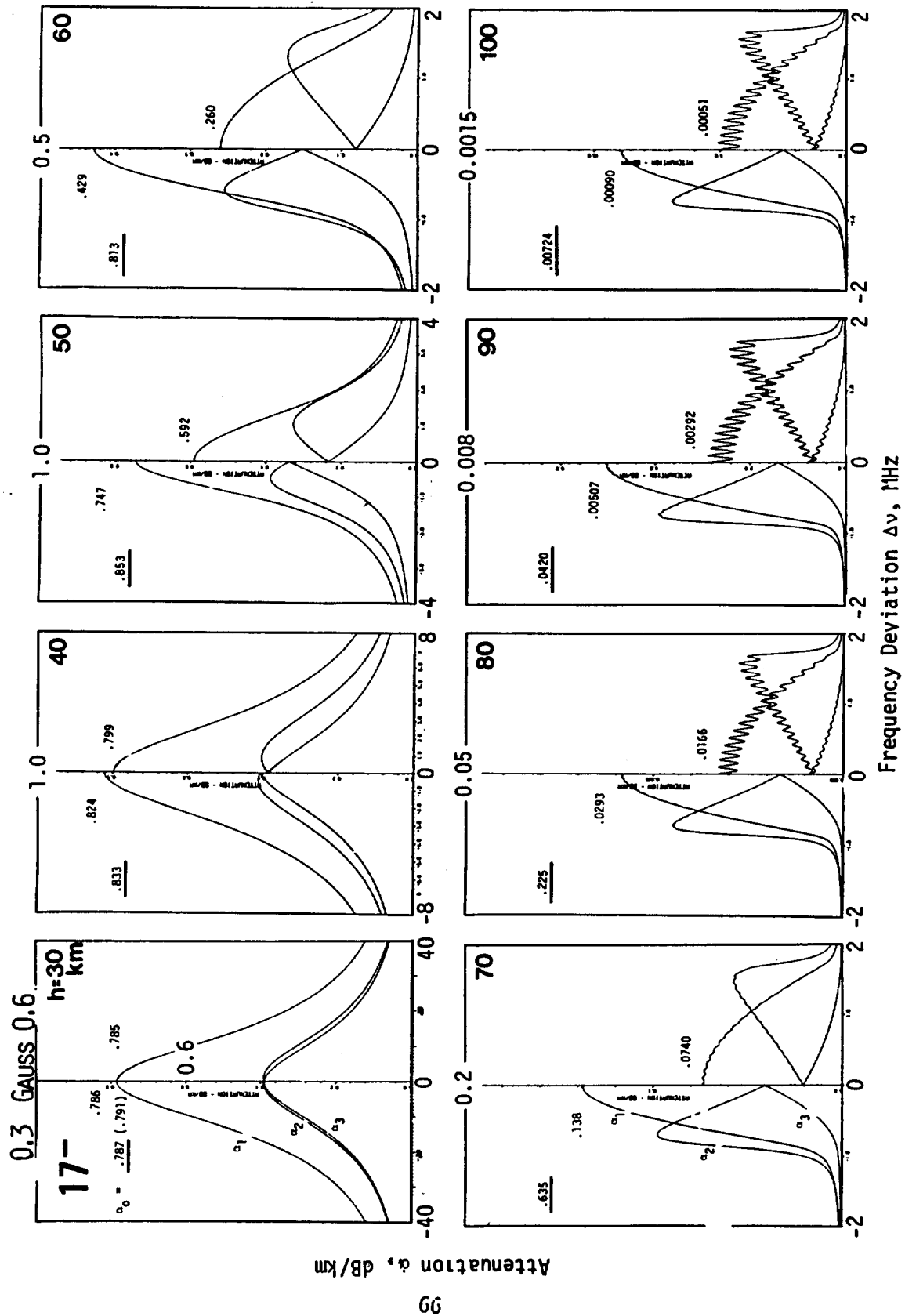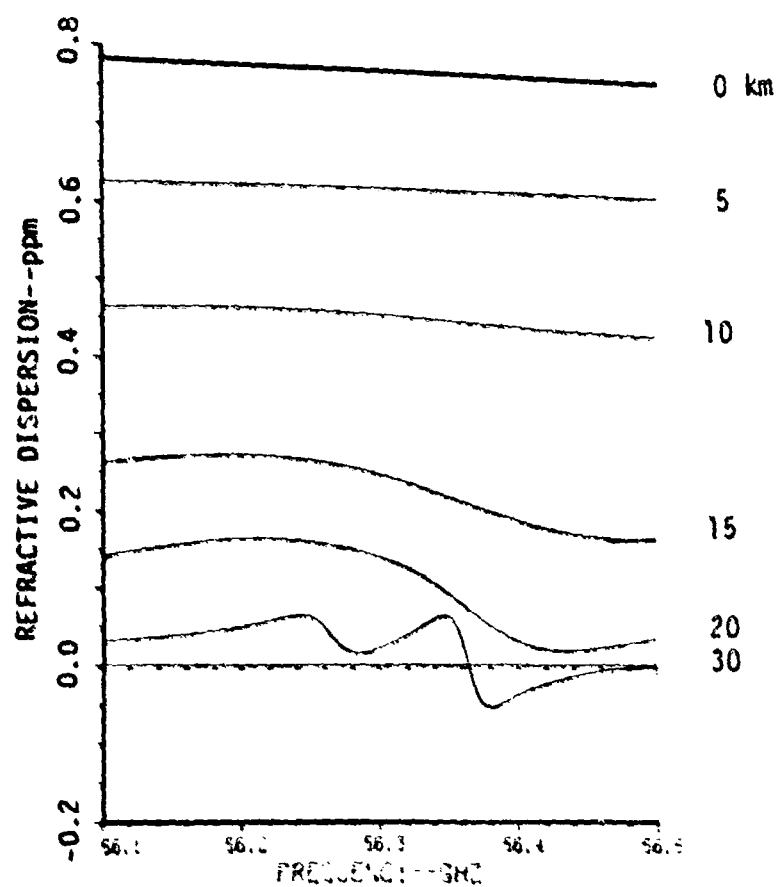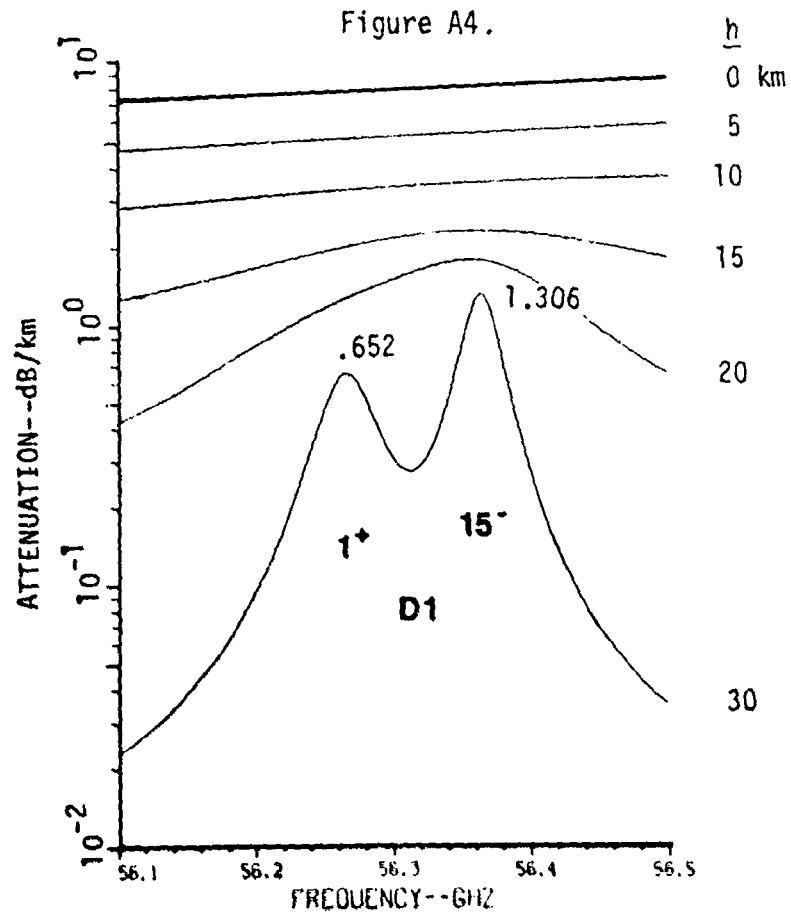
Figure A4. continued

Figure A5.

70

Figure A5. continued

Frequency Deviation Δν, MHz

Attenuation α, dB/km

71

Figure A5. continued

Attenuation α, dB/km

Frequency Deviation $\Delta\nu$, MHz
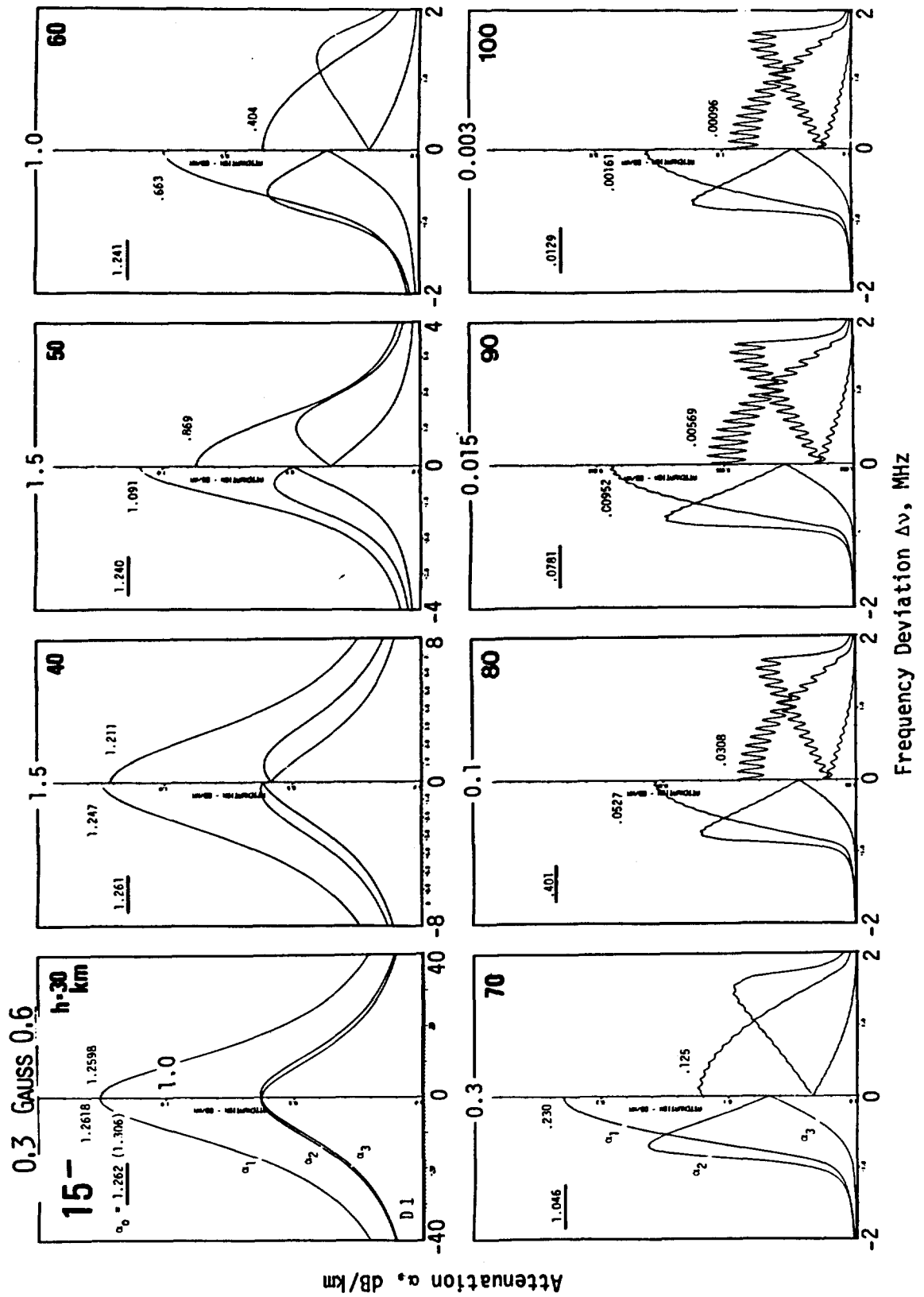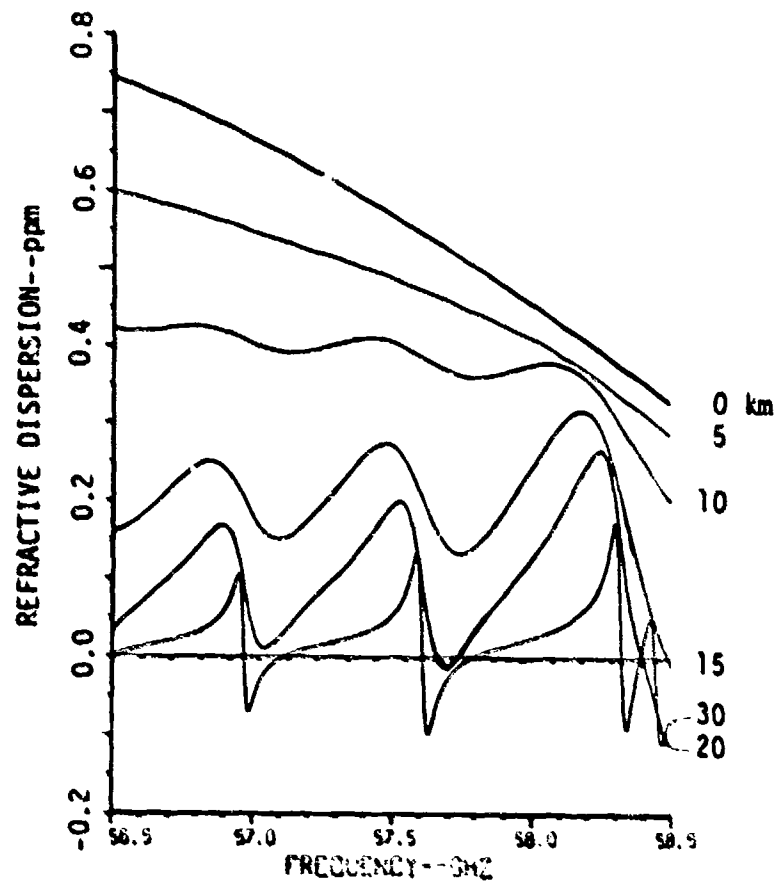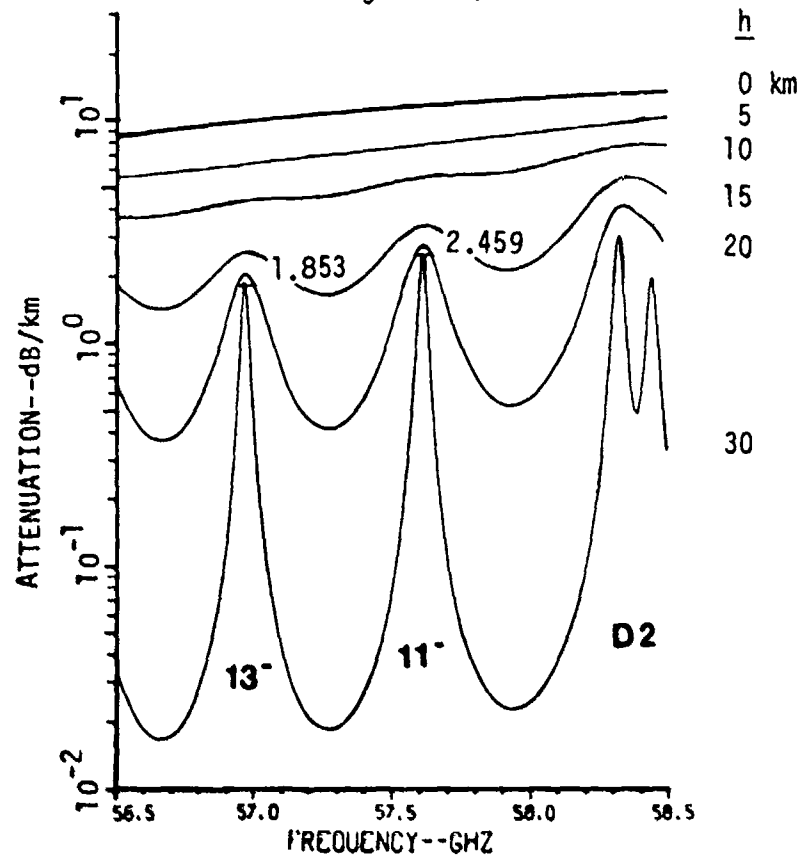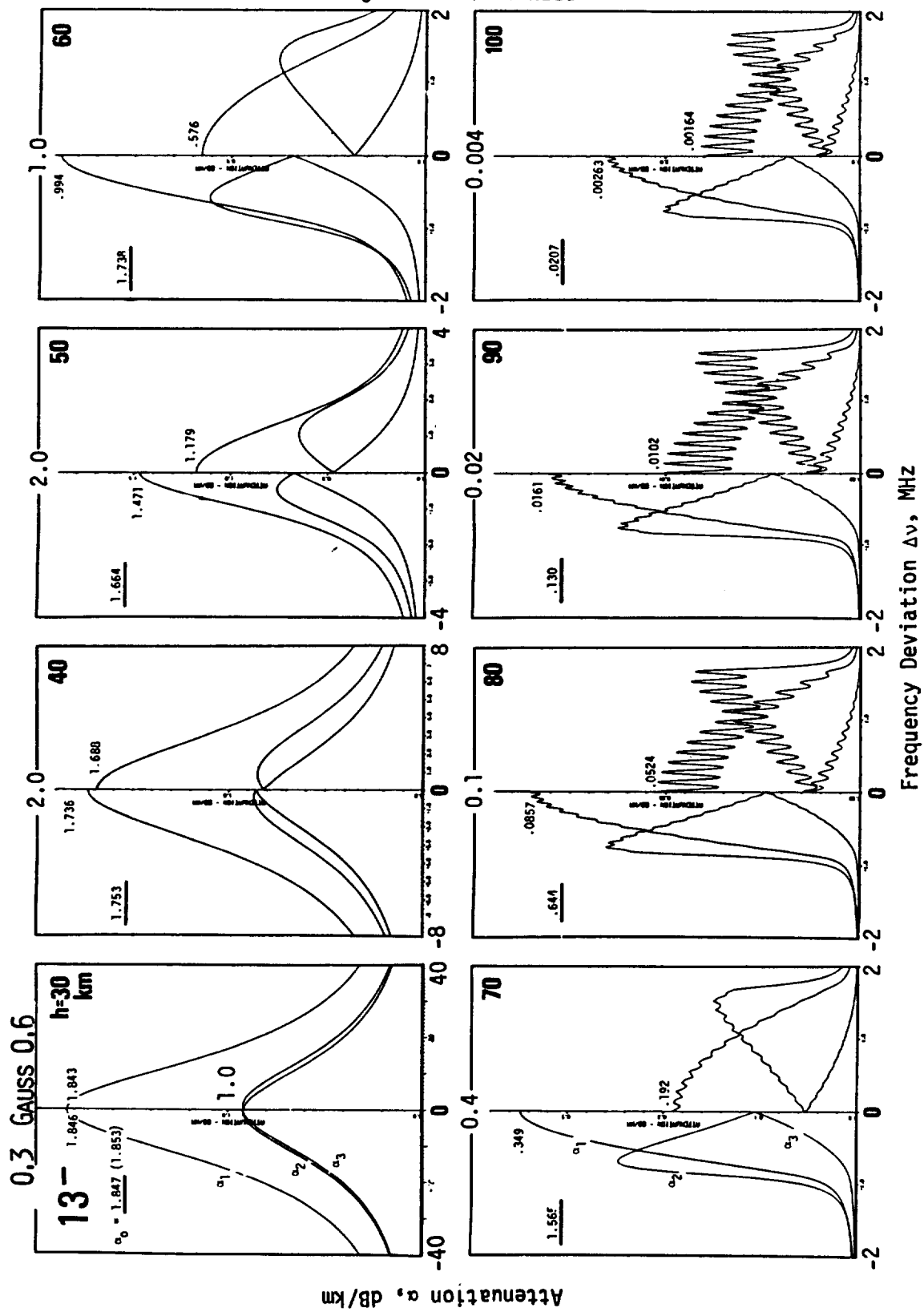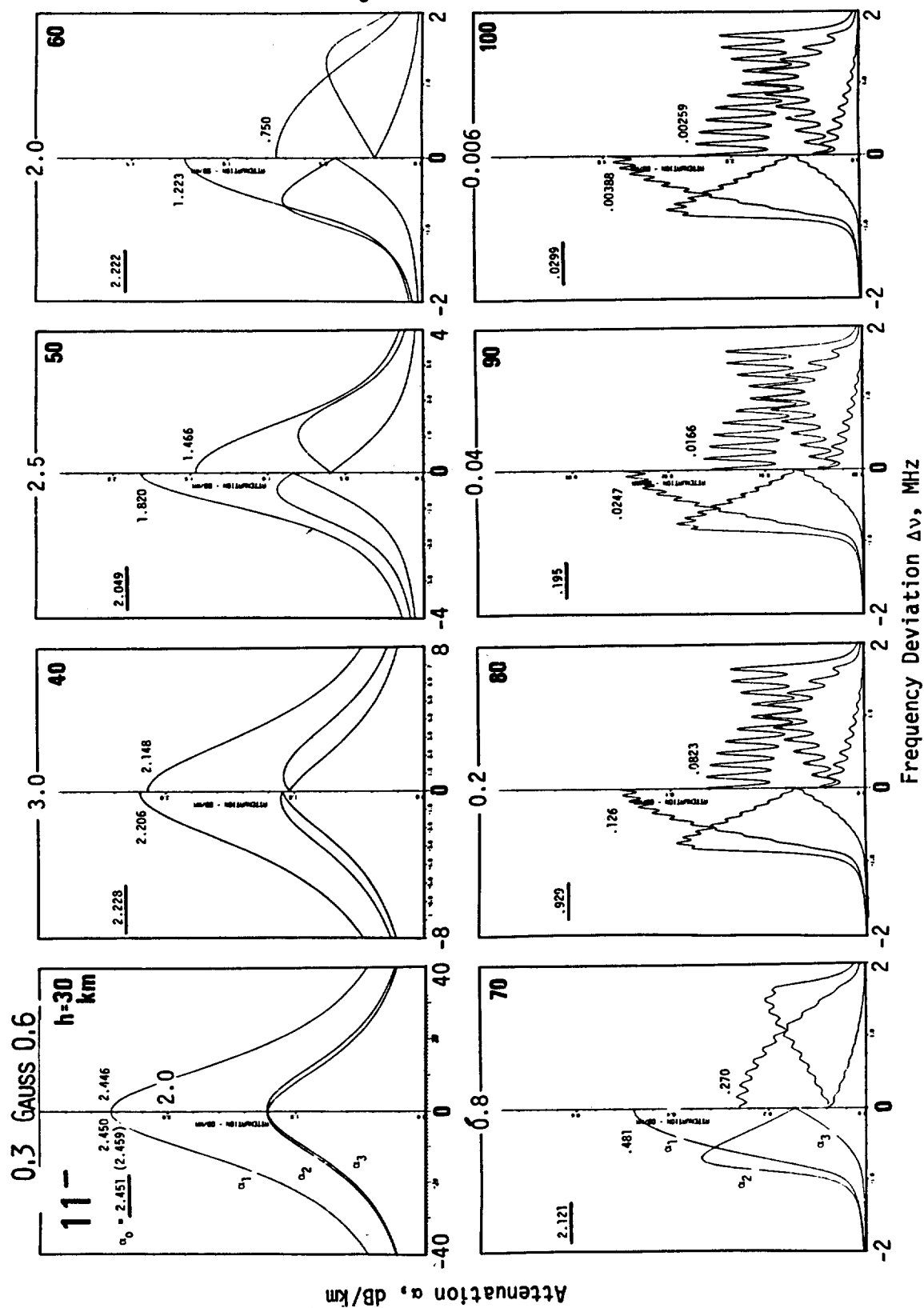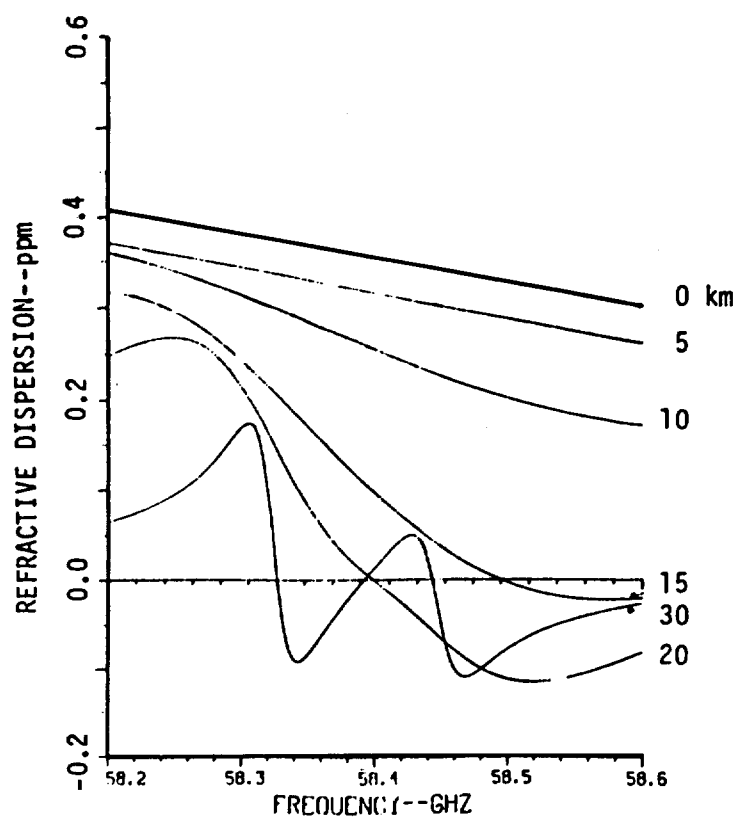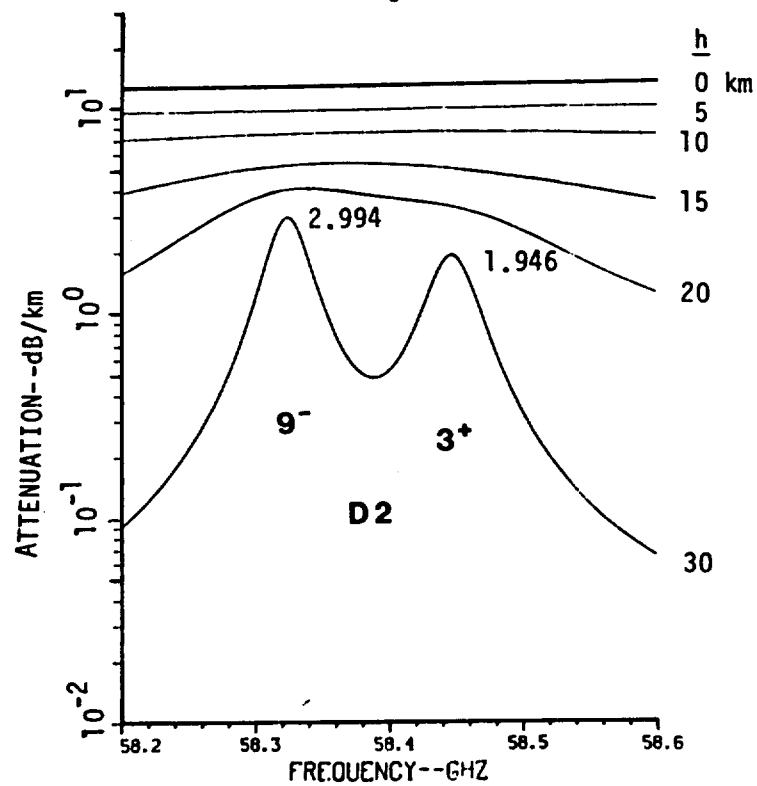
Figure A6.

Figure A6. continued
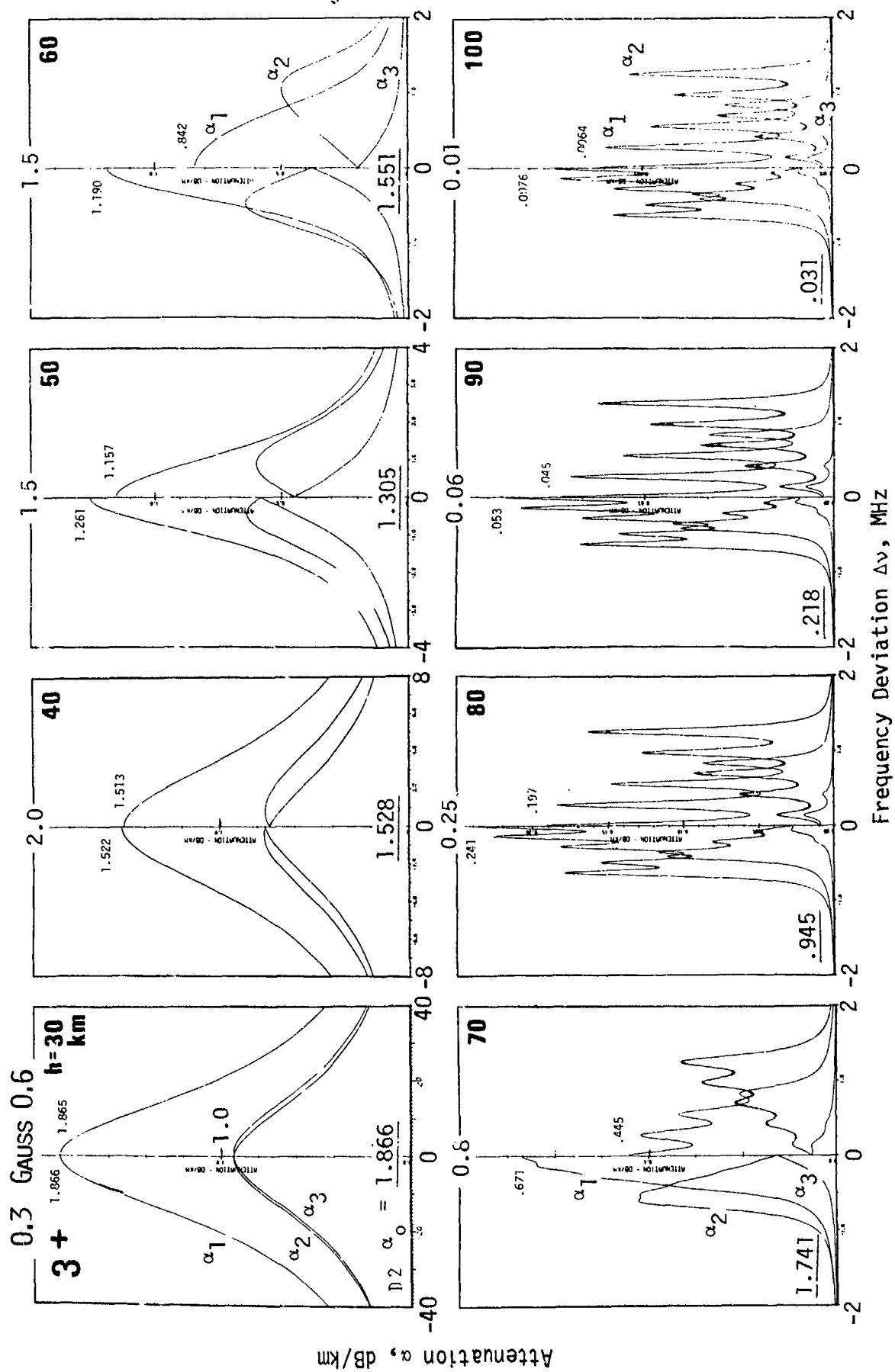
Figure A7.
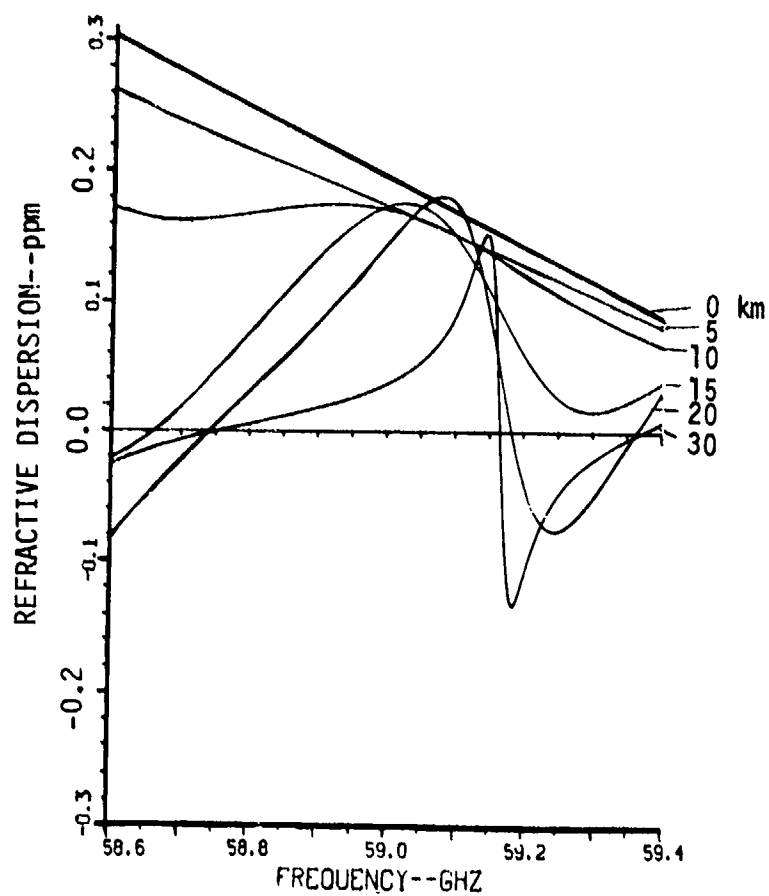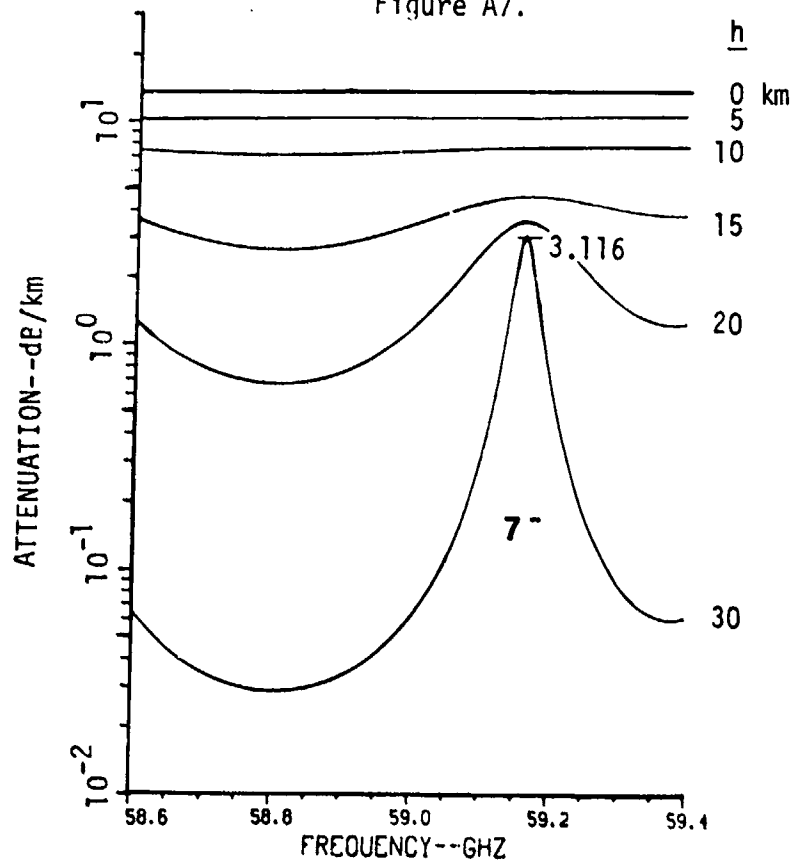
Figure A7. continued

Figure A8.

78

Figure A8. continued

Attenuation α, dB/km

Frequency Deviation Δν, MHz

79
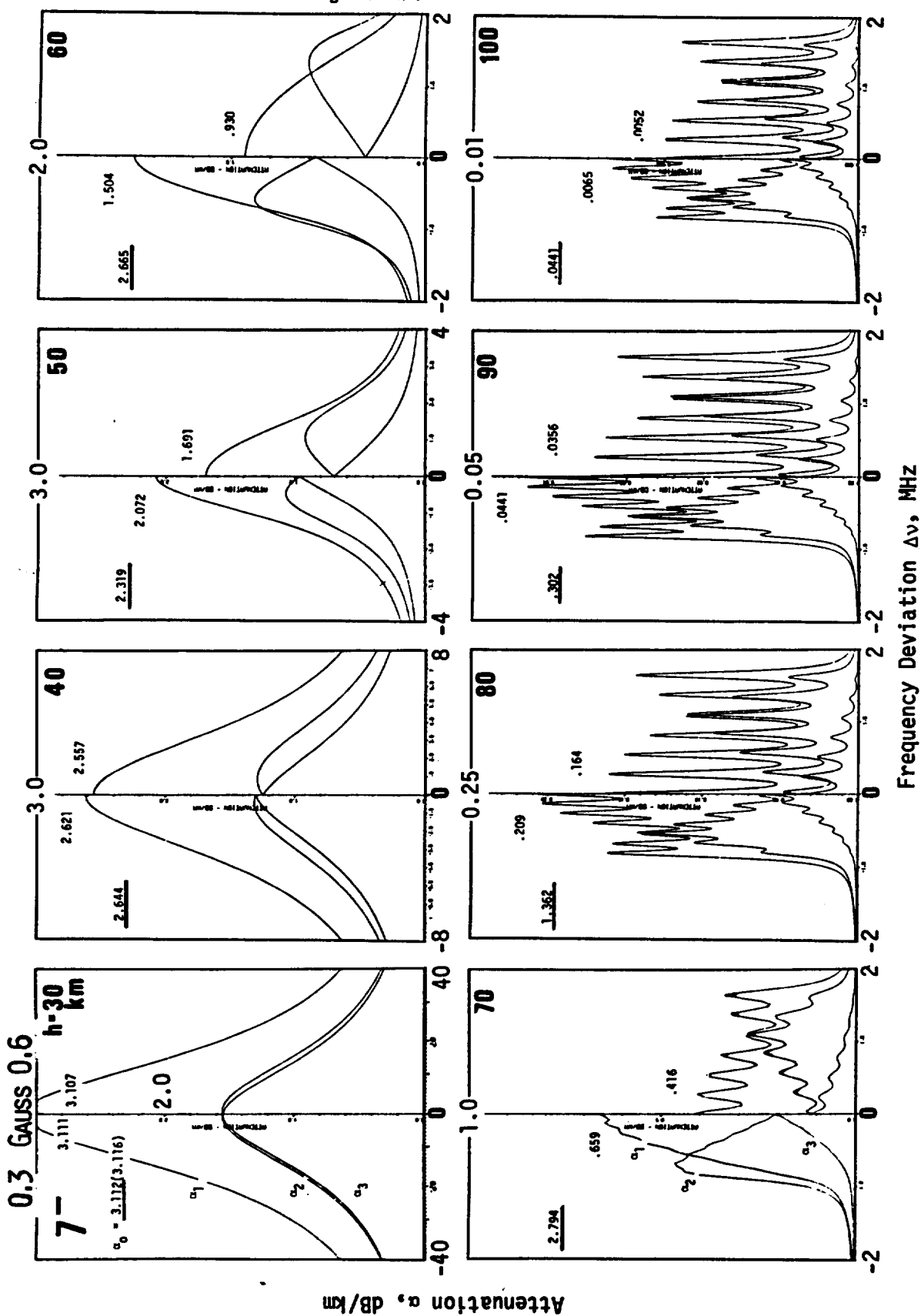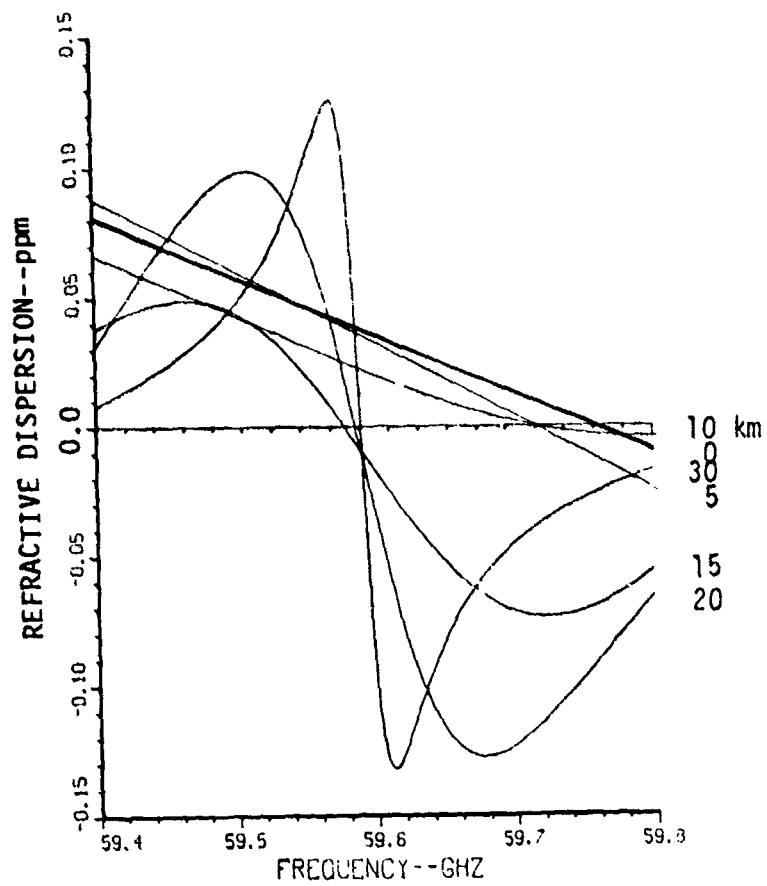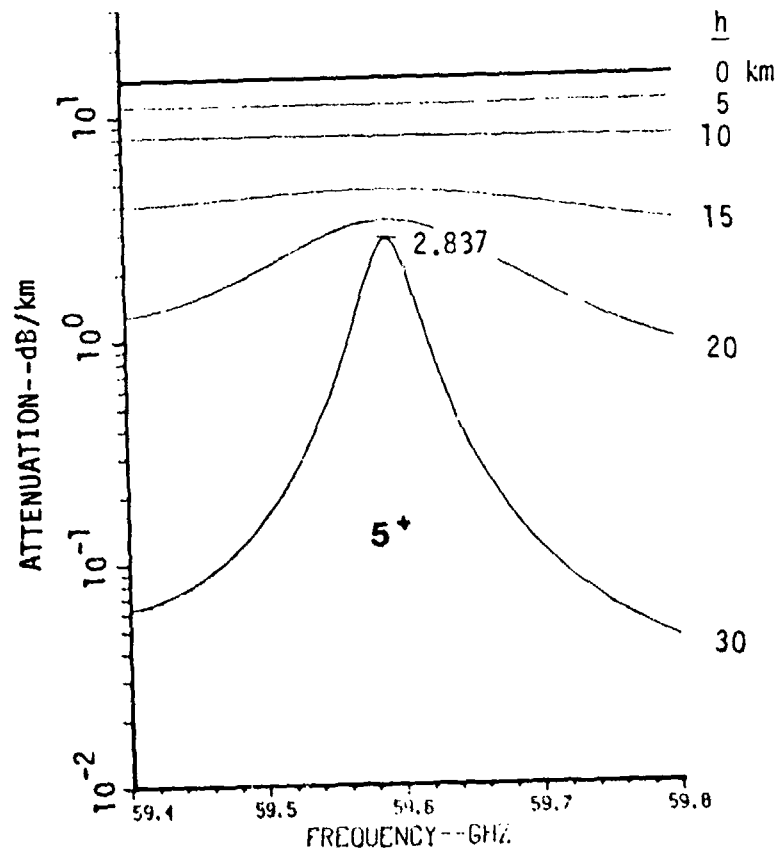
Figure A9.

Figure A9. continued

81

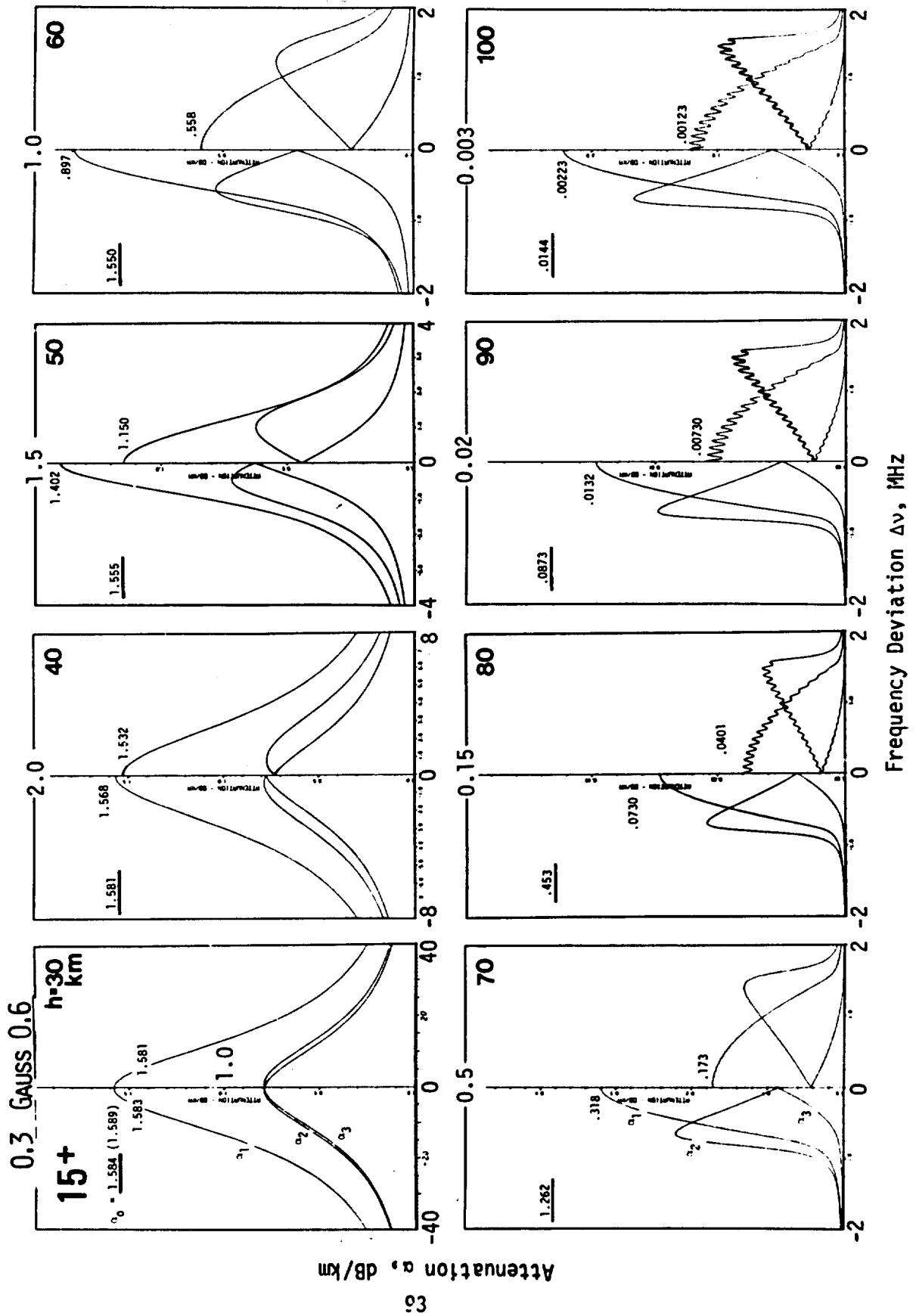# Figure A9. continued

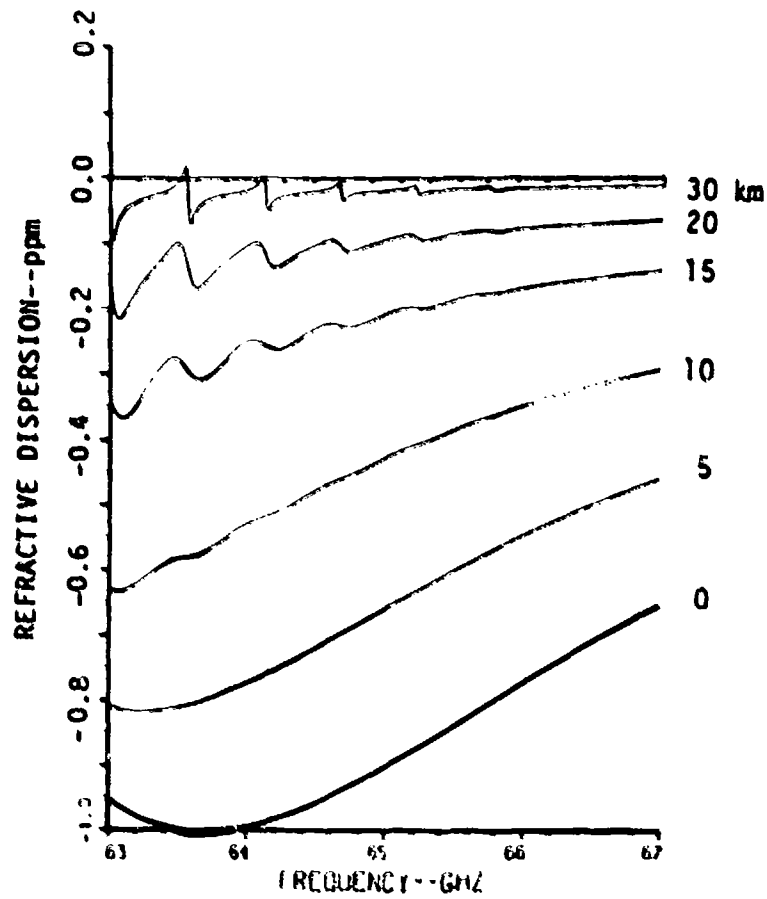Attenuation α, dB/km

Frequency Deviation Δν, MHz

32
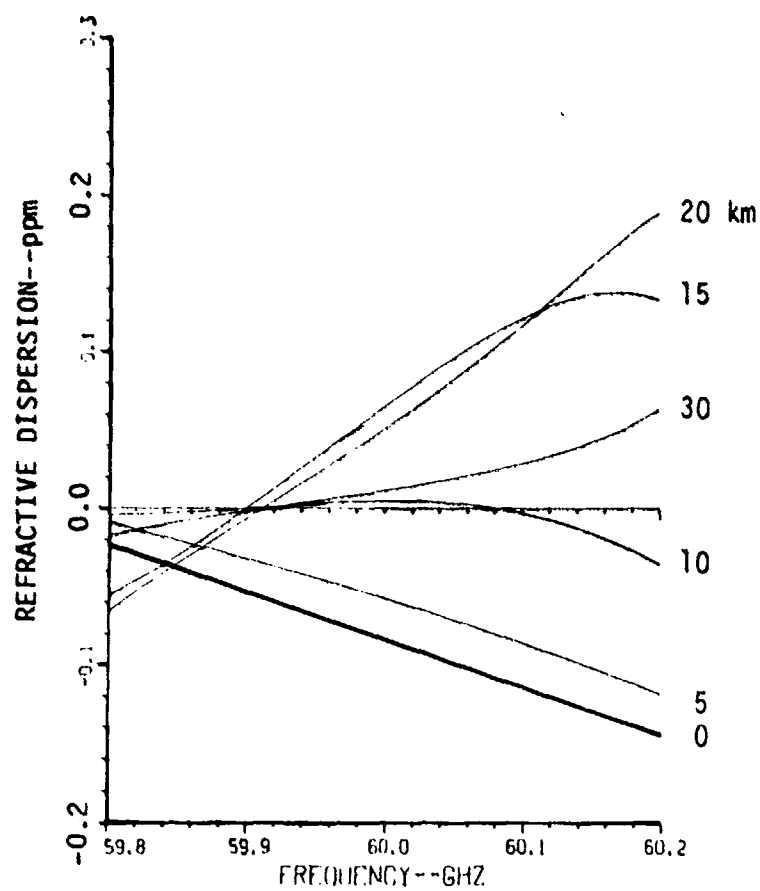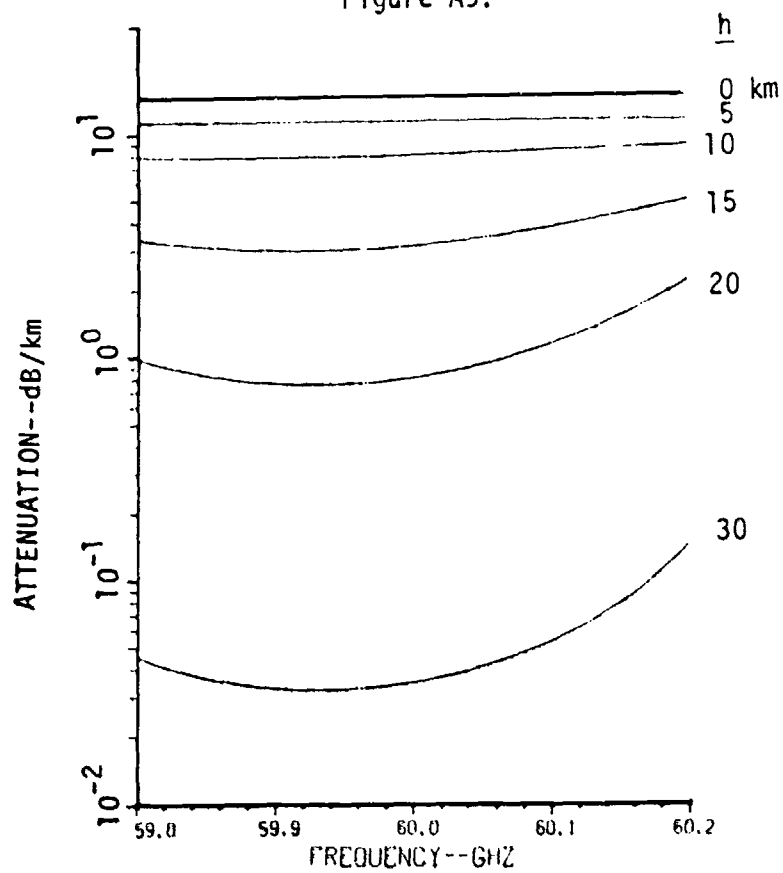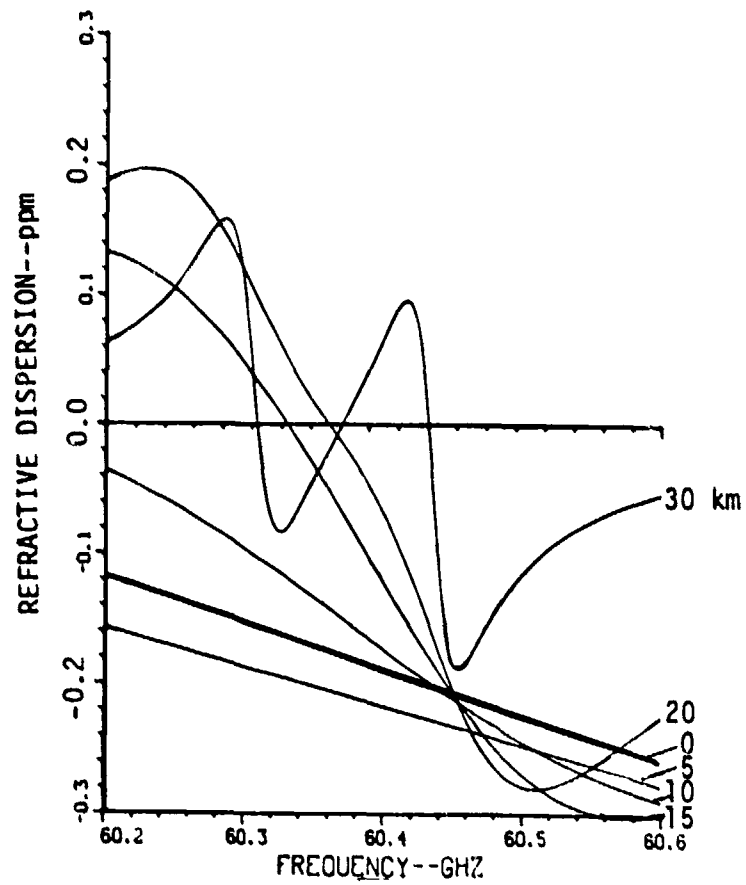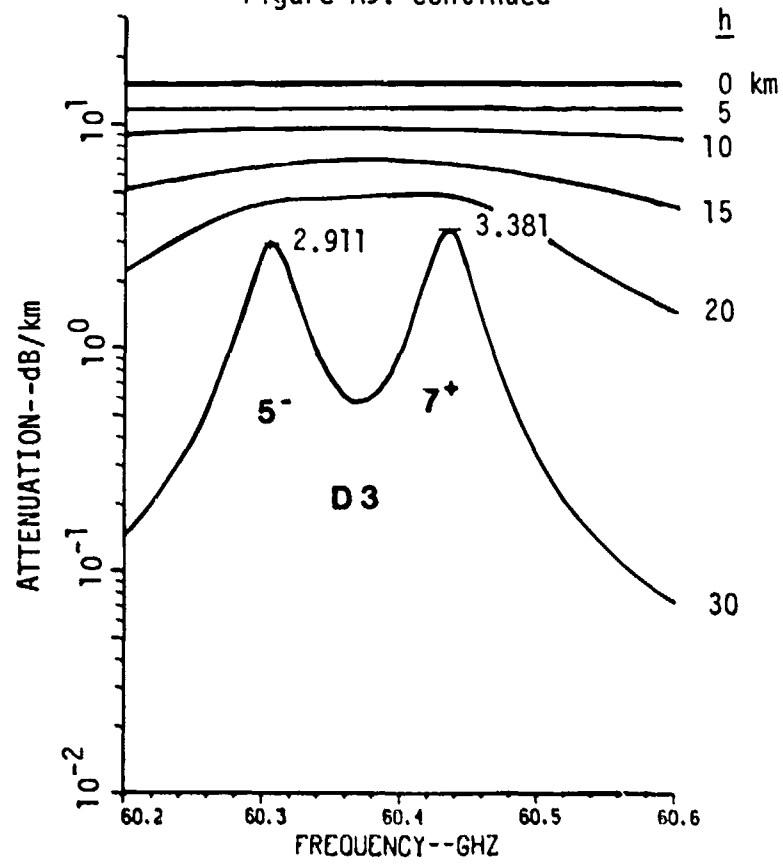
Figure A9. continued

Figure A10.

Figure A10. continued

85

Figure A10. continued

Frequency Deviation Δν, MHz

Attenuation α, dB/km

Figure A11.

Figure A12.

Frequency Deviation Δν, MHz

Attenuation α, dB/km
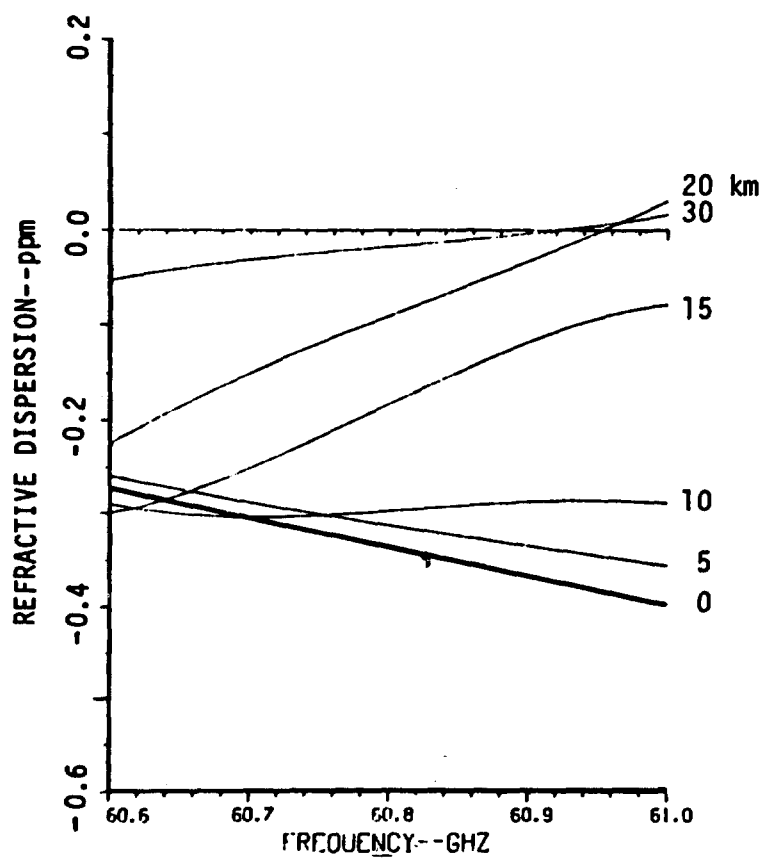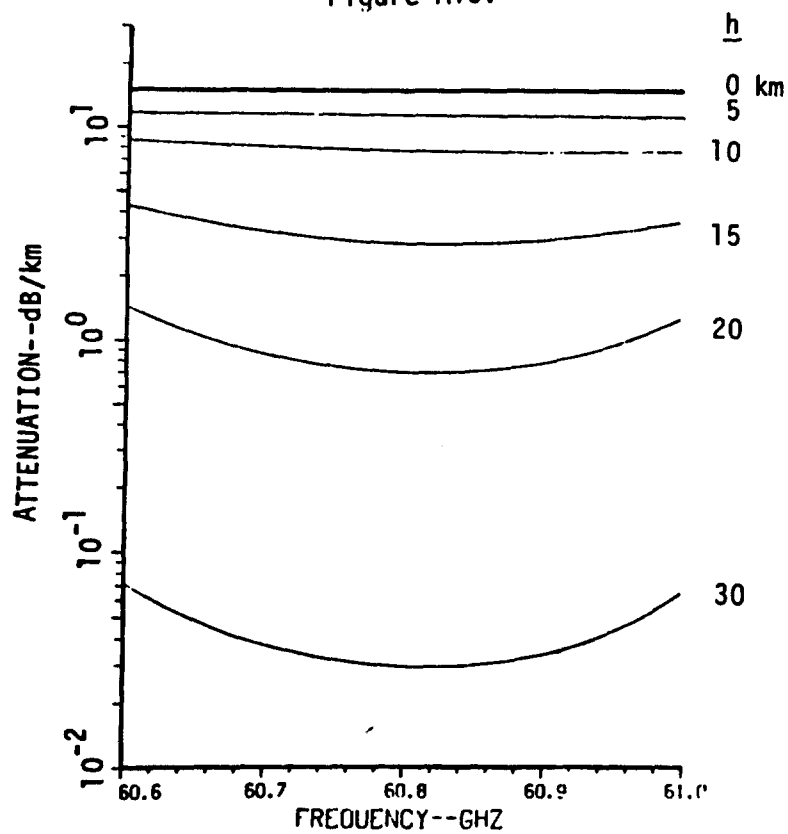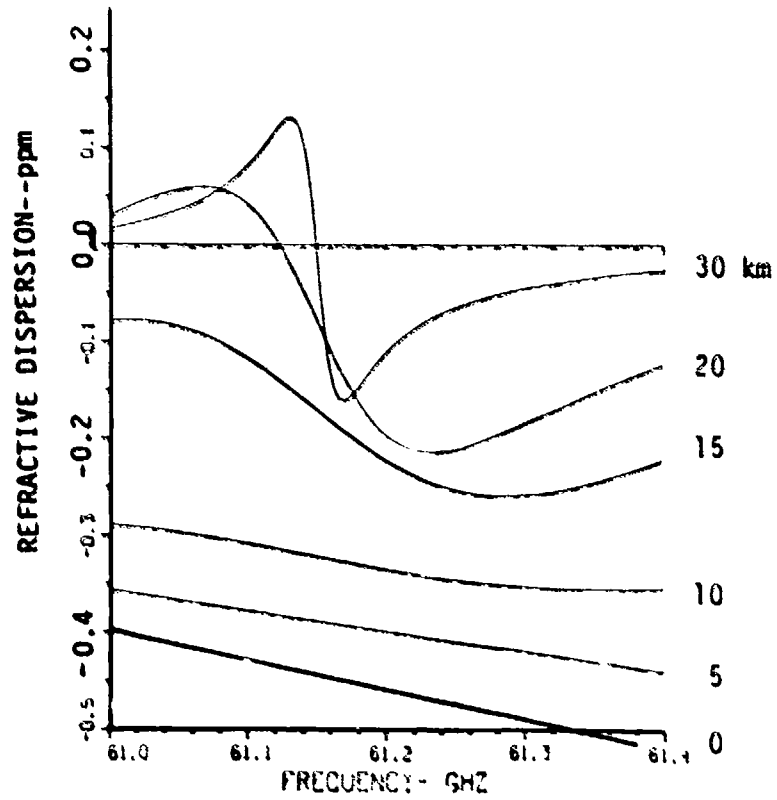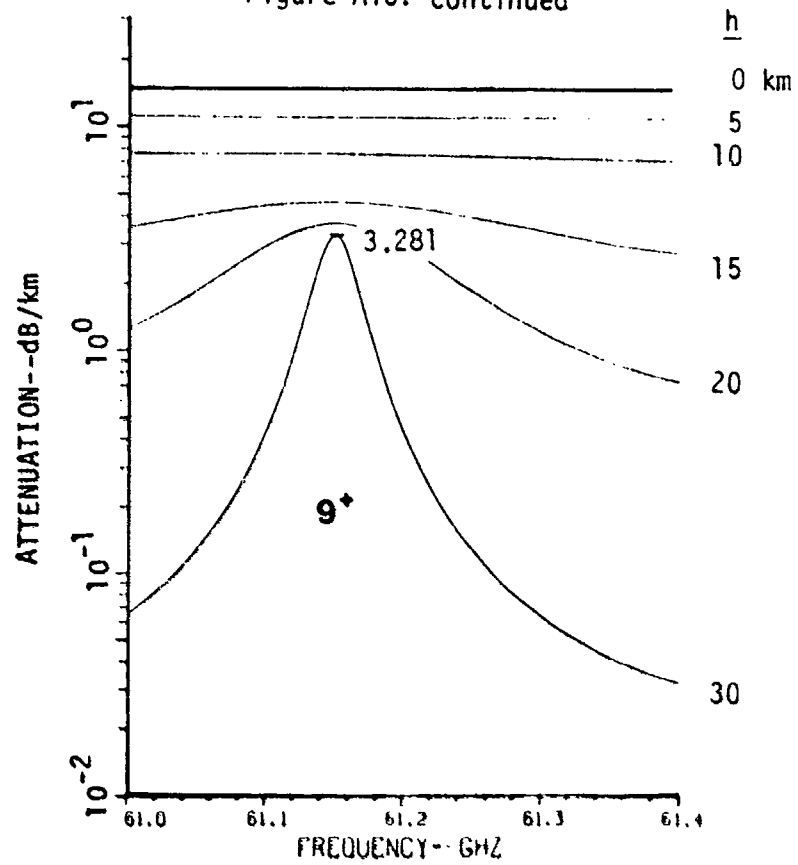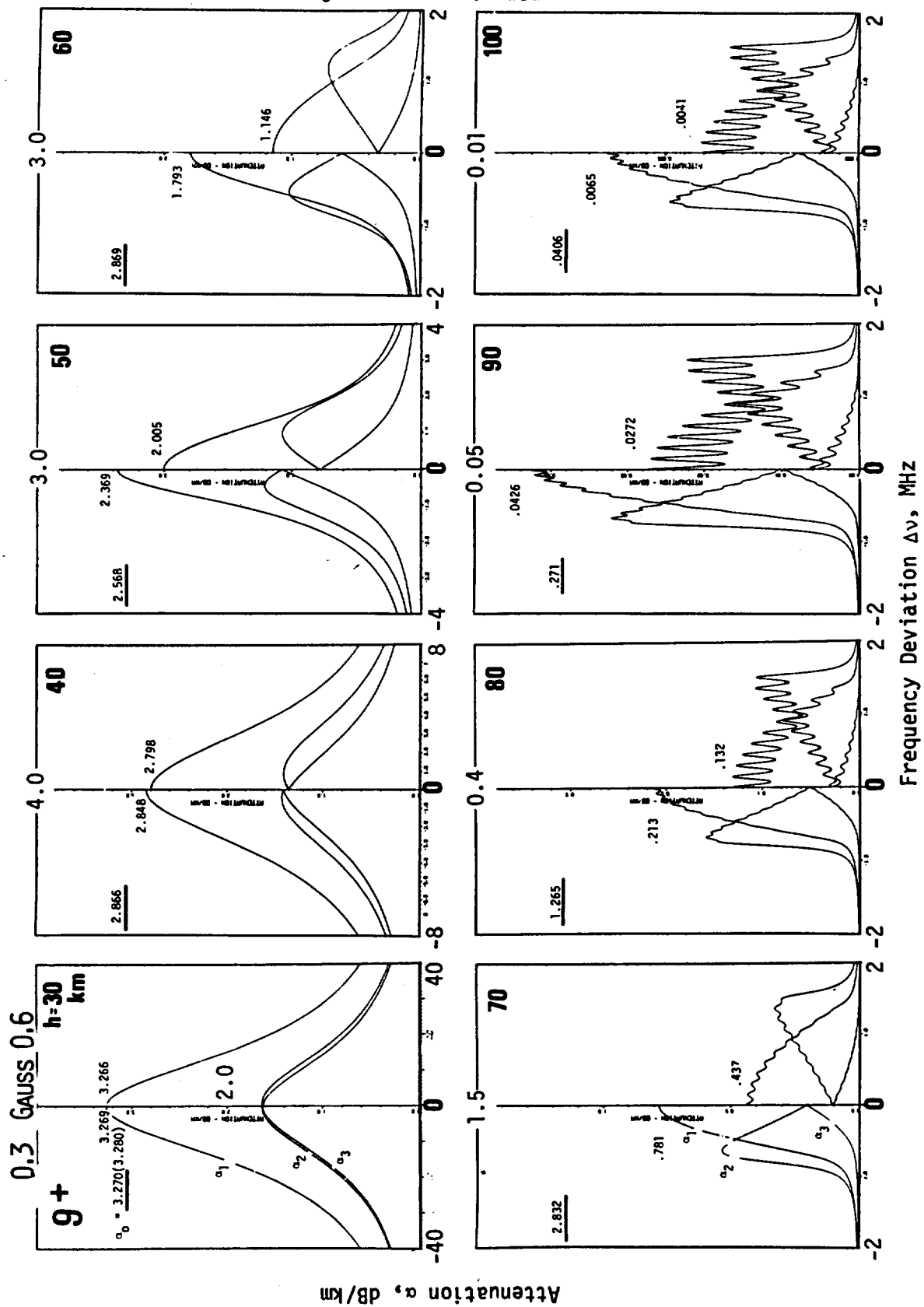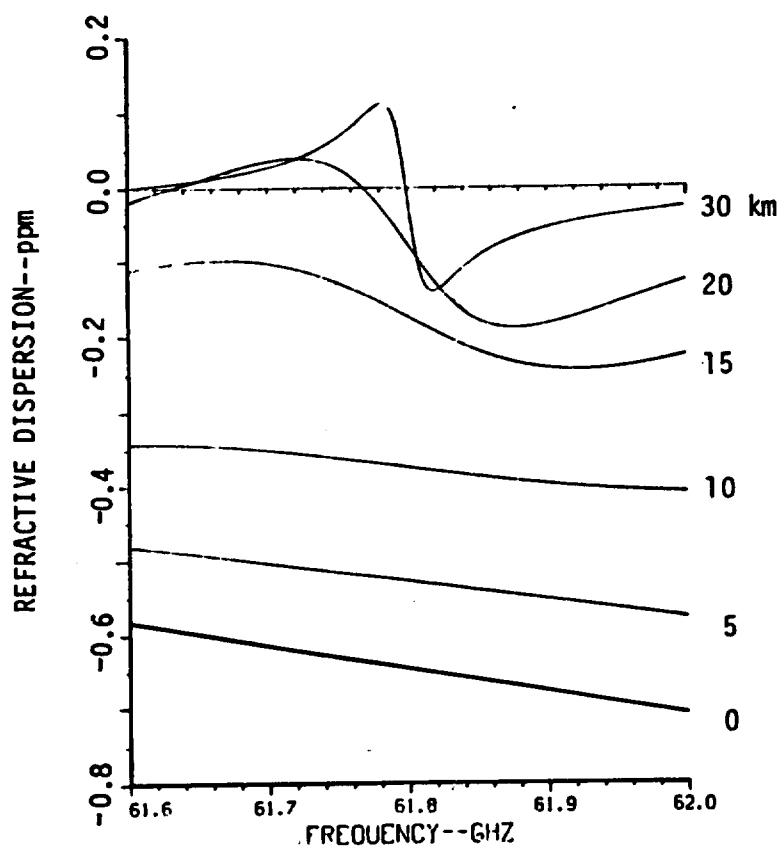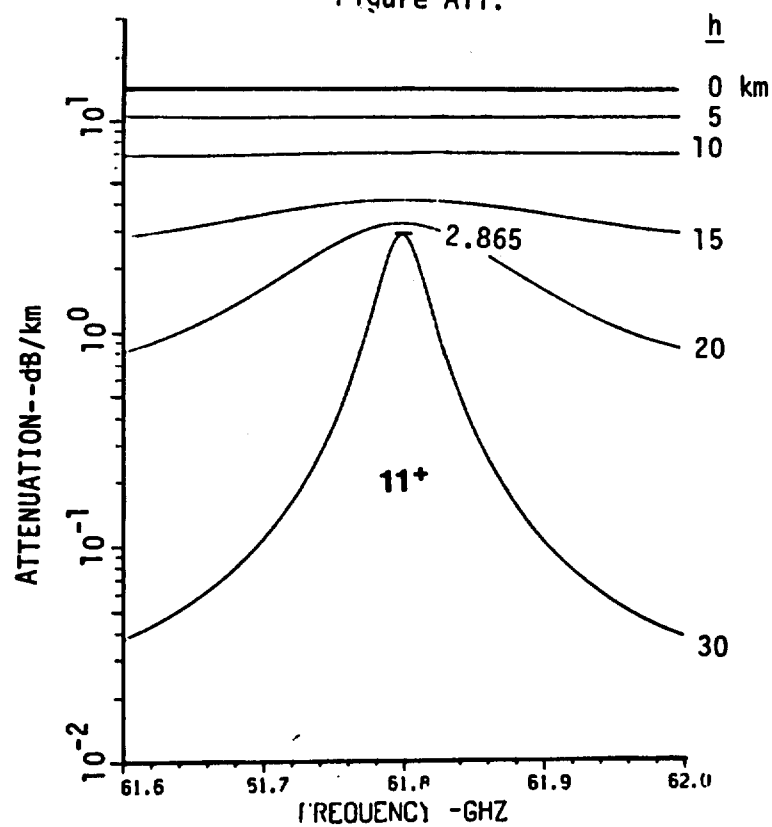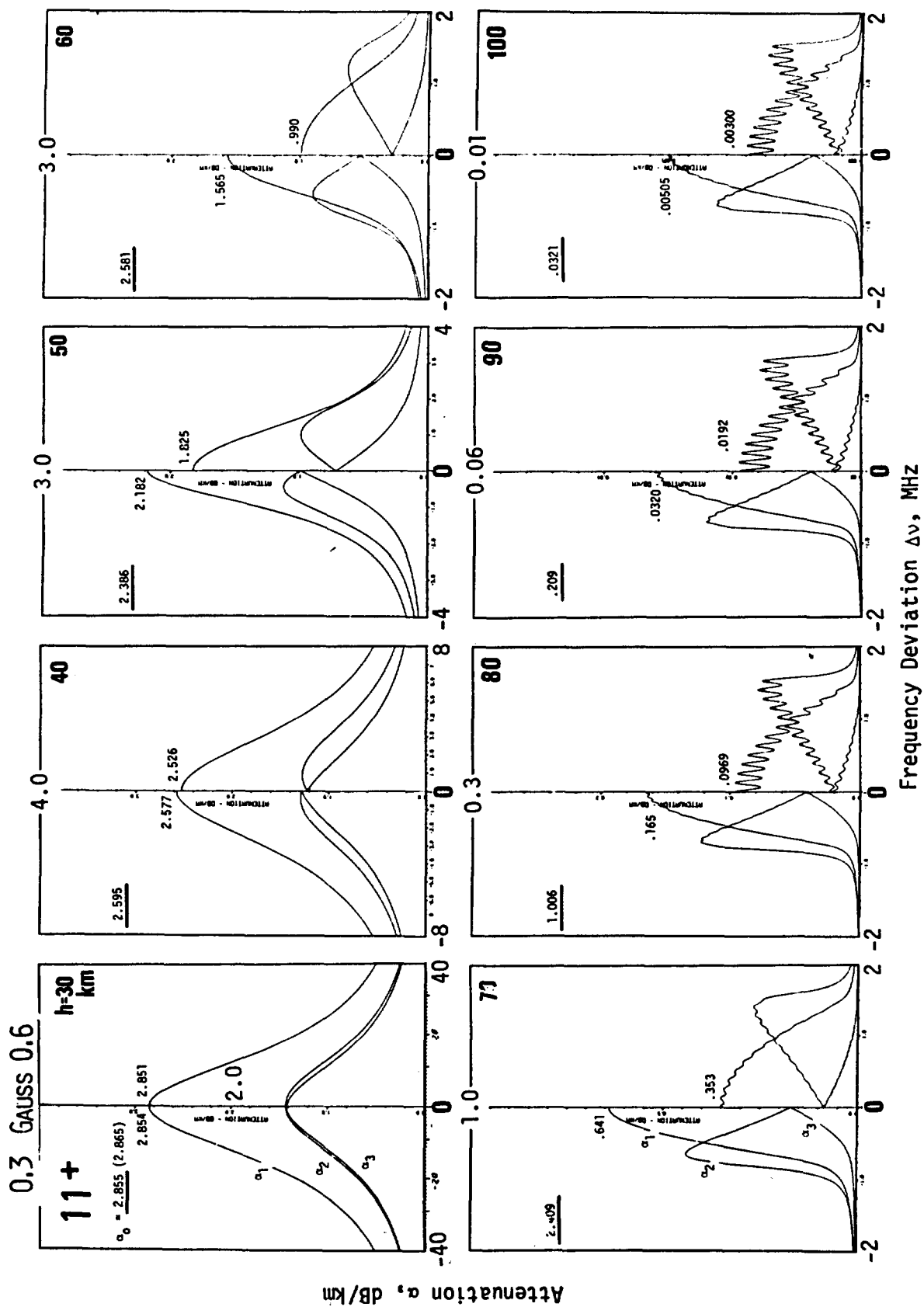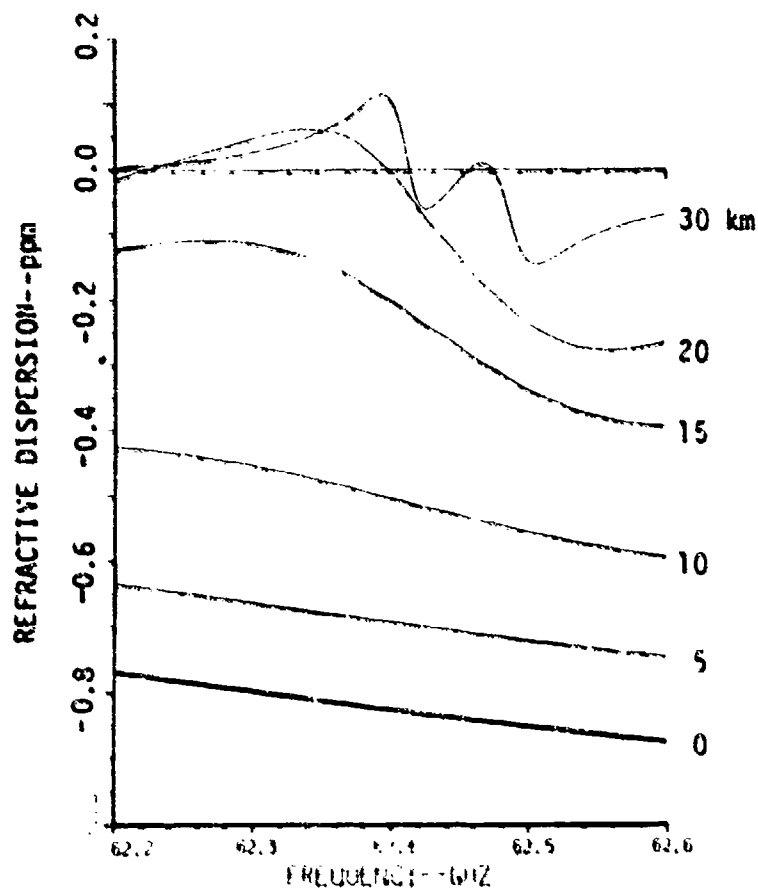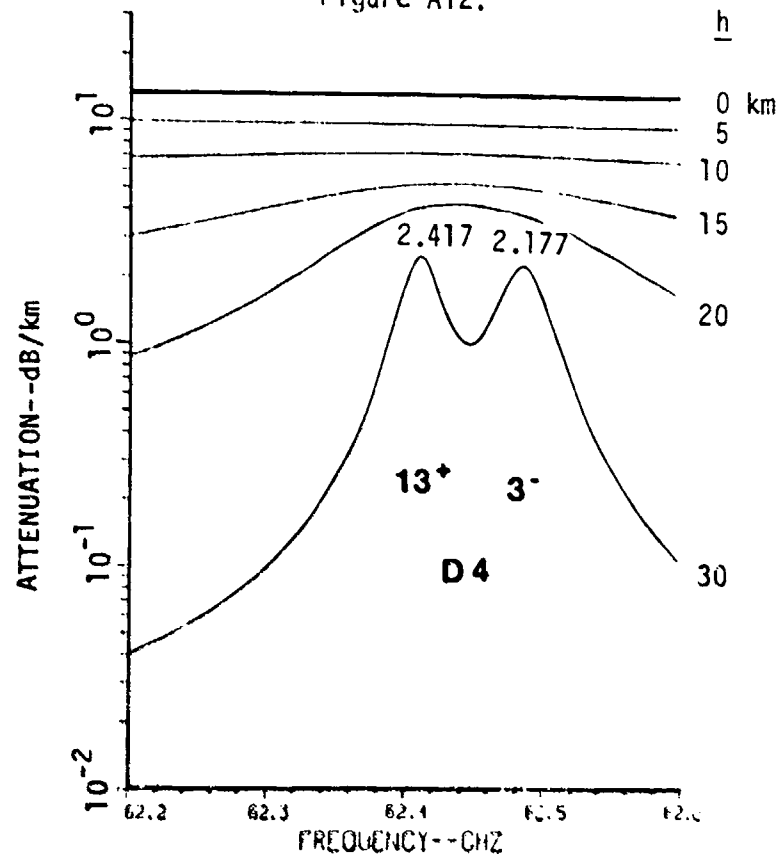
Figure A12. continued

Figure A13.
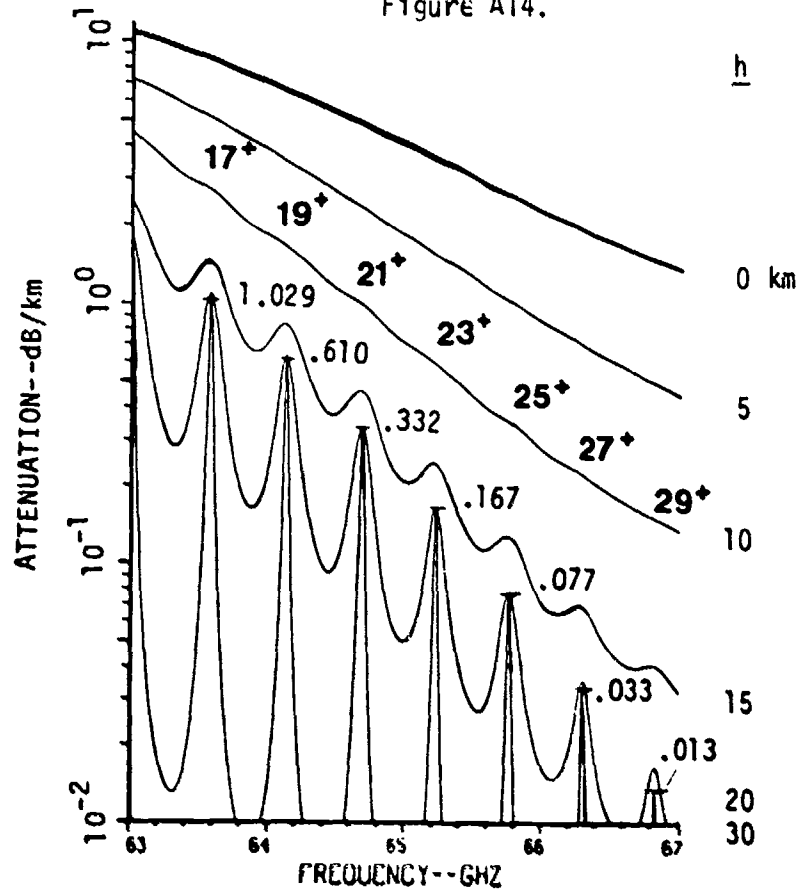
92

Figure A13. continued

Frequency Deviation Δν, MHz

Attenuation α, dB/km
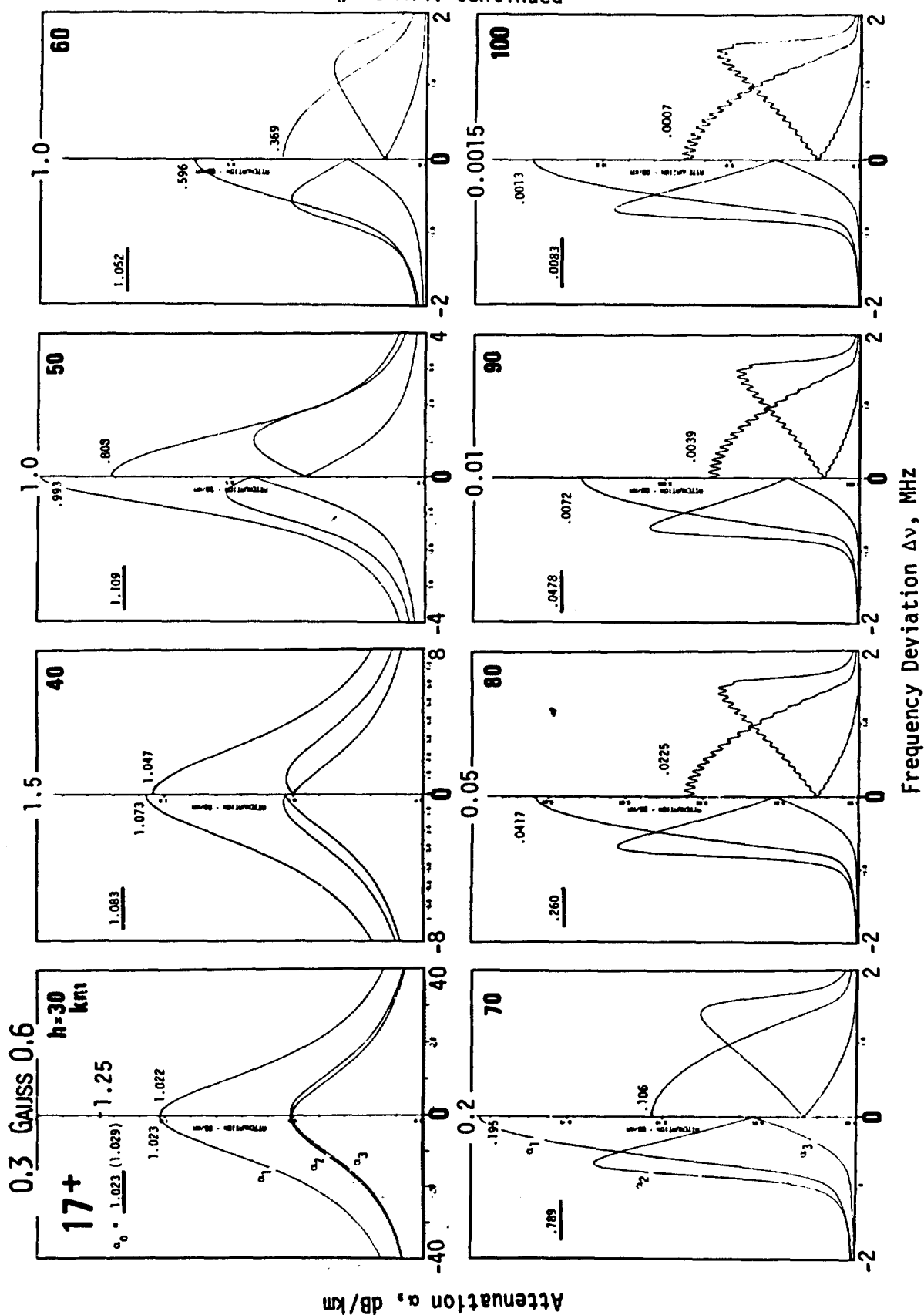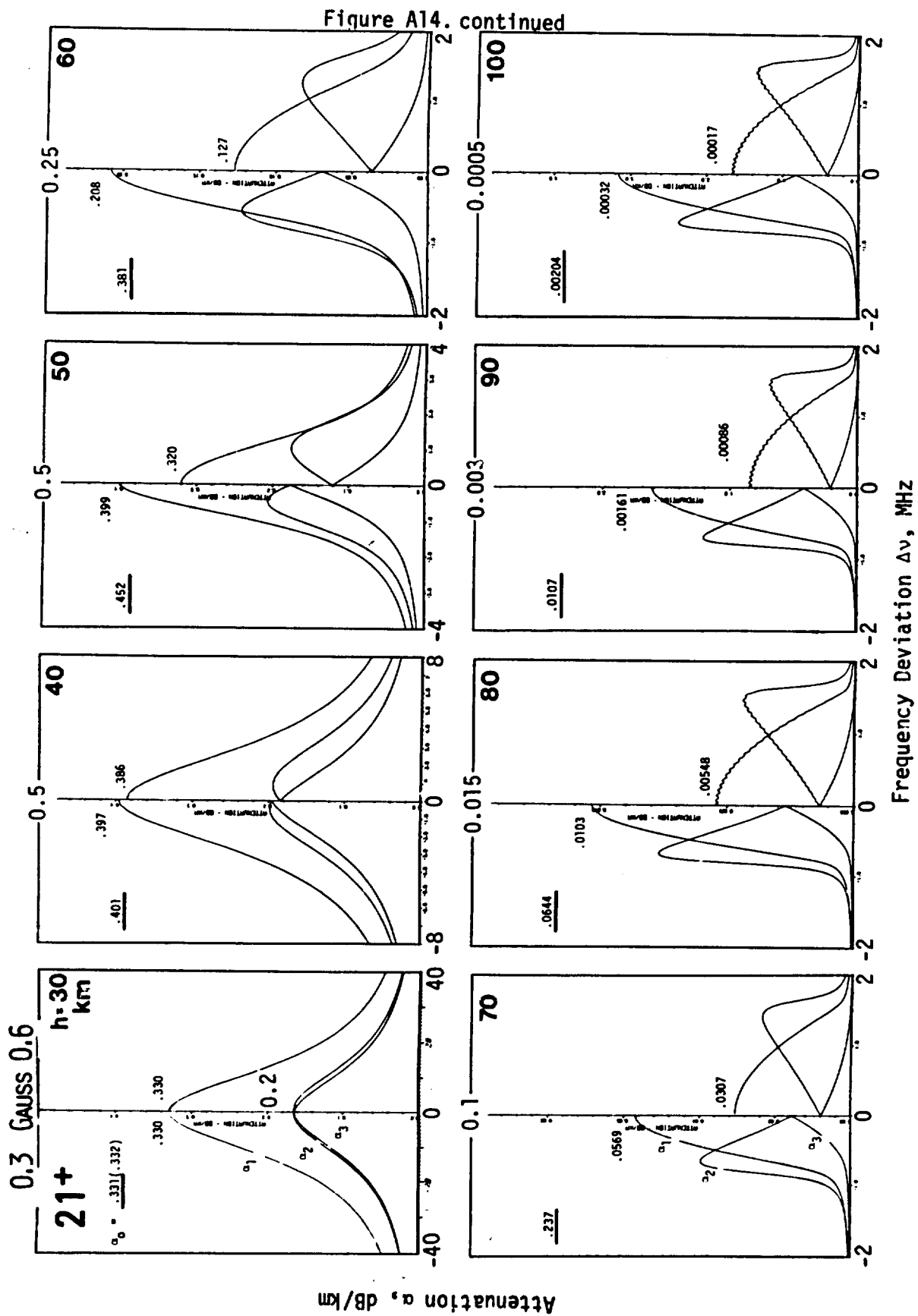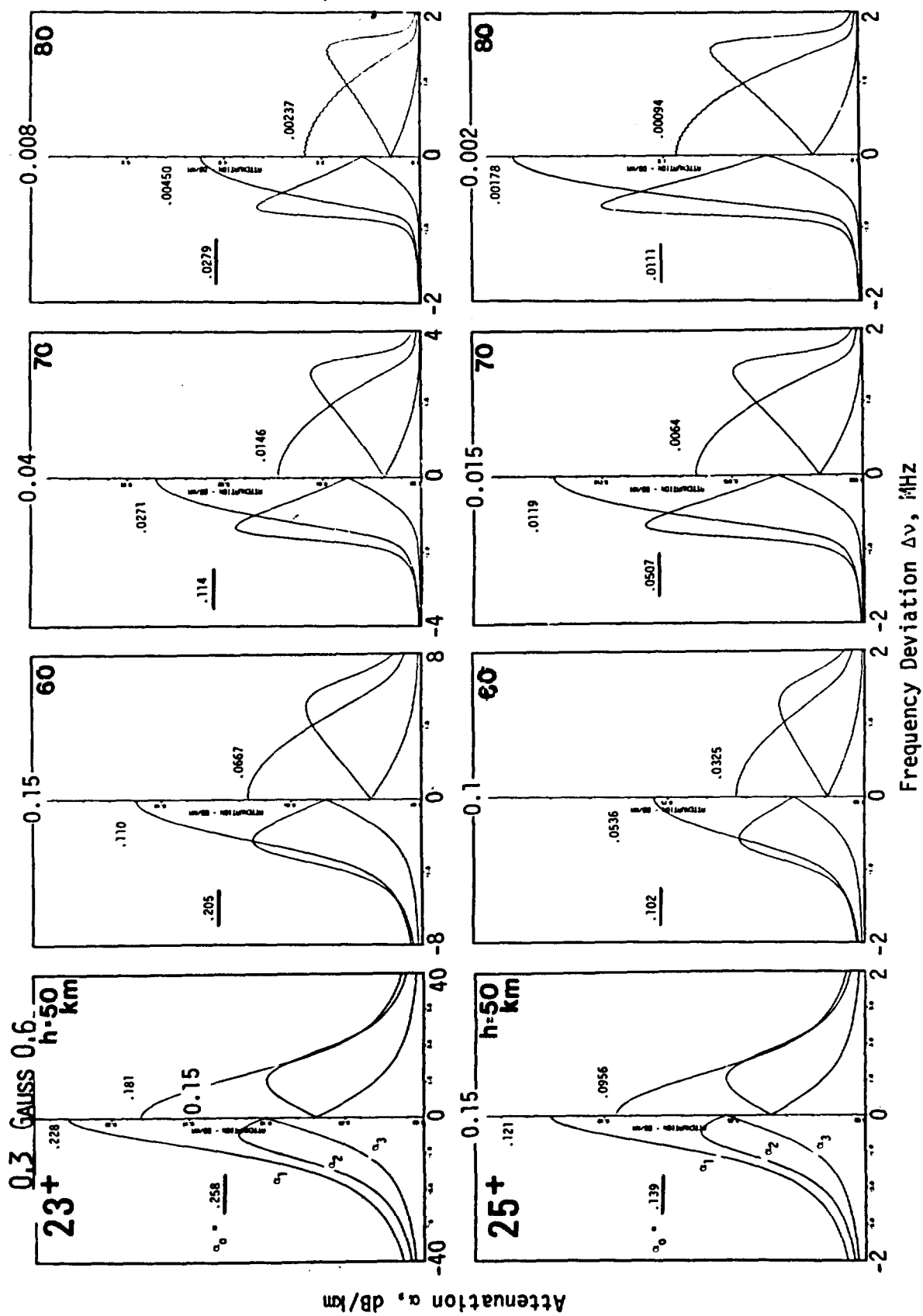
Figure A14.

Figure A14. continued
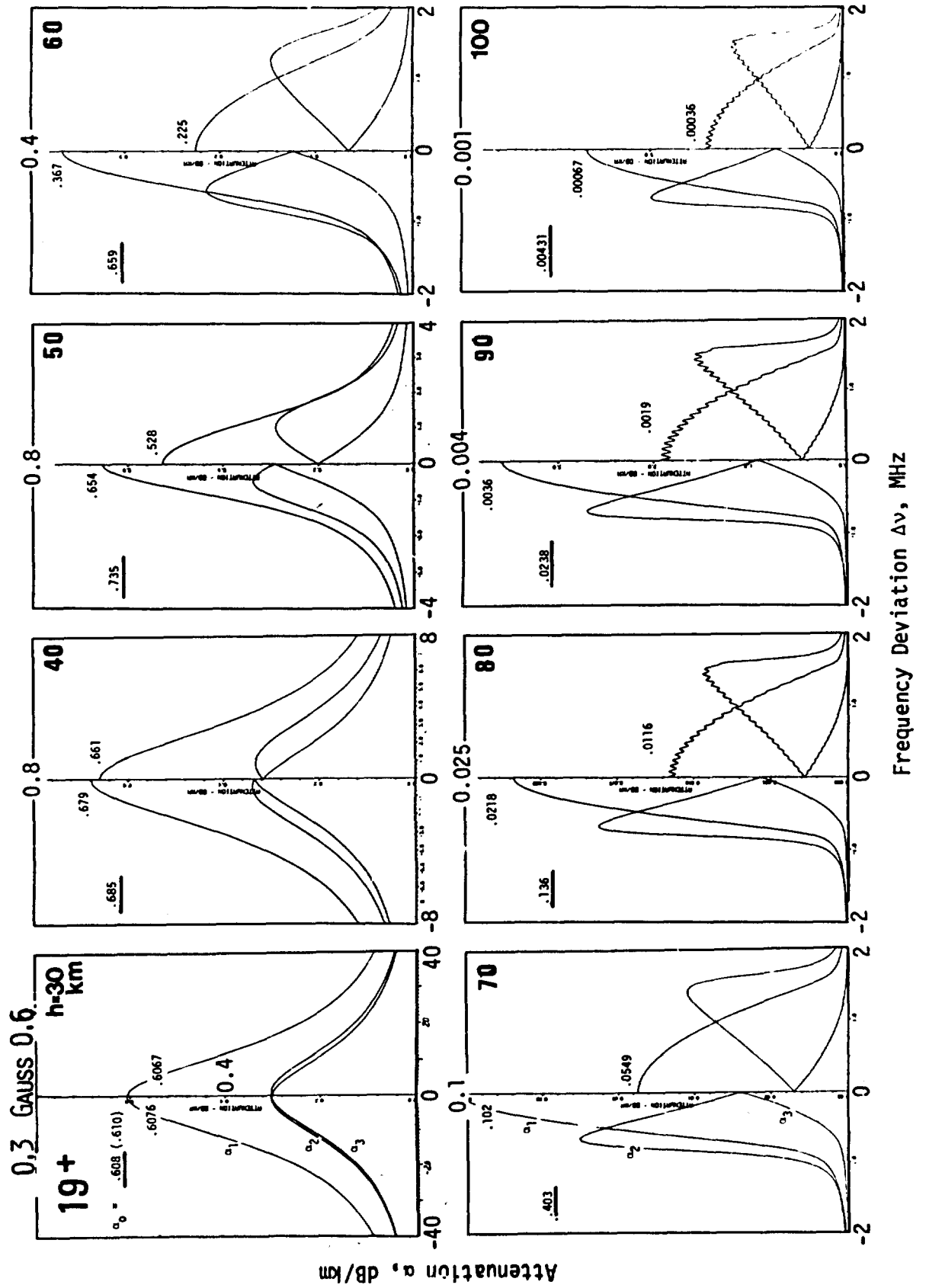
Figure A14. continued

Frequency Deviation Δν, MHz

Attenuation α, dB/km

Figure A14. continued

Figure A14. continued

Frequency Deviation $\Delta\nu$, MHz

Attenuation α, dB/km

99

66
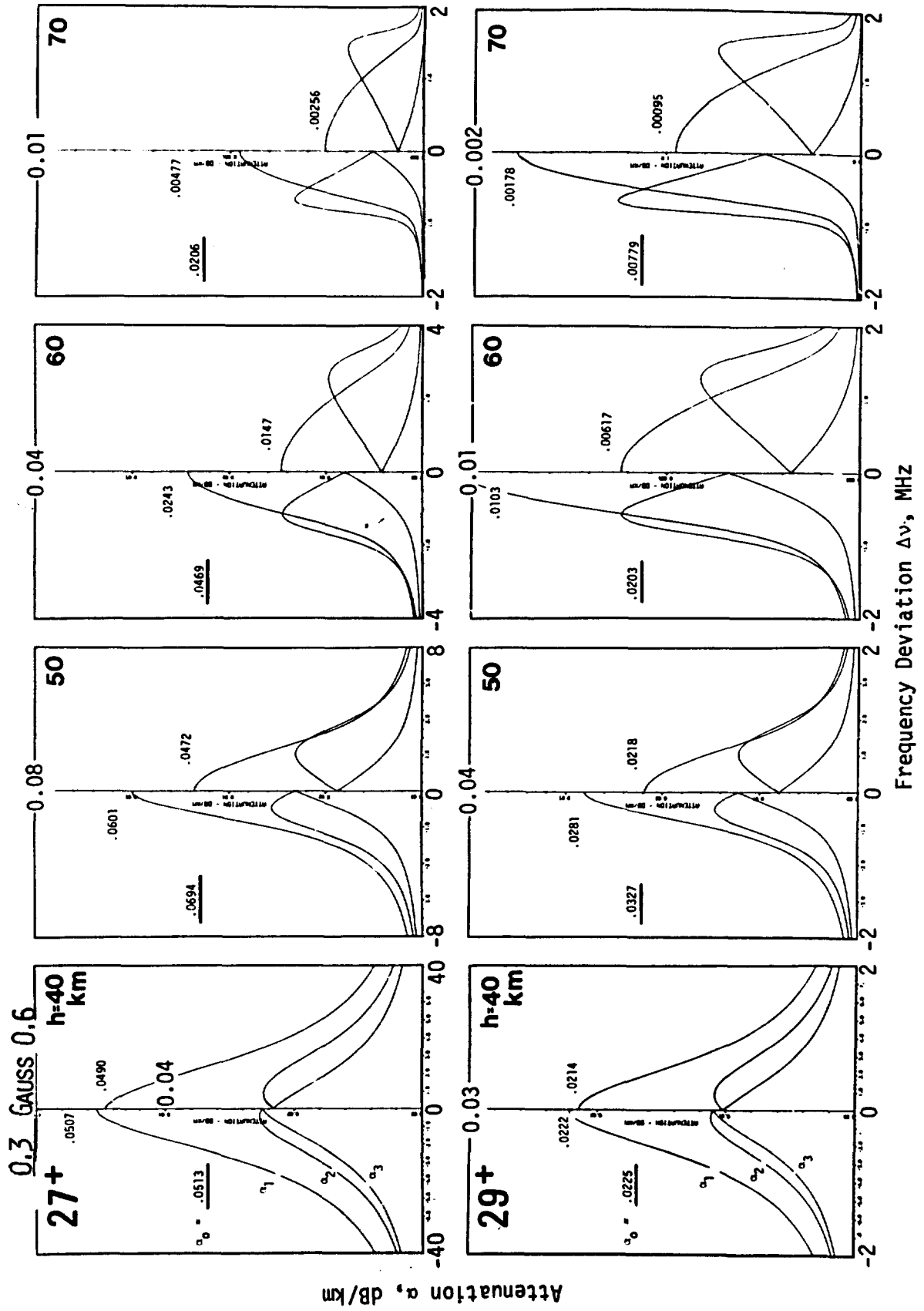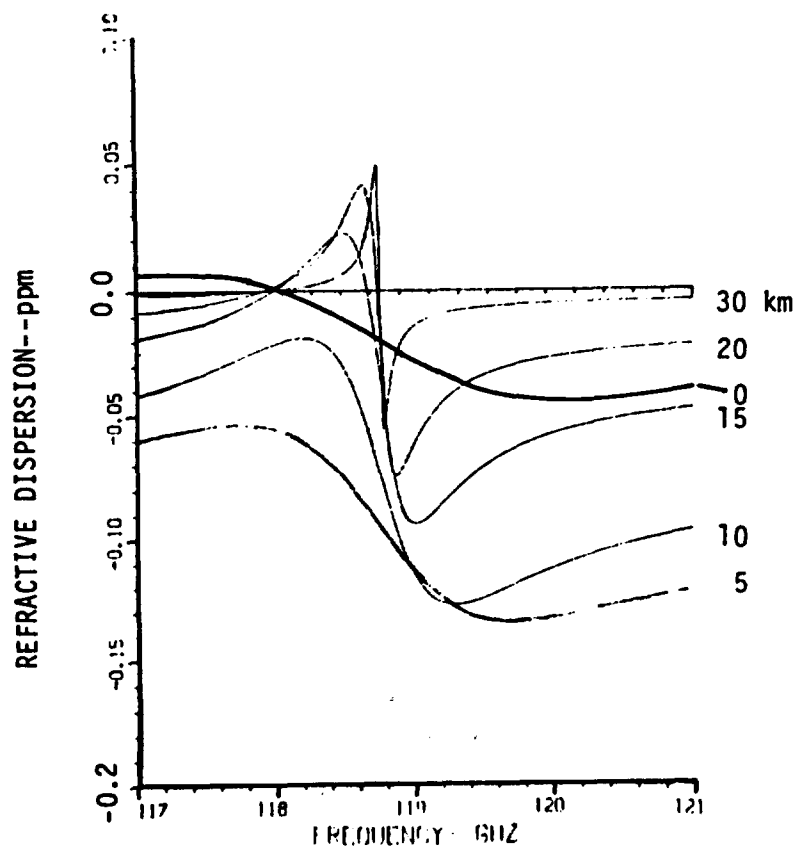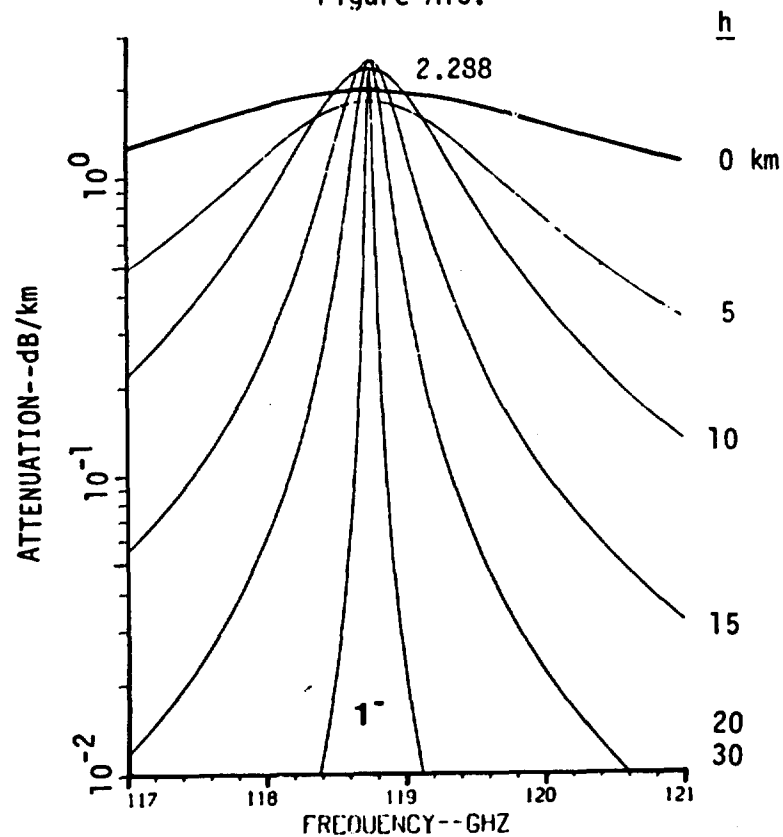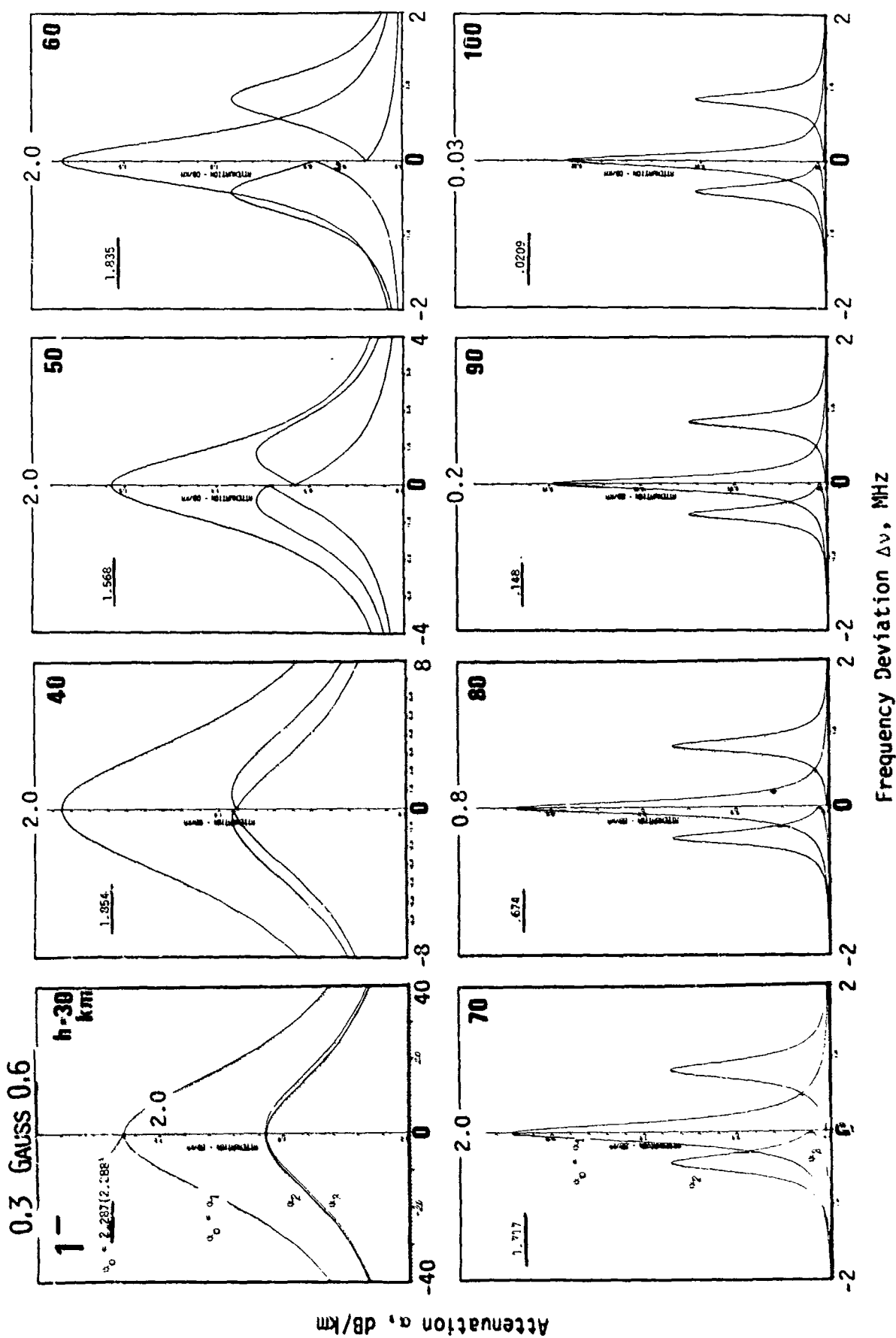
Figure A15.

APPENDIX B.

AB INITIO CALCULATION OF O_2 LINE STRENGTHS

We present here briefly the assumptions, and the molecular and fundamental constants that are used in an ab initio calculation of line strengths S_i (8) for O_2 lines in air. The absorption spectrum $N''(f)$ of a pressure-broadened line is given in molecular terms by

$$N''(f) = \frac{2\pi^2 10^{-6} M}{3h \, Q} \, g_\ell \mu^2 |\phi|^2 (e^{-E_\ell/kT} - e^{-E_m/kT}) \, F(f) \quad \text{ppm} \tag{B1}$$

For spectral lines in the millimeter wave range, the approximation

$$e^{-E_\ell/kT} - e^{-E_m/kT} \simeq (h\nu_0/kT) e^{-E_\ell/kT}$$

is valid, which leads via (see Equations 8,17)

$$N''(f) = \text{...} F(\text{...}) = SF''(f) \quad \text{ppm}$$

to the definition of a line strength

$$S = 2\pi 10^{-6} \nu_0 M \, g_\ell \mu^2 |\phi|^2 [\exp(-E_\ell/kT)]/3kTQ \quad \text{Hz} \tag{B2}$$

A numerical evaluation of (B2) for the linear rotor molecule $^{16}O_2$ (99.76%) in air (20.946%) assumes the ideal gas law

$$M = 0.20946 \times 0.9976 \, p/kT = 1.5135 \times 10^{19} \, p/T \quad cm^{-3}$$

for the number density of molecular absorbers; and the appropriate molecular parameters are

$$g_\ell = 1$$

$$\mu^2 = 3.44034 \times 10^{-40} \ (erg/Gauss)^2$$

$$B = 43.100518 \ GHz$$

$$E_\ell/kT \simeq hBK(K + 1)/kT = 2.06852 \ K(K + 1)/T$$

$$Q = 3kT/2hB = 0.72516 \ T$$

$$h = 6.62618 \times 10^{-27} \ erg \cdot s$$

$$k = 1.38066 \times 10^{-16} \ erg/K$$

With these values inserted into (B2), one obtains

$$S = 1.0892 \times 10^{-4} \nu_0 (p/T^3) |\phi|^2 \exp[-2.0685K(K + 1)/T] \quad \text{kHz} \quad , \tag{B3}$$

when the line center frequency ν_0 is in GHz.

The matrix elements for O_2 microwave lines are

$$|\phi^+|^2 = k_J K^+ (2K^+ + 3)/K^+ + 1) \quad ,$$

$$|\phi^-|^2 = k_J (K^- + 1)(2K^- - 1)/K^- \quad ,$$

and k_J is a correction factor for deviations from Hund's case "b" as listed below

K+	K-	J	k_J
	1-	0	1.0000
1+	3-	2	.9808
3+	5-	4	.9941
5+	7-	6	.9972
7+	9-	8	.9984
9+	11-	10	.9989
11+	13-	12	.9992
$\geq$13+	$\geq$15-	$\geq$14	1.0000

The spectroscopic coefficient a_1 is defined at the temperature $T = 300$ K by means of (B3) to (Table 1)

$$a_1 = S(300)/p = 4.0342 \times 10^{-12} \nu_0 |\phi|^2 \exp[-0.006895K(K + 1)] \text{ kHz/kPa}, \tag{B4}$$

and Equation (B3) is reduced to expression (19), which is used for the Millimeter-Wave Propagation Model (MPM). These involved calculations have been reported many times with more or less slightly differing constants and definitions. This appendix is meant to reveal the extent of simplifications and reductions that had to be performed before the millimeter wave properties of dry air could be entered into an MPM version. The expert recognizes our numerical assumptions in calculating a_1 and a_2; however, we refrain from defining the numerous terms (see Section 2.1.1) but refer to standard references (e.g., Waters, 1976; Endo and Mizushima, 1982; Poynter and Pickett, 1981).

104

APPENDIX C.
COMPARISON OF MODEL (MPM) PREDICTIONS WITH
SELECTED LABORATORY/FIELD DATA

The millimeter wave propagation model (MPM) is a conglomerate of individual routines addressing formally via (7) and (8) line sums of O_2 and H_2O, continuum spectra of dry air and H_2O, as well as fog and rain contributions. Each routine has been developed separately, based on underlying theory and supportive experiments. This appendix presents several examples that are suitable as test cases for demonstrating the performance of the MPM in actual atmospheric situations. It was difficult to find corroborative data of sufficient quality in the literature that might serve such a role. Reliability, precision, and limited scope of supporting meteorological data often compromise the accuracy of results deduced from field observations. Generally, controlled laboratory experiments provide more serious tests by simulating atmospheric conditions crucial to MPM validations.

We selected some recent, and one set of rather classic, attenuation results from laboratory (Figure C1) and field (Figures C2 to C5) experiments conducted at frequencies (21, 32, 96, 110, and 337 GHz) that are particularly sensitive to the new water vapor continuum (24). Continuum absorption has been a major source of uncertainty in past modeling efforts, including the MPM. The comparison between laboratory data and MPM predictions, as depicted in Figure C1, indicates good agreement. A second comparison is made with data from field measurements on horizontal paths. Figures C2 and C3 demonstrate a reasonable fit considering the scatter in data points that indicates difficulties plaguing an absolute calibration. For example, the 72 data points in Figure C2 were obtained over a three-week summer period in Boulder, Colorado, as hourly averages taken during stable weather conditions (afternoons). The vapor pressure e was deduced from microwave refractivity readings $N_0(e,p,T)$ at the receiver site by applying (4).

The last example, Figure C4, is more complex since it involves zenith attenuation A_z at two frequencies (20.6 and 31.6 GHz), measured radiometrically by means of atmospheric brightness $T_B(11)$ from three locations (h_0 = 0, 0.8, and 1.6 km) in the United States. The authors successfully fitted straight lines (LF) to the water vapor dependences as summarized in Figure C4. The experimental conditions were simulated with the MPM by assuming the U. S. Standard Atmosphere. Adjusting the dry air cut-offs A_0 to the calculated values (BF) had the effect of slightly changing the water vapor slopes $(A_v/V)_z$ within data scatter, which allowed a
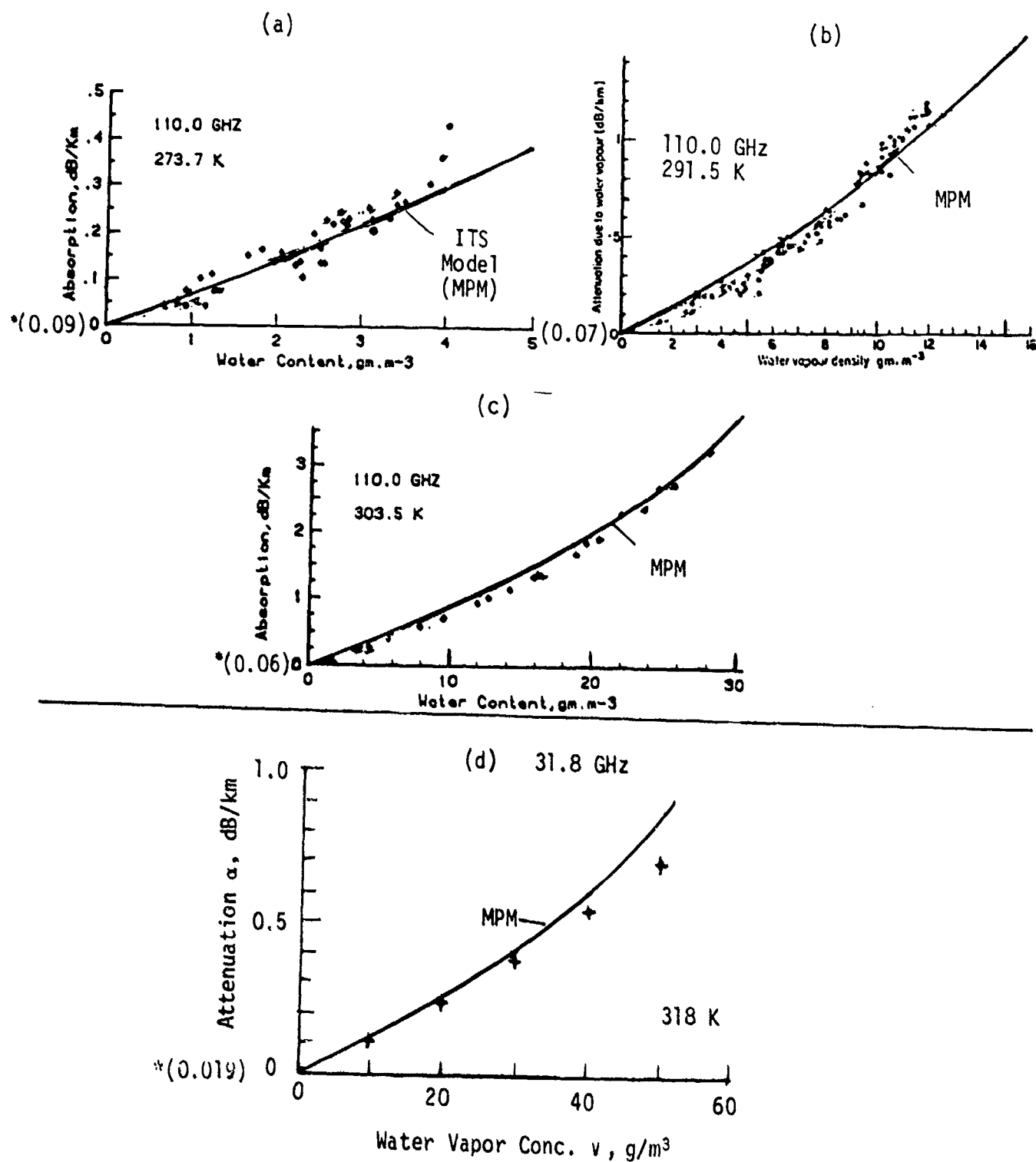
LABORATORY DATA
(Moist Air, 1013 mb)

Figure C1. Laboratory measurements of moist air attenuation at 110 GHz and three temperatures: (a) 273.7 K, (c) 303.5 K (Knight and Llewellyn-Jones, 1982), (b) 291.5 K (Llewellyn-Jones and Knight, 1981) and (d) at 31.8 GHz, 318 K (Becker and Autler, 1946).
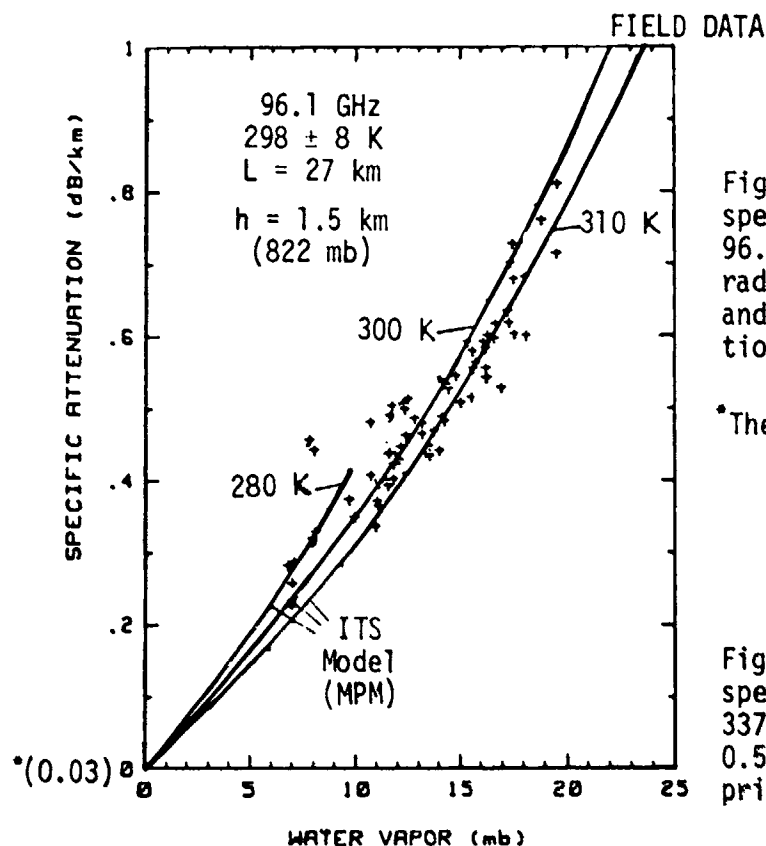
106

Figure C2 (left). Measurements of specific water vapor attenuation at 96.1 GHz over a 27 km horizontal radio path (K. Allen, E. Violette, and R. Espeland, private communication, 1983).

*The value ( ) at α = 0 is the dry air attenuation

Figure C3 (below). Measurements of specific water vapor attenuation at 337 GHz and two temperatures over a 0.5 km horizontal path (A. Gasiewski, private communication, 1983).
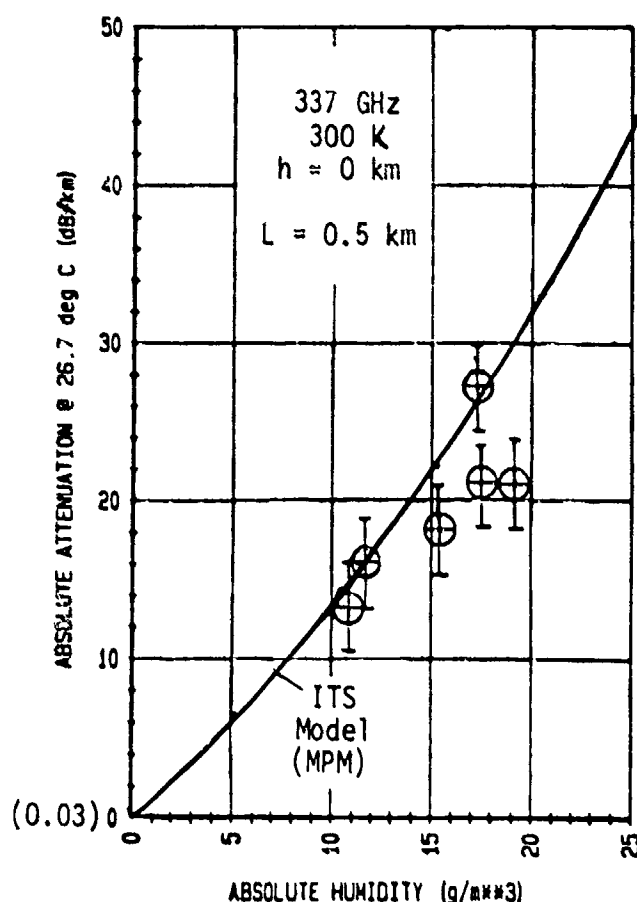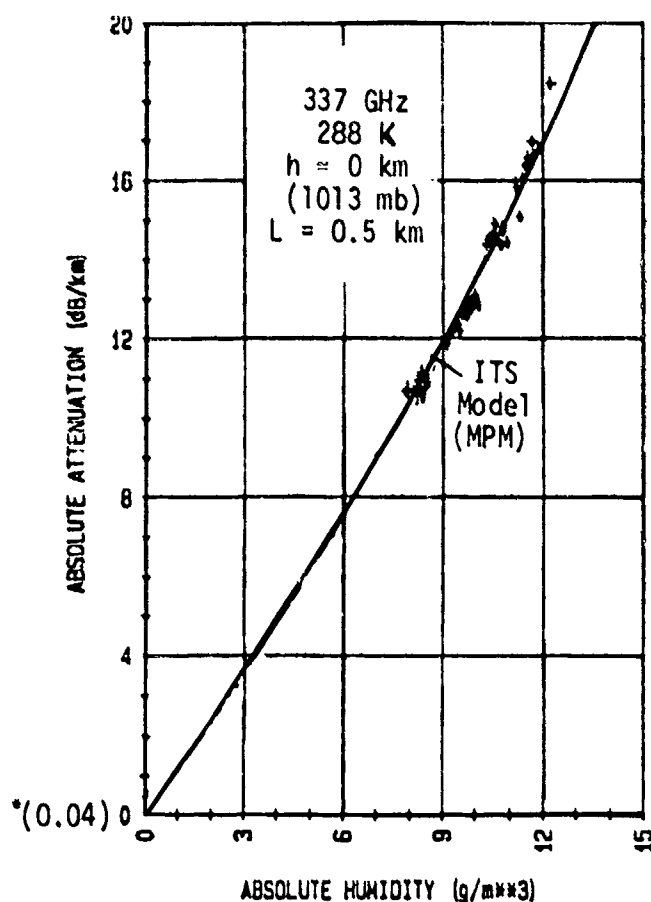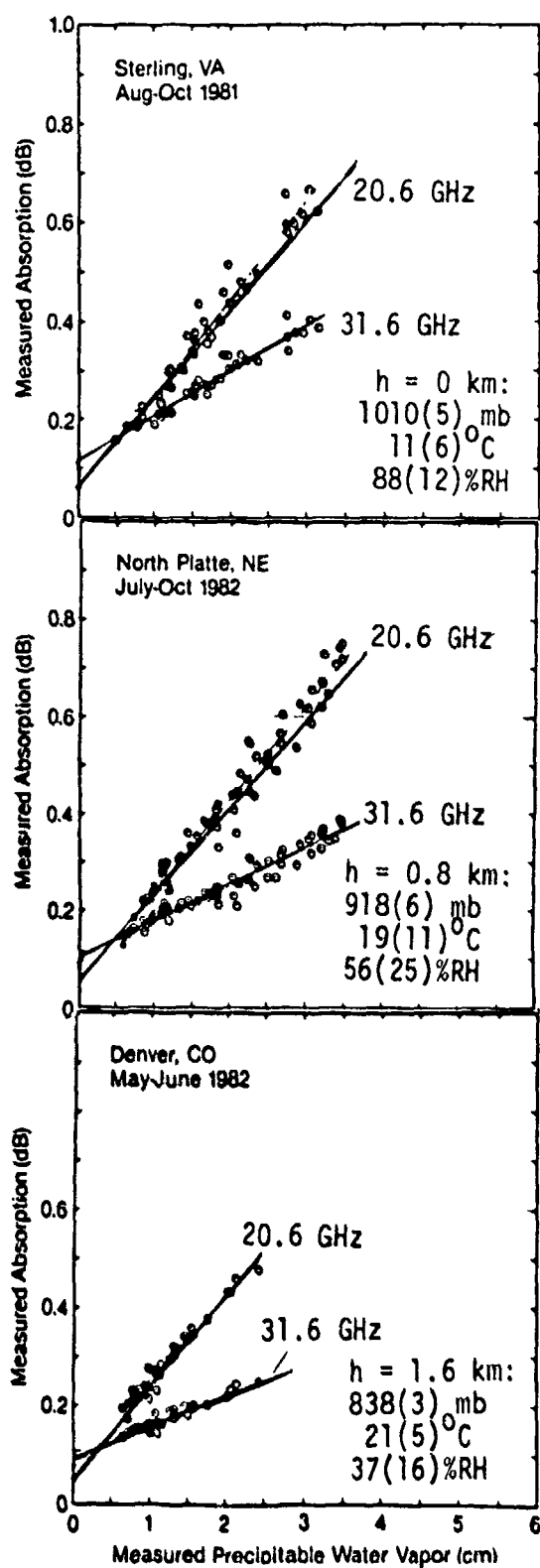
	A_o	A_v/V
	dB	dB/cm
20.6 GHz		
LF	0.049(10)	0.199(7)
BF		0.175
MF	0.060	0.167(2)
rms = 0.030dB		
31.6 GHz		
LF	0.115(6)	0.092(4)
MF	0.119	0.089(3)
rms = 0.016dB		
20.6 GHz		
LF	0.044(8)	0.192(5)
BF		0.175
MF	0.048	0.169(2)
rms = 0.017dB		
31.6 GHz		
LF	0.103(4)	0.076(2)
MF	0.100	0.076(3)
rms = 0.017dB		
20.6 GHz		
LF	0.076(7)	0.173(6)
BF	0.045	
MF	0.045	0.170(2)
rms = 0.014dB		
31.6 GHz		
LF	0.096(4)	0.064(4)
BF	0.090	
MF	0.085	0.070(3)
rms = 0.008dB		

LF = linear fit, BF = biased fit,
MF = model fit (MPM).

Plot labels:
Sterling, VA Aug-Oct 1981; 20.6 GHz; 31.6 GHz; h = 0 km: 1010(5) mb, 11(6)°C, 88(12)%RH

North Platte, NE July-Oct 1982; 20.6 GHz; 31.6 GHz; h = 0.8 km: 918(6) mb, 19(11)°C, 56(25)%RH

Denver, CO May-June 1982; 20.6 GHz; 31.6 GHz; h = 1.6 km: 838(3) mb, 21(5)°C, 37(16)%RH

Measured Absorption (dB) vs Measured Precipitable Water Vapor (cm)

Figure C4. MPM predictions for radiometric measurements of dry air zenith attenuation A_o(dB) and water vapor zenith attenuation slope A_v/V (dB/cm) from ground level observations at h_o = 0, 0.8, and 1.6 km: (a) 20.6 GHz (D. Hogg, F. Guiraud, and E. Westwater, private communication, 1983), (b) 31.6 GHz (Hogg et al., 1983).
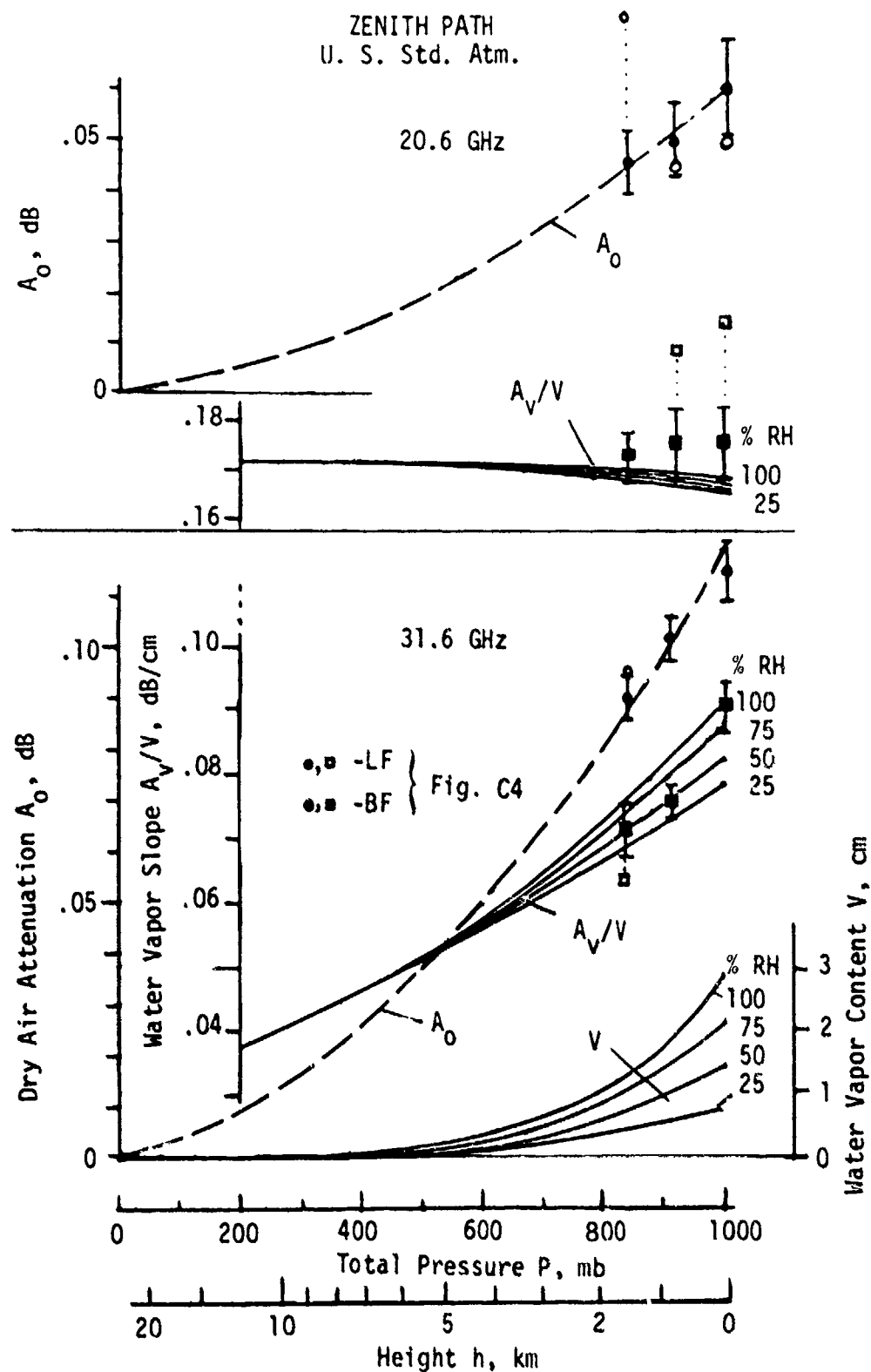
Figure C5. Predicted (MPM) total pressure P (or height h) dependence of dry air attenuation A_o and water vapor attenuation slope A_v/V (P > 200 mb, h < 12 km) at 20.6 and 31.6 GHz for a zenith path through the U. S. Std. Atm. (NOAA, 1976). Four water vapor contents V(h) are assumed and the experimental results from Figure C4 are shown.

satisfactory fit to model predictions. Only one data point (A_o at 20.6 GHz, h_o = 1.6 km) out of twelve is not explained by the simulation.

A more complete picture of modeling the data given in Figure C4 is exhibited in Figure C5. Dependences on total pressure P (height h) and four values for height-limited (h $\leq$ 12 km) water vapor contents V are shown. At 20.6 GHz, about 2/3 of the water vapor attenuation A_V comes from the 22.235 GHz H_2O line; at 31.6 GHz, the picture is reversed in favor of the water vapor continuum (24). In the first case, line pressure-broadening defeats increases in the slope A_V/V that are caused at 31.6 GHz by the e^2-term of (24). Data at 20.6 GHz indicate a possibility that the 22 GHz line strength (b_1 = 0.112, Table 2) is a little bit too low.

In summary, good agreement between MPM-predicted attenuation and selected data taken under a variety of conditions (that is, frequencies between 21 and 337 GHz, v = 0 to 50 g/m^3, V = 0 to 3.5 cm, T = 274 to 318 K, P_o = 1013 to 820 mb) lends credibility to the millimeter wave propagation model MPM presented in this report.

ADDITIONAL REFERENCES FOR APPENDIX C

Becker, G. E., and S. H. Autler (1946), Water vapor absorption of electromagnetic radiation in the centimeter wave-length range, Phys. Rev. 70, No. 5/6, pp. 300-307.

Hogg, D. C., F. O. Guiraud, and E. R. Westwater (1983), Emission measurements of 31.6 GHz absorption by atmospheric water vapor, Radio Sci. 18, No. 6, pp. 1295-1300.

Knight, R. J., and D. T. Llewellyn-Jones (1982), Measurements of water vapour absorption in the RAL untuned cavity, Rutherford Appleton Lab. Research Note RL-82-051, July.

Llewellyn-Jones, D. T., and R. J. Knight (1981), Molecular absorption by atmospheric gases in the 100-1000 GHz region, IEE Conf. Publ. 195 (ICAP 81), pp. 81-83.

BIBLIOGRAPHIC DATA SHEET

	1. PUBLICATION NO	2 Gov't Accession No.	3 Recipient's Accession No
	NTIA Report 83-137	AD-A139154	

4 TITLE AND SUBTITLE	5 Publication Date
AN ATMOSPHERIC MILLIMETER WAVE PROPAGATION MODEL	December 1983
	6 Performing Organization Code
	NTIA/ITS.S3

7 AUTHOR(S)	9. Project/Task/Work Unit No
H. J. Liebe	

8 PERFORMING ORGANIZATION NAME AND ADDRESS

U. S. Department of Commerce
National Telecommunications & Information Administration
Institute for Telecommunication Sciences/S3
325 Broadway
Boulder, CO 80303

9. Project/Task/Work Unit No

910 8108

10 Contract/Grant No.

MIPR'a 30-79, 42-80
51-81, 6-82, 101-83

12. Type of Report and Period Covered

1 Aug 79 - 31 Dec 83
FR 0

13.

14. SUPPLEMENTARY NOTES

15 ABSTRACT (A 200-word or less factual summary of most significant information. If document includes a significant bibliography or literature survey, mention it here.)

The neutral atmosphere is characterized for the frequency range from 1 to 300 GHz as a nonturbulent propagation medium. Attenuation and propagation delay effects are predicted from meteorological data sets: pressure, temperature, humidity, suspended particle concentration, and rain rate. The physical data base of the propagation model consists of four terms: (a) resonance information for 30 water vapor and 48 oxygen absorption lines in the form of intensity coefficients and center frequency for each line; (b) a composite (oxygen, water vapor, and nitrogen) continuum spectrum; (c) a hydrosol attenuation term for haze, fog, and cloud conditions; and (d) a rain attenuation model. Oxygen lines extend into the mesosphere, where they behave in a complicated manner due to the Zeeman effect. The geomagnetic field strength H is required as an additional input parameter. Each O_2 line splits proportionally with H into numerous sub-lines, which are juxtaposed to form a Zeeman pattern spread over a megahertz scale. Patterns for three main polarization cases are calculated. Detailed examples for model atmospheres provide basic millimeter wave propagation information over the height range 0 to 100 km of the neutral atmosphere.

16 Key Words (Alphabetical order, separated by semicolons)

atmospheric attenuation; delay effects; millimeter wave properties of air; propagation model; oxygen Zeeman patterns

17. AVAILABILITY STATEMENT	18 Security Class (This report)	20. Number of pages
☒ UNLIMITED	UNCLASSIFIED	115
	19 Security Class (This page)	21 Price
☐ FOR OFFICIAL DISTRIBUTION.	UNCLASSIFIED	